# Driver lines for studying associative learning in Drosophila

Yichun Shuai[1*], Megan Sammons[1,2], Gabriella Sterne[1,3], Karen Hibbard[1], He Yang[1], Ching-Po Yang[1,4], Claire Managan[1], Igor Siwanowicz[1], Tzumin Lee[1,4], Gerald M. Rubin[1], Glenn Turner[1], Yoshinori Aso[1*]

[1] Janelia Research Campus, Howard Hughes Medical Institute, 19700 Helix Drive, Ashburn, VA 20147, USA

[2] Current address: Technion-Israel Institute of Technology, 1 Efron St., Haifa 32000, Israel.

[3] Current address: Department of Biomedical Genetics, University of Rochester Medical Center, Rochester, NY, USA.

[4] Current address: Life Sciences Institute, University of Michigan, Ann Arbor, USA.

[*] Correspondence to: shuaiy@janelia.hhmi.org asoy@janelia.hhmi.org

**Abstract**

The mushroom body (MB) is the center for associative learning in insects. In Drosophila, intersectional split-GAL4 drivers and electron microscopy (EM) connectomes have laid the foundation for precise interrogation of the MB neural circuits. However, investigation of many cell types upstream and downstream of the MB has been hindered due to lack of specific driver lines. Here we describe a new collection of over 800 split-GAL4 and split-LexA drivers that cover approximately 300 cell types, including sugar sensory neurons, putative nociceptive ascending neurons, olfactory and thermo-/hygro-sensory projection neurons, interneurons connected with the MB-extrinsic neurons, and various other cell types. We characterized activation phenotypes for a subset of these lines and identified the sugar sensory neuron line most suitable for reward substitution. Leveraging the thousands of confocal microscopy images associated with the collection, we analyzed neuronal morphological stereotypy and discovered that one set of mushroom body output neurons, MBON08/MBON09, exhibits striking individuality and asymmetry across animals. In conjunction with the EM connectome maps, the driver lines reported here offer a powerful resource for functional dissection of neural circuits for associative learning in adult Drosophila.

## Introduction

In the insect brain, the mushroom body (MB) serves as the center for associative learning (Figure 1A-C; reviewed in Modi et al., 2020; Davis, 2023). Information regarding conditioned stimulus (CS), such as odors and colors, is conveyed by projection neurons (PNs) to the calyx, the input region of the MB. In Drosophila, approximately 2,000 Kenyon cells (KCs), the MB's primary intrinsic neurons, represent the identity of sensory stimuli by their sparse activity patterns (Perez-Orive et al., 2002; Turner et al., 2008). Dopaminergic neurons (DANs) mediate signals of the unconditioned stimulus (US), such as sugar reward or electric shock punishment, to the MB (Burke et al., 2012; Kirkhart and Scott, 2015; Liu et al., 2012; Mao and Davis, 2009; Schwaerzel et al., 2003). DANs and MB output neurons (MBONs) collectively form 15 compartmental zones that tile down the length of the KC axons in the MB lobes (Aso et al., 2014a; Tanaka et al., 2008). Memories are stored as altered weights of synaptic connections between KCs and MB output neurons (MBONs) in each compartment (Hige et al., 2015a; Owald et al., 2015). Relative activity levels of MBONs across compartments represent the valence of the learned CS and drive memory-based behaviors (Aso et al., 2014b; Owald et al., 2015).

The recently completed electron microscopy (EM) connectomes of the Drosophila brain in larvae and adults revealed thousands of interneurons upstream of DANs, which convey reinforcement signals to the MB, and downstream of MBONs, which link the MB to premotor pathways and other higher-order brain centers (Dorkenwald et al., 2023; Eichler et al., 2017; Eschbach et al., 2020; Li et al., 2020; Scheffer et al., 2020; Winding et al., 2023; Zheng et al., 2018). Functional investigation of these interneuron cell types has been limited by the lack of cell-type-specific driver lines.

Using the intersectional split-GAL4 method (Luan et al., 2020, 2006), we previously generated 93 split-GAL4 driver lines that allowed for precise genetic access to 60 MB cell types, including most of the KCs, DANs, MBONs and other modulatory neurons in the MB lobe regions (Aso et al., 2014a). These lines have been instrumental in revealing the neural circuit logic by which the MB forms associative memories (Aso et al., 2019, 2014b; Awata et al., 2019; Berry et al., 2018; Dolan et al., 2018; Felsenberg et al., 2017; Handler et al., 2019; Hattori et al., 2017; Hige et al., 2015a, 2015b; Ichinose et al., 2015; König et al., 2019; Martinez-Cervantes et al., 2022; Masek et al., 2015; McCurdy et al., 2021; Pavlowsky et al., 2018; Plaçais et al., 2017; Sayin et al., 2019; Shyu et al., 2017; Tsao et al., 2018; Vogt et al., 2016; Wu et al., 2017; Yamada et al., 2023; Zhang et al., 2019).

Since the MB split-GAL4 lines were generated, new genetic and computational tools have expanded the cell types that can be targeted and facilitated the split-GAL4 design. Critically, a new collection of ZpGAL4DBD and p65ADZp hemidrivers became available (Dionne et al., 2018; Tirian and Dickson, 2017) and the expression patterns of the original GAL4 driver lines were imaged with higher-resolution confocal microscopy and Multi-Color-Flip-Out (MCFO) stochastic labeling method to reveal the morphology of individual neurons (Meissner et al., 2023; Nern et al., 2015). Additionally, advanced tools for computational neuroanatomy were developed to aid the design of split-GAL4 driver lines (Bogovic et al.,

2020; Costa et al., 2016; Masse et al., 2012; Meissner et al., 2023; Otsuna et al., 2018). Leveraging these tools and resources, we have generated a collection of new split-GAL4 lines labeling MBONs, including the majority of atypical MBONs that have dendritic input both within the MB lobes and in adjacent brain regions (Rubin and Aso, 2023). In this report, we introduce a novel collection of approximately 800 split-GAL4 lines, covering sensory neurons for sugar, wind and nociception, projection neurons for olfactory, thermo/hygro-sensory and gustatory signals, ascending neurons from ventral nerve cord (VNC), cell types within the MB, and interneurons that connect with DANs and/or MBONs. While our primary objective was to generate driver lines for studying associative learning, the collection also includes cell types tailored for various other functions. We provide a lookup table that maps the corresponding EM neurons in the hemibrain connectome for these drivers to facilitate connectome-guided investigation of neural circuits. This expanded collection of driver lines will be instrumental for many future studies of Drosophila associative learning and beyond.

## Results and Discussions

### Split-GAL4 design and anatomical screening

To gain genetic access to the cell types that convey CS and US information to the MB and those mediating memory-based actions, we designed screening to examine the expression patterns of over 4,000 intersections of split-GAL4 hemidrivers (Figure 1D). We selected 1,183 split-GAL4 lines representing various cell types in the central brain and the VNC for further characterization. For these lines, we employed higher resolution confocal microscopy and visualized the individual neurons that compose each split-GAL4 pattern with the MCFO method. We eventually identified 828 useful lines based on their specificity, intensity and non-redundancy. These fly lines are now publicly available through the webpage of the Janelia Flylight team project (http://www.janelia.org/split-gal4), where we have deposited a total of 28,376 confocal images from 6,374 tissue samples to document their expression patterns. We included lines with off-targeted expression, as they can be valuable for anatomical, developmental or functional imaging experiments, even if not suitable for behavioral experiments. Additionally, we retained drivers that intersected unintended cell types from the screening. Examples of confocal microscopy images are shown in Figure 1F and Figure 1-figure supplement 1.

We have annotated our split-GAL4 lines by matching the labeled neurons to their counterparts in the hemibrain connectome volume (Scheffer et al., 2020). We utilized confocal images registered to a standard brain, and matched neuronal cell types in each split-GAL4 line with those present in other lines and with the EM-reconstructed neurons (Figure 2A-D, see Materials and Methods). This light microscopy (LM) to EM matching process allows us to locate the cell type of each driver line in the connectome map, enabling users to select driver lines for further functional investigations based on their upstream and downstream synaptic partners (Figure 2E; Figure 2-figure supplement 1-20).

Among the 828 lines, 355 lines exhibit relatively high specificity to a non-redundant set of at least 319 cell types. Figure 1E provides an overview of the categories of covered cell

113 types. Detailed information, including genotype, expression specificity, matched EM cell
114 type(s), and recommended driver for each cell type, can be found in Supplementary File 1. A
115 small subset of these lines have been previously used in studies (Aso et al., 2023; Dolan et al.,
116 2019; Gao et al., 2019; Scaplen et al., 2021; Schretter et al., 2020; Takagi et al., 2017; Xie et
117 al., 2021; Yamada et al., 2023). All transgenic lines newly generated in this study are listed in
118 Supplementary File 2.
119
120 **Drivers for the MB cell types, MBON-downstream and DAN-upstream**
121 Prior to the completion of the EM connectome map, we conducted parallel efforts to identify
122 cell types downstream of MBONs or upstream of DANs using confocal images of GAL4 drivers
123 registered to a standard brain (Bogovic et al., 2020). We searched for GAL4 drivers containing
124 cell types with potential connections to MBONs or DANs by quantifying the number of voxels
125 overlapping with MBON axons or DAN dendrites (Otsuna et al., 2018). We then built split-
126 GAL4 intersections from selected pairs of drivers from the established hemidriver library
127 (Dionne et al., 2018; Tirian and Dickson, 2017).
128 After matching with EM-reconstructed neurons, these efforts resulted in split-GAL4
129 drivers encompassing 111 cell types that connect with the DANs and MBONs (Figure 3).
130 Several of the cell types originally selected by LM were found to be not directly connected
131 with MBONs or DANs. Nevertheless, these lines can be valuable for investigating other
132 behaviors. For example, one such line, SS32237, was found to exhibit robust female-female
133 aggression when activated (Schretter et al., 2020).
134 In the hemibrain EM connectome, there are about 400 interneuron cell types that
135 have over 100 summed synaptic inputs from MBONs and/or synaptic outputs to DANs. Our
136 newly developed collection of split-GAL4 drivers covers 30 of these major interneuron cell
137 types (Figure 3C). While this constitutes a small fraction, it includes cell types with remarkable
138 connectivity patterns. For instance, CRE011, presented as a single neuron per hemisphere,
139 integrates over 2,000 inputs from 9 types of MBONs. This is the highest number of synaptic
140 inputs from MBONs among all interneurons (Figure 3C). CRE011 provides cholinergic input to
141 reward DANs (Figure 2E) and neurons in the lateral accessory lobe, a premotor center housing
142 dendrites of multiple descending neurons (Kanzaki et al., 1994; Namiki et al., 2018). Another
143 notable example is SMP108, which receives inputs from multiple glutamatergic MBONs and
144 makes the highest number of cholinergic connections to DANs involved in appetitive memory
145 (Figure 3C). We recently reported on SMP108's role in second-order conditioning (Yamada et
146 al., 2023) and its upstream neurons labeled in SS33917 in transforming appetitive memory
147 into wind-directed locomotion (Aso et al., 2023). Supplementary File 3 contains connectivity
148 information of the MB major interneurons, along with the predicted neurotransmitters
149 (Eckstein et al., 2023) and the available driver lines.
150 The current collection also contains 189 lines for cell types that have innervations
151 within the MB (Figure 3-figure supplement 1). These lines offer valuable tools to study cell
152 types that may have been overlooked previously. Notably, the SS48794 driver labels OA-
153 VUMa2 octopaminergic neurons, which are the Drosophila counterparts to the honeybee OA-

154 VUMmx1 neurons, the first neurons identified as mediating US signals in an insect brain
155 (Hammer, 1993). Moreover, several drivers in this collection provide improved specificity.
156 When combined with previous collections (Aso et al., 2014a; Rubin and Aso, 2023), we now
157 have coverage for 7 types of Kenyon cells and 58 out of 68 cell types within the MB (excluding
158 PNs) using split-GAL4 drivers. Overall, this amounts to about 87% coverage for non-PN cell
159 types within the MB and about 10% coverage for MBON-downstream and DAN-upstream cell
160 types (Supplementary File 3 and 4, Figure 3B-C).
161
162 **Drivers for the antennal lobe projection neurons**
163 In Drosophila, the primary CS pathway to the MB involves the antennal lobe PNs that convey
164 olfactory signals. We have developed a set of driver lines for PNs and other cell types in the
165 antennal lobe (Supplementary File 1). This set includes 191 lines, covering more than 48 of
166 the approximately 190 PN types identified through EM connectome and LM studies (Bates et
167 al., 2020; Li et al., 2020; Lin et al., 2007; Tanaka et al., 2004; Zheng et al., 2022), encompassing
168 both uni- and multi-glomerular PNs (Figure 4 and 5; Supplementary File 5).
169 The antennal lobe, in addition to the 51 olfactory glomeruli, contains 7 glomeruli
170 involved in processing thermo- and hygro-sensory information (Enjin et al., 2016; Frank et al.,
171 2015; Gallio et al., 2011; Jenett et al., 2012; Liu et al., 2015; Marin et al., 2020; Stocker et al.,
172 1990; Tanaka et al., 2012). We provide 8 lines that cover sensory neurons projecting into
173 these non-olfactory glomeruli and 18 lines covering the projection neurons emanating from
174 them (Figure 6; Supplementary File 1 and 5).
175
176 **Drivers for reinforcement pathways**
177 Our understanding of the neural pathways that encode the US has been greatly advanced by
178 experiments that have tested the sufficiency of various neuronal cell types to substitute for
179 the US (Aso et al., 2010; Aso and Rubin, 2016; Chiang et al., 2011; Claridge-Chang et al., 2009;
180 Hige et al., 2015a; Huetteroth et al., 2015; Liu et al., 2012; Saumweber et al., 2018; Schroll et
181 al., 2006; Yamagata et al., 2015). These experiments leveraged thermogenic or optogenetic
182 tools expressed in specific neuronal cell types, especially DANs, to assess their functions in
183 associative learning. The approach to directly stimulate DANs, although valuable, bypasses
184 the earlier US processing pathways and potential feedback in the circuit. Because of this
185 experimental caveat, it is preferable to activate neurons at the sensory level of reward or
186 punishment pathways to faithfully replicate the natural activity of these DANs. In that way,
187 DANs can be regulated by both US sensory pathways and feedback pathways from MBONs.
188 That is likely to be essential for the successful execution of more continual learning tasks in
189 which flies update memories based on the current and past experiences (Felsenberg et al.,
190 2017; Jiang and Litwin-Kumar, 2021; McCurdy et al., 2021; Rajagopalan et al., 2022).
191 Our collection provides the starting point for generating the genetic tools needed for
192 this approach. For example, we have generated drivers for the cell types in the thermo-
193 sensory pathways, as well as PNs for odors with innate preference, such as CO2 and cVA

194 (Datta et al., 2008; Lin et al., 2013; Suh et al., 2004). These cell types are candidates to convey
195 the reinforcement signals to the MB and other brain regions for associative learning.
196 On the other hand, gustatory sensory neurons constitute the first layer of neurons
197 that detect food-related sensory signals (taste), which are conveyed to the MB through
198 largely uncharacterized pathways (Bohra et al., 2018; Burke et al., 2012; Deere et al., 2023;
199 Kim et al., 2017; Miyazaki et al., 2015; Sterne et al., 2021). GAL4 driver lines that recapitulate
200 expression patterns of gustatory receptors (GRs) have been generated and utilized for
201 functional studies (Dahanukar et al., 2007; Harris et al., 2015; Miyamoto et al., 2012; Wang
202 et al., 2004; Yavuz et al., 2014). However, these driver lines tend to contain a morphologically
203 and functionally heterogeneous set of sensory neurons (see for examples: Chen et al., 2022;
204 Thoma et al., 2016) and may contain off-targeted expressions. To address these limitations,
205 we have developed split-GAL4 drivers specific to different subsets of gustatory sensory
206 neurons by generating hemidrivers for GR-gene promoters and screening intersections with
207 existing hemidrivers (Figure 7A).
208 We used this strategy to generate Gr64f-split-GAL4 lines and create clean drivers for
209 reward sensory neurons. In fruit flies, sugar is detected by sensory neurons located on
210 different taste organs of the body and also inside the brain (Fujii et al., 2015; Hiroi et al., 2002;
211 Miyamoto et al., 2012; Rodrigues and Siddiqi, 1978). Gr64f-Gal4, in which Gal4 is expressed
212 under the control of the promoter of the sugar receptor gene *Gr64f*, broadly labels sugar
213 sensory neurons (Dahanukar et al., 2007 and Figure 7 – figure supplement 1). Gr64f-Gal4
214 expression can be found in heterogeneous sets of sensory neurons in the labellum, the tarsi
215 and the labral sense organ (LSO) located along the pharynx. In addition, Gr64f-Gal4 also labels
216 subsets of olfactory receptor neurons and neurons innervating the abdominal ganglion (Park
217 and Kwon, 2011)(Figure 7-figure supplement 1), despite that whether these cells
218 endogenously express Gr64f is yet to be confirmed. Such heterogeneity in Gr64f-Gal4
219 expression could limit its usage to substitute reward in complex associative learning.
220 To refine Gr64f-Gal4 expression, we intersected Gr64f-GAL4DBD with various AD lines
221 selected based on the projection patterns of Gr64f-Gal4, and obtained 16 stable split-GAL4
222 lines that have expression in distinct subsets of Gr64f neurons (Figure 7). We examined the
223 ability of these lines to serve as US in olfactory learning (Aso and Rubin, 2016) and their
224 potency to drive local search behaviors (Corfas et al., 2019)(Figure 8 and Figure 8-figure
225 supplement 1). Additionally, we measured the walking speed of flies, as flies decrease walking
226 while feeding (Thoma et al., 2016).
227 Among the Gr64f-split-GAL4 lines, SS87269 emerged as the best driver for substituting
228 sugar reward in olfactory learning given its specificity and the utility in long training protocols
229 (Figure 8E). SS87269 expresses in the labellum and at least two types of tarsal sensory
230 neurons, namely the ascending (atGRN) and the non-ascending segment-specific (stGRN)
231 types (Figure 7E-F). The driver does not label pharyngeal sensory neurons, and importantly,
232 it lacks expression in abdominal ganglion and olfactory sensory neurons that could be off-
233 targeted neurons found in the original Gr64f-GAL4. When odor presentation was paired with
234 the activation of SS87269 neurons, flies formed robust appetitive memories even after

extended training with high LED intensity (Figure 8E, Figure 8-figure supplement 1 and Video 1). Furthermore, and consistent with the idea that this subset of sensory neurons encodes appetitive food-related taste information, flies with SS87269 activation showed proboscis extension and reduced locomotion (Figure 8F-I; Figure 8-figure supplement 2, Video 2 and 4). These flies also showed robust local search behavior during the post-activation period, i.e., an increased probability of revisiting the area where they experienced the activation (Video 3). Notably, the revisiting phenotype of SS87269 was stronger than the original Gr64f-GAL4 and any other Gr64f-split-GAL4 drivers (Figure 8F and Figure 8-figure supplement 2A).

Two other lines SS88801 and SS88776, which label stGRNs or stGRNs along with labial sensory neurons, respectively (Figure 7K-L,I), showed appetitive learning and reduced locomotion during activation (Figure 8E-F). Interestingly, however, the activation of stGRNs with SS88801 did not induce significant local search behaviors (Figure 8F and Figure 8-figure supplement 2A). This finding could be valuable for understanding circuits underlying local search behavior and invites further investigation to compare pathways from labial and tarsal sensory neurons to the MB and the central complex.

In contrast to SS87269, two other resulting lines, SS87278 and SS87279, express in cells that appear to convey aversive signals. Activation of these lines induced an increase in walking speed during activation and reduced the probability of return at the offset of LED activation (Figure 8F and Figure 8-figure supplement 2). Also, flies became progressively less mobile during the inter-trial interval period (Figure 8G). The reduced locomotion in the interval period was also observed with the original Gr64f-GAL4 (Figure 8G) and a bitter-taste driver, Gr66a-GAL4 (data not shown). With extended training using SS87278 and SS87279, the preference to the paired odor eventually became negative (Figure 8E). These drivers label distinct subsets of sensory neurons projecting to the abdominal ganglion (Figure 7O,P). The innervation of SS87278 inside the abdominal ganglion is similar to that of Gr66a-GAL4 (Figure 7P) (Dunipace et al., 2001), which is known to label multidendritic sensory neurons in the adult Drosophila abdomen (Shimono et al., 2009). Examining projection patterns in fly bodies with whole-animal agar sections, we found that sensory neurons in SS87278 also project to the abdominal body surface (Figure 7J), likely representing the class IV multidendritic neurons that detect multimodal nociceptive stimuli (Hwang et al., 2007; Ohyama et al., 2015). GAL4 expression in these aversive sensory neurons may thereby explain the compromised learning performance with the original Gr64f-GAL4.

Overall, the refinement of Gr64f-Gal4 expression with SS87269 now allows for specific manipulation of the rewarding subset of gustatory sensory neurons and thereby permits training with an extended number of trials. While we have not yet conducted anatomical screening, LexADBD lines generated with Gr64f, Gr43a, Gr66a, Gr28b.d promoters (Figure 7A) should enable similar refinement of these sensory neuron lines. We also made a small number of lines for cell types in the subesophageal zone (SEZ) area (Figure 8-figure supplement 3), which complement previous collections of drivers for gustatory interneurons (Otto et al., 2020; Sterne et al., 2021).

275 Lastly, we generated driver lines for putative ascending nociceptive pathways. We
276 determined the activation preference for 581 combinations of ZpGAL4DBD and p65ADZp
277 hemidrivers in the circular arena (Figure 9A, Supplementary File 1). We found one driver,
278 SS01159, which showed the most robust avoidance of LED quadrants and demonstrated
279 behavioral components that are characteristic to nociception, including backward walking,
280 turning, increased speed, and jumping upon activation (Figure 9B-D, and Video 5). This driver
281 labels a group of ascending neurons (Figure 9E), which likely carry nociceptive signals from
282 the body and legs to the brain. We then generated drivers for subsets of these ascending
283 neurons guided by single neuron morphologies of cells in SS01159 determined by MCFO
284 stochastic labeling (Nern et al., 2015). Other than SS01159, the collection in total contains
285 approximately 100 split-GAL4 lines covering ascending neurons. While not completely
286 matched to EM cell types due to only a portion of their morphologies being available in the
287 hemibrain volume, these lines serve as a valuable resource for querying the reinforcement
288 pathways.
289
290 **Morphological individuality and asymmetry**
291 Despite the recent progress in the EM connectome field, EM-based methods remain
292 prohibitively expensive and morphological variability of neurons has been compared only
293 across two individuals and three hemispheres (Schlegel et al., 2023). As a part of Janelia
294 Flylight team project to generate cell-type-specific driver lines, we have imaged over 6,000
295 fly brains for the present study. While annotating those confocal images of split-GAL4 lines,
296 we occasionally encountered samples with atypical morphologies (Figure 10). For example,
297 one V_l2PN neuron, which typically projects to the lateral horn of the ipsilateral hemisphere,
298 exhibited a peculiar morphology in one brain sample, where its axon crossed the midline and
299 projected to the contralateral hemisphere, yet it still reached the correct target area within
300 the lateral horn of the opposite side (Figure 10A). Another instance involved a DPM neuron,
301 the sole serotonergic neuron of the MB lobes. While typical brain samples contain only one
302 DPM neuron per hemisphere, we found a brain with two DPM neurons in one hemisphere
303 (Figure 10B). In this case, the DPM projections exhibited an atypical innervation of the calyx
304 of the mushroom body. We also found examples involving MBONs. The dendrites of MBON-
305 α1 are typically confined inside the α lobe of the MB, but we discovered a case of MBON-α1
306 in addition projecting to the ellipsoid body (Figure 10C). MBON-α3 displayed striking
307 variability in soma positions, but only subtle variability in axonal projections (Figure 10D). The
308 table in Figure 10E summarizes additional examples of the atypical morphologies of MBONs.
309 Overall in 1241 brain hemispheres examined, we found mislocalization of dendrites and
310 axons in 3.14% and 0.97% of MB cell types, respectively. If this rate of mislocalization is
311 generalizable to other brain regions, a fly brain of ~130,000 neurons (Dorkenwald et al., 2023)
312 would have a few thousands of neurons with mislocalized dendrites or axons. These examples
313 of atypical morphology were observed only once in dozens of samples, and thus can be
314 considered as erroneous projections either resulting from stochastic developmental

processes, or possibly caused by ectopic expression of reporter proteins on the plasma membrane at a high level.

In contrast to these rare, and seemingly erroneous, morphological variations, we observed much more frequent and reproducible variations in the composition as well as morphologies in the two MBONs labeled by MB083C, which may amount to "individuality". This split-GAL4 driver line invariably labels two cells in each hemisphere in 169 brain samples examined with four different reporters and in both sexes (57 males and 112 females; Figure 11-figure supplement 1). In all samples, these MBONs arborized dendrites in the γ3 and β'1 compartments. An obvious mistargeting of the axon was observed in only one sample, suggesting highly consistent development of these MBONs (Figure 11A-B). However, MCFO method visualized two distinct morphologies of these MBONs: MBON08 arborizes dendrites in the γ3 compartment of both hemispheres, whereas MBON09 arborize dendrites in ipsilateral γ3 and contralateral β'1 (Figure 11C-H)(Aso et al., 2014a). β'1 compartment was always labeled in both hemispheres for all 169 samples, suggesting that MBON09 represents at least one of the two cells in each hemisphere. The second cell can be either MBON08 or MBON09. In MCFO experiments, we observed 21 instances of MBON08 (8 in the left and 13 in the right hemisphere) and 188 instances of MBON09 (Figure 11I). Based on the likelihood, we expect 65% of flies contain four MBON09, while the remaining 35% of flies likely have at least one MBON08. In 71 hemispheres, two cells were visualized in different colors of MCFO: 52 contained two MBON09 and 19 contained one MBON08 and MBON09. We never observed a brain with MBON08 on both hemispheres or two MBON08 in one hemisphere (Figure 11J). When MBON08 and MBON09 coexist, MBON09 arborized in the lateral part of the ipsilateral γ3 and MBON08 arborize in the medial part of the contralateral γ3 (Figure 11E-H). This seemingly extended γ3 compartment innervated by MBON08 is not part of γ4, because it did not overlap with DANs in the γ4 (Figure 11-figure supplement 2A-B).

Although MBON08 was not found in brain samples used for the hemibrain or FAFB EM connectome (Dorkenwald et al., 2023; Scheffer et al., 2020; Zheng et al., 2018), DANs in the γ3 could be subdivided to two groups that innervate the medial or lateral part of the γ3 (Figure 11-figure supplement 2C) (Li et al., 2020). Therefore, subdivision of the γ3 compartment may exist irrespective of heterogeneity on the MBON side. In larval brains, two MBONs that correspond to adult MBON08/09 exhibit identical morphology (Eichler et al., 2017; Saumweber et al., 2018; Truman et al., 2023). Therefore, one of these MBONs acquires distinct morphology as MBON08 during metamorphosis at 21/209 odds, resulting in an asymmetric output pathway of the MB; We have never observed a brain with MBON08 on both hemispheres, and therefore MBON08 likely to appear in only one hemisphere, if at all (Figure 11J). This asymmetry could be one source of turning handedness and idiosyncratic learning performance (de Bivort et al., 2022; Smith et al., 2022), given that MBON09 forms extensive connection with other MBONs and fan-shaped body neurons (Li et al., 2020) and the activity of MBON08/MBON09 has strong influence on turning (Aso et al., 2023, 2014b; Matheson et al., 2022).

356 **Conversion to split-LexA**
357 Split-GAL4 lines can be converted into split-LexA lines by replacing the GAL4 DNA binding
358 domain with that of LexA (Ting et al., 2011). To broaden the utility of our collection, we have
359 generated over 20 LexADBD lines to test the conversions of split-GAL4 to split-LexA. The
360 majority (22 out of 34) of the resulting split-LexA lines exhibited very similar expression
361 patterns to their corresponding original split-GAL4 lines (Figure 12). For the failed cases, the
362 expression level was either undetectable or too weak.
363
364 **Concluding Remarks**
365 The ability to define and manipulate a small group of neurons is crucial for studying neural
366 circuits. Here, we have generated and characterized driver lines targeting specific cell types
367 that are likely to be a part of associative learning circuits centered on the MB. We have
368 provided these driver lines with a comprehensive lookup table linking these cell types with
369 the EM hemibrain connectome. These lines, together with preceding collections of drivers
370 (Aso et al., 2014a; Aso and Rubin, 2016; Davis et al., 2020; Dolan et al., 2018; Rubin and Aso,
371 2023; Shuai et al., 2015; see for examples: Sterne et al., 2021; Strother et al., 2017; Truman
372 et al., 2023; Tuthill et al., 2013; Wang et al., 2021; Wolff and Rubin, 2018; Wu et al., 2016),
373 collectively constitute a powerful resource for precise functional interrogation of associative
374 learning in adult Drosophila melanogaster, and will be a foundation to reveal conserved
375 principles of neural circuits for associative learning.
376
377 **Materials and Methods**
378 **Fly strains**
379 *Drosophila melanogaster* strains were reared at 22°C and 60% humidity on standard cornmeal food
380 in 12:12 hour light:dark cycle. The genotypes of all split-GAL4 and split-LexA driver lines released here
381 are listed in the Supplementary File 1. The new collection of split-GAL4 drivers reported here was
382 designed based on confocal image databases (http://flweb.janelia.org) (Jenett et al., 2012; Tirian and
383 Dickson, 2017), and screening expression patterns of p65ADZp and ZpGAL4DBD combinations was
384 performed as described previously (Aso et al., 2014a; Pfeiffer et al., 2010).
385
386 **Immunohistochemistry**
387 Brains and ventral nerve cords of 3-10 days old flies were dissected, fixed and immunolabeled and
388 imaged with confocal microscopes (Zeiss LSM710, LSM780 or LSM880) as previously described (Aso
389 et al., 2014a; Jenett et al., 2012; Meissner et al., 2023; Nern et al., 2015). The detailed protocols and
390 videos are available at https://www.janelia.org/project-team/flylight/protocols.
391
392 **Whole-body sections**
393 For sample preparation, flies were anesthetized on ice and briefly washed with 70% ethanol. Small
394 incisions were made in the flanks of the thorax and abdomen under 2% paraformaldehyde in PBS with
395 0.1% Triton X-100 (PBS-T), and the flies were fixed in this solution overnight at 4°C. After washing in
396 PBS containing 1% Triton X-100, the samples were embedded in 7% agarose and sectioned on Leica
397 Vibratome (VT1000s) sagittally in slices of 0.3 mm. The slices were incubated in PBS with 1% Triton X-
398 100, 0.5% DMSO, 3% normal goat serum, Texas Red-X Phalloidin (1:50, Life Technologies #T7471) and

399 anti-GFP rabbit polyclonal antibodies (1:1000, Thermo Fisher, #A10262) at room temperature with
400 agitation for 24 hours. After a series of three washes in PBS-T, the sections were incubated for another
401 24 hours in the solution containing secondary antibodies (1:1000, goat anti-rabbit, Thermo Fisher
402 #A32731). The samples were then washed in PBS-T and mounted in Tris-HCL (pH 8.0)-buffered 80%
403 glycerol + 0.5% DMSO. For imaging and rendering, serial optical sections were obtained at 2 µm
404 intervals on a Zeiss 880 confocal microscope with a pan-apochromat 10x/0.45 NA objective using 488
405 and 594 nm lasers. Images were processed in Fiji (http://fiji.sc/) and Photoshop (Adobe Systems Inc.).
406

407 **Behavioral assays**

408 For flies expressing CsChrimson (Klapoetke et al., 2014), the food was supplemented with retinal (0.2
409 mM all-trans-retinal prior to eclosion and then 0.4 mM). Two- to six-day old adult females were
410 collected and sorted on a Peltier cold plate 2-4 days before testing in behavioral assays. Flies were
411 starved for 40–48 hr on 1% agar before they were subjected to behavioral experiments. Olfactory
412 conditioning and optogenetic activation experiments were performed as previously described using
413 the modified four-field olfactory arena equipped with the 627 nm LED board and odor mixers (Aso
414 and Rubin, 2016; Pettersson, 1970). The odors were diluted in paraffin oil: pentyl acetate (PA,
415 1:10000, v/v) and ethyl lactate (EL, 1:10000, v/v). Videos were taken at 30 frames per second and
416 analyzed using Fiji and Caltech FlyTracker (Eyjolfsdottir et al., 2014).
417

418 **LM-EM matching**

419 The confocal microscopy images of different split-GAL4 lines were registered to a common template
420 JRC2018_unisex (Bogovic et al., 2020) and organized in Janelia Workstation software
421 (https://github.com/JaneliaSciComp/workstation). Color depth MIP mask search (Otsuna et al., 2018)
422 was used to search through the EM neuron library (hemibrain 1.2.1) for matching candidates. The
423 searching target was obtained by either creating a mask on the full confocal image or using neurons
424 of interest manually segmented in VVD viewer (https://github.com/takashi310/VVD_Viewer)(Wan et
425 al., 2012). SWC files of top-matching EM neuron candidates were loaded into VVD viewer together
426 with the confocal microscopy images in the same standard brain coordinates. By rotating the 3d
427 images and manually scrutinizing the branching patterns, we picked the best matching candidate.
428 Typically, we had high confidence of LM-to-EM matching for the line that labels only one cell per
429 hemishere. For instance, we could unambiguously match the cell in SS67721 with SMP108 in the EM
430 hemibrain volume. Our confidence of LM-to-EM matching tended to be lower for the lines that label
431 multiple cells, because neurons of similar morphologies could be labeled together in those lines.
432

433 **Connectivity analysis**

434 Connectivity information was retrieved from neuPrint (neuprint.janelia.org), a publicly accessible
435 website hosting the "hemibrain" dataset (Scheffer et al., 2020). For cell types, we used cell type name
436 assignments reported in Sheffer et al., 2020. Only connections of the cells in the right hemisphere
437 were used due to incomplete connectivity in the left hemisphere. The 3D renderings of neurons
438 presented were generated using the visualization tools of NeuTu (Zhao et al., 2018) or VVD viewer .
439

440 **Statistics**

441 Statistical comparisons were performed on GraphPad Prism 7.0 using one-way ANOVA followed by
442 Dunnett's test for multiple comparisons. Sample size was not predetermined based on pilot
443 experiments.

444

445 **Data Availability**

446 The confocal images of expression patterns are available online (http://www.janelia.org/split-gal4).
447 The values used for figures are summarized in Source Data.

448

449 **Detailed fly genotypes used by figures**

450

| | |
|---|---|
| Figure 1F | *w/w, 20xUAS-CsChrimson-mVenus attP18; +/split-GAL4*<br>*w/w, 20xUAS-CsChrimson-mVenus attP18; +/P{Gr64f-GAL4.9.7}5; +/P{Gr64f-GAL4.9.7}1* |
| Figure 2A | *w/w, 20xUAS-CsChrimson-mVenus attP18;+/SS45245-split-GAL4* |
| Figure 2B | w/w, pBPhsFlp2::PEST in attP3;;<br>pJFRC201-10XUAS-FRT>STOP>FRT-myr::smGFP-HA in VK00005,<br>pJFRC240-10XUAS-FRT>STOP>FRT-myr::smGFP-V5-THS-10XUAS-FRT>STOP>FRT-myr::smGFP-FLAG in su(Hw)attP1/SS45245-*split-GAL4* |
| Figure 2C | w/w;pJFRC225-5XUAS-IVS-myr::smFLAG in VK00005,<br>pJFRC51-3XUAS-IVS-Syt::smHA in su(Hw)attP1/SS45245-*split-GAL4* |
| Figure 7E-J | *w/w, 20xUAS-CsChrimson-mVenus attP18;+/SS87269-split-GAL4*<br>*w/w, 20xUAS-CsChrimson-mVenus attP18;+/SS87272-split-GAL4*<br>*w/w, 20xUAS-CsChrimson-mVenus attP18;+/SS88801-split-GAL4*<br>*w/w, 20xUAS-CsChrimson-mVenus attP18;+/SS87278-split-GAL4* |
| Figure 7K-Q | *w/w, 20xUAS-CsChrimson-mVenus attP18;+/Gr64f-split-GAL4s*<br>*w/w, 20xUAS-CsChrimson-mVenus attP18;+/Gr66a-GAL4* |
| Figure 7 - figure supplement 1 | *w/w; +/ P{Gr64f-GAL4.9.7}5; 5xUAS-myr-smFLAG in VK00005/P{Gr64f-GAL4.9.7}1* |
| Figure 8E-F, Figure 8 - figure supplement 2 | *w/w, 20xUAS-CsChrimson-mVenus attP18; +/Gr64f-split-GAL4s*<br>*w/w, 20xUAS-CsChrimson-mVenus attP18; +/ P{Gr64f-GAL4.9.7}5; +/P{Gr64f-GAL4.9.7}1*<br>*w/w, 20xUAS-CsChrimson-mVenus attP18; +/empty-split-GAL4* |
| Figure 8 - figure supplement 1A | *w/w, 20xUAS-CsChrimson-mVenus attP18; +/SS87269-split-GAL4* |
| Figure 8 - figure supplement 1C | *w/w, 20xUAS-CsChrimson-mVenus attP18; +/SS87269-split-GAL4*<br>*w/w, 20xUAS-CsChrimson-mVenus attP18; +/SS87278-split-GAL4*<br>*w/w, 20xUAS-CsChrimson-mVenus attP18; +/empty-split-GAL4* |
| Figure 8I | *w/w, 20xUAS-CsChrimson-mVenus attP18;+/SS87269-split-GAL4*<br>*w/w, 20xUAS-CsChrimson-mVenus attP18;+/SS88801-split-GAL4*<br>*w/w, 20xUAS-CsChrimson-mVenus attP18;+/empty-GAL4* |
| Figure 9B-D | *w/w, 20xUAS-CsChrimson-mVenus attP18;+/SS01159-split-GAL4*<br>*w/w, 20xUAS-CsChrimson-mVenus attP18;+/empty-GAL4* |
| Figure 10A | w/w;pJFRC225-5XUAS-IVS-myr::smFLAG in VK00005,<br>pJFRC51-3XUAS-IVS-Syt::smHA in su(Hw)attP1/*SS01336-split-GAL4* |
| Figure 10B | w/w;pJFRC225-5XUAS-IVS-myr::smFLAG in VK00005,<br>pJFRC51-3XUAS-IVS-Syt::smHA in su(Hw)attP1/ *SS01241-split-GAL4* |

| | |
|---|---|
| Figure 10C | w/w, pBPhsFlp2::PEST in attP3;;<br>pJFRC201-10XUAS-FRT>STOP>FRT-myr::smGFP-HA in VK00005,<br>pJFRC240-10XUAS-FRT>STOP>FRT-myr::smGFP-V5-THS-10XUAS-FRT>STOP>FRT-myr::smGFP-FLAG in su(Hw)attP1/*MB310C-split-GAL4* |
| Figure 10D | w/w, pBPhsFlp2::PEST in attP3;;<br>pJFRC201-10XUAS-FRT>STOP>FRT-myr::smGFP-HA in VK00005,<br>pJFRC240-10XUAS-FRT>STOP>FRT-myr::smGFP-V5-THS-10XUAS-FRT>STOP>FRT-myr::smGFP-FLAG in su(Hw)attP1/*MB082C-split-GAL4* |
| Figure 11A-B, Figure 11 - figure supplement 1 | w/w;;pJFRC225-5XUAS-IVS-myr::smFLAG in VK00005,<br>pJFRC51-3XUAS-IVS-Syt::smHA in su(Hw)attP1/ *MB083C-split-GAL4*<br><br>*w/w;UAS-mCD8::GFP/MB083C-split-GAL4*<br><br>*w/w, 20xUAS-CsChrimson-mVenus in attP18;;+/ MB083C-split-GAL4*<br><br>*w/w, pJFRC12-10XUAS-IVS-myr::GFP in attP18/ MB083C-split-GAL4* |
| Figure 11 - figure supplement 2 | *w, 10xUAS-IVS-myr::smGdP-HA in attP18, 13xLexAop2-IVS-myr::smGdP-V5 in su(Hw)attP8; +/R52G04-LexA (MBON08/09);+/MB312C-split-GAL4 (PAM-γ4)*<br><br>*w, 10xUAS-IVS-myr::smGdP-HA in attP18, 13xLexAop2-IVS-myr::smGdP-V5 in su(Hw)attP8; +/R52G04-LexA (MBON08/09);+/MB441B-split-GAL4 (PAM-γ3)*<br><br>*w/w;;VT006202-LexAp65 in attP2/pJFRC19-13XLexAop2-IVS-myr::GFP in attP2* |
| Figure 12 | *w/w, 20xUAS-CsChrimson-mVenus attP18; +/split-GAL4s*<br>*w/w, 13xLexAop2-CsChrimson-mVenus attp18; +/split-LexAs* |

## Supplemental information

**Supplementary File 1 A list of released driver lines and their corresponding EM neurons.**

Listed are stable split-GAL4 lines (SS, MB) and split-LexA lines (SL). Drivers are grouped by the anatomical regions where they have their primary expression. Recently released MBON lines (Rubin and Aso, 2023) are also included. Matching to EM cell types in the hemibrain v1.2.1 dataset was performed by an algorithmic search of the morphologies of EM skeletons, followed by manual evaluation of proposed matches using 3D visualization software. The best-matching candidates are listed. Where multiple candidates seem valid, the alternatives are listed in the note column. In some cases, a matching EM BodyId can be found in the hemibrain v1.2.1 dataset but an EM cell type has not been defined; these are listed as TBD. Number of cells observed in light microscopy (LM) or electron microscopy (EM) are from one hemisphere, unless otherwise stated. A descriptive cell type column is included, which uses conventional names (if available) to facilitate searching and includes cell types with weak/stochastic expression (bracketed) or putative cell types with less matching confidence. When there are multiple drivers for the same cell type(s), one is chosen as the primary driver based on specificity, consistency, and expression strength. Abbreviations: AL, antennal lobe; ORNs, olfactory receptor neurons; AL LNs, antennal lobe local interneurons; PNs, projection neurons; MB, mushroom body; KCs, Kenyon cells; MBONs, mushroom body output neurons; DANs, dopaminergic neurons; LH, lateral horn; LHONs, lateral horn output neurons; LHLNs, lateral horn local neurons; SNP, superior neuropils; CRE, crepine; CX, central complex; LAL, lateral accessory lobe; ANs, ascending neurons; DNs, descending neurons; OANs, octopaminergic neurons; 5-HT, serotonergic neurons; OL, optic lobe; VLNP, ventrolateral neuropils; INP, inferior neuropils (other than crepine); VMNP, ventromedial neuropils; PENP, periesophageal neuropils; GNG, gnathal ganglia; VNC, ventral nerve cord; N.D., not determined.

476
477 **Supplementary File 2 New transgenic flies generated in this study.**
478 The enhancer fragments, insertion sites, and inserted chromosomes used to construct the lines are
479 listed. For some of the transgenes, an additional version with a *p10* 3'-UTR (Pfeiffer et al., 2012) was
480 generated to increase the expression.
481
482 **Supplementary File 3 Coverage of MBON-downstream and DAN-upstream**
483 Connection matrix between MB interneurons and DANs and MBONs. A threshold was set to exclude
484 connections with a low number of neuron-neuron connections, specifically, 10 connections for MBON
485 to a downstream neuron and 5 connections for upstream neurons to a DAN (Li et al., 2020). Recurrent
486 neurons are defined as cell types receiving input from MBONs and supplying output to DANs.
487 Neurotransmitter (NT) prediction data were from (Eckstein et al., 2023), and the fraction of synapses
488 predicted for the neurotransmitter was pooled from all cells of the cell type.
489
490 **Supplementary File 4 Updated list of driver lines for cell types within the MB excluding**
491 **Kenyon cells.**
492 This includes new or improved split-GAL4 and split-LexA lines from the present study, lines from the
493 Aso 2014 collection (Aso et al., 2014a), a recent MBON collection (Rubin and Aso, 2023), MB630B (Aso
494 and Rubin, 2016), SS01308 (Aso et al., 2019), MB063B (Dolan et al., 2019), SS46348 (Otto et al., 2020),
495 and some regular Gal4 lines VT43924-Gal4.2 (Amin et al., 2020) and G0239 (Chiang et al., 2011). Lines
496 listed in boldface are generally of higher quality.
497
498 **Supplementary File 5 Coverage of PN cell types**
499 A list of split-GAL4 lines and their coverage of PNs of the antennal lobe. Shading indicates expression
500 level. Many of the multi-glomerular PN (mPN) cell types cannot be easily differentiated based on light
501 microscopy images, so they are listed as a broad mPN category in the table.
502
503 **Video 1 Olfactory arena learning experiment with SS87269**
504 An exemplar video of learning of flies of the genotype SS87269/UAS-CsChrimson-mVenus attP18.
505 Movies were tracked with Caltech FlyTracker (Eyjolfsdottir et al., 2014). Trailing trajectories of
506 individual flies in the last 5 s were overlaid. Delivery of odor A and B to the quadrants along with the
507 625 nm LED activation are indicated. Experiment movie and data from the first 1x 1 m training and
508 test are presented with the gray line indicating session transition.
509
510 **Video 2 Activation phenotypes with SS87269**
511 An exemplar video of activation of flies of the genotype SS87269/UAS-CsChrimson-mVenus attP18.
512 Flies receive six consecutive 60s trials; during each trial a 10s LED activation was presented (from 10-
513 20s) as indicated. The trajectories of individual flies over the previous 5 s are shown.
514
515 **Video 3 Return phenotype of SS87269 at LED offset**
516 Behaviors of individual flies with their trajectories from LED offset up to 15 s after LED offset. Videos are
517 centered to the positions of flies at LED offset. The two white circles indicate 3 mm and 10 mm
518 boundaries from the position. Flies were sorted by the time they re-entered the 3-mm inner circle after
519 they exited the 10-mm outer circle. Flies at the bottom row did not return within the 15-s time frame.

520

521 **Video 4 Proboscis extension upon SS87269 activation for flies walking on a ball**

522 Flies were thorax-fixed by tethering to a pin and allowed to walk on an air-floated foam ball. Proboscis
523 activities were tracked with the Animal Part Tracker (https://github.com/kristinbranson/APT) (Kabra
524 et al., 2022).

525

526 **Video 5 Activation preference of SS01159 in the LED choice experiment.**

527 An exemplar video of LED choices of flies of the genotype SS01159/UAS-CsChrimson-mVenus attP18.
528 The trajectories of individual flies over the previous 5 s are shown. 625 nm LED was on from 30 s to
529 60 s and from 90 s to 120 s, and the lit quadrants are indicated.

530

531 **Appendix 1—key resources table**

| Reagent type (species) or resource | Designation | Source or reference | Identifiers | Additional information |
|---|---|---|---|---|
| strain, strain background (*Drosophila melanogaster*) | New split-GAL4 and split-LexA lines | This paper | https://splitgal4.janelia.org/cgi-bin/splitgal4.cgi | Available from Aso lab |
| strain, strain background (*Drosophila melanogaster*) | 20xUAS-CsChrimson-mVenus attP18 | (Klapoetke et al., 2014); PMID: 24509633 | N.A. | |
| strain, strain background (*Drosophila melanogaster*) | pJFRC200-10xUAS-IVS-myr::smGFP-HA in attP18 | (Nern et al., 2015); PMID: 25964354 | N.A. | |
| strain, strain background (*Drosophila melanogaster*) | pJFRC225-5xUAS-IVS-myr::smGFP-FLAG in VK00005 | (Nern et al., 2015); PMID: 25964354 | N.A. | |
| strain, strain background (*Drosophila melanogaster*) | pBPhsFlp2::PEST in attP3 | (Nern et al., 2015); PMID: 25964354 | N.A. | |
| strain, strain background (*Drosophila melanogaster*) | pJFRC201-10XUAS-FRT>STOP > FRT-myr::smGFP-HA in VK0005 | (Nern et al., 2015); PMID: 25964354 | N.A. | |
| strain, strain background (*Drosophila melanogaster*) | pJFRC240-10XUAS-FRT>STOP > FRT-myr::smGFP-V5-THS-10XUAS-FRT>STOP > FRT-myr::smGFP-FLAG_in_su(Hw)attP1 | (Nern et al., 2015); PMID: 25964354 | N.A. | |

| | | | | |
|---|---|---|---|---|
| strain, strain background (*Drosophila melanogaster*) | empty-split-GAL4 (p65ADZp attP40, ZpGAL4DBD attP2) | (Hampel et al., 2015); PMID: 26344548 | RRID:BDSC_79603 | |
| strain, strain background (*Drosophila melanogaster*) | empty-Gal4 (pBDPGal4U attP2) | (Pfeiffer et al., 2008); PMID: 18621688 | RRID:BDSC_68384 | |
| strain, strain background (*Drosophila melanogaster*) | MB083C split-GAL4 | (Aso et al., 2014a) ; PMID: 25535793 | RRID:BDSC_68287 | Available from Aso lab |
| strain, strain background (*Drosophila melanogaster*) | w*; P{Gr64f-GAL4.9.7}5/CyO; P{Gr64f-GAL4.9.7}1/TM3, $Sb^1$ | (Haberkern et al., 2019); PMID: 31056392 | RRID: BDSC_57668, BDSC_57669 | |
| strain, strain background (*Drosophila melanogaster*) | Gr66a-Gal4 | (Joseph and Heberlein, 2012); PMID: 22798487 | N.A. | |
| antibody | anti-GFP (rabbit polyclonal) | Invitrogen | A11122 RRID:AB_221569 | 1:1000 |
| antibody | anti-Brp (mouse monoclonal) | Developmental Studies Hybridoma Bank | nc82 RRID:AB_2341866 | 1:30 |
| antibody | anti-HA-Tag (mouse monoclonal) | Cell Signaling Technology | C29F4; #3724 RRID:AB_10693385 | 1:300 |
| antibody | anti-FLAG (rat monoclonal) | Novus Biologicals | NBP1-06712 RRID:AB_1625981 | 1:200 |
| antibody | anti-V5-TAG Dylight-549 (mouse monoclonal) | Bio-Rad | MCA2894D549GA RRID:AB_10845946 | 1:500 |
| antibody | anti-mouse IgG(H&L) AlexaFluor-568 (goat polyclonal) | Invitrogen | A11031 RRID:AB_144696 | 1:400 |
| antibody | anti-rabbit IgG(H&L) AlexaFluor-488 (goat polyclonal) | Invitrogen | A11034 RRID:AB_2576217 | 1:800 |

| | | | | |
|---|---|---|---|---|
| antibody | anti-mouse IgG(H&L) AlexaFluor-488 conjugated (donkey polyclonal) | Jackson Immuno Research Labs | 715-545-151 RRID:AB_2341099 | 1:400 |
| antibody | anti-rabbit IgG(H&L) AlexaFluor-594 (donkey polyclonal) | Jackson Immuno Research Labs | 711-585-152 RRID:AB_2340621 | 1:500 |
| antibody | anti-rat IgG(H&L) AlexaFluor-647 (donkey polyclonal) | Jackson Immuno Research Labs | 712-605-153 RRID:AB_2340694 | 1:300 |
| antibody | anti-mouse IgG(H&L) ATTO 647 N (goat polyclonal) | ROCKLAND | 610-156-121 RRID:AB_10894200 | 1:100 |
| antibody | anti-rabbit IgG(H+L) Alexa Fluor 568 (goat polyclonal) | Invitrogen | A-11036 RRID:AB_10563566 | 1:1000 |
| chemical compound, drug | Pentyl acetate | Sigma-Aldrich | 109584 | 1:10000 in paraffin oil |
| chemical compound, drug | Ethyl lactate | Sigma-Aldrich | W244015 | 1:10000 in paraffin oil |
| chemical compound, drug | Paraffin oil | Sigma-Aldrich | 18512 | |
| software, algorithm | ImageJ and Fiji | NIH; (Schindelin et al., 2012) | https://imagej.nih.gov/ij/ http://fiji.sc/ | |
| software, algorithm | MATLAB | MathWorks | https://www.mathworks.com/ | |
| software, algorithm | Adobe Illustrator CC | Adobe Systems | https://www.adobe.com/products/illustrator.html | |
| software, algorithm | GraphPad Prism 9 | GraphPad Software | https://www.graphpad.com/scientific-software/prism/ | |
| software, algorithm | Python | Python Software Foundation | https://www.python.org/ | |

| | | | | |
|---|---|---|---|---|
| software, algorithm | Caltech FlyTracker(Eyjolfsdottir et al., 2014) | (Eyjolfsdottir et al., 2014) | https://github.com/kristinbranson/FlyTracker | |
| software, algorithm | Animal Part Tracker | (Kabra et al., 2022) | (https://github.com/kristinbranson/APT) | |
| software, algorithm | neuPrint | (Plaza et al., 2022) | https://neuprint.janelia.org/ | |
| software, algorithm | Cytoscape | (Shannon et al., 2003) | https://cytoscape.org/ | |
| software, algorithm | Janelia workstation | HHMI Janelia | https://doi.org/10.25378/janelia.8182256.v1 | |
| software, algorithm | NeuTu | (Zhao et al., 2018) | https://github.com/janelia-flyem/NeuTu | |
| software, algorithm | VVD Viewer | (Wan et al., 2012) | https://github.com/takashi310/VVD_Viewer | |
| other | Grade 3 MM Chr Blotting Paper | Whatman | 3030–335 | Used in glass vials with paraffin-oil diluted odors |
| other | mass flow controller | Alicat | MCW-200SCCM-D | Mass flow controller used for the olfactory arena |

## Acknowledgments

We thank Toshihide Hige, Daisuke Hattori, members of the Y.A., G.M.R. and G.T. laboratories for valuable comments on the manuscript. We thank all the members of Janelia Flylight (https://www.janelia.org/project-team/flylight) and Project Technical Resources (https://www.janelia.org/support-team/project-technical-resources) for technical assistance for constructing split-GAL4 drivers and generating confocal microscopy images. During this effort, the FlyLight Project Team and Project Technical Resources included Gudrun Ihrke, Megan Atkins, Shelby Bowers, Kari Close, Gina DePasquale, Zack Dorman, Kaitlyn Forster, Jaye Anne Gallagher, Theresa Gibney, Asish Gulati, Joanna Hausenfluck, Yisheng He, Kristin Hendersen, Hsing Hsi Li, Nirmala Iyer, Jennifer Jeter, Lauren Johnson, Rebecca Johnston, Rachel Lazarus, Kelley Lee, Hua-Peng Liaw, Oz Malkesman, Geoffrey Meissner, Brian Melton, Scott Miller, Reeham Motaher, Alexandra Novak, Omatara Ogundeyi, Alyson Petruncio, Jacquelyn Price, Sophia Protopapas, Susana Tae, Athreya Tata, Jennifer Taylor, Allison Vannan, Rebecca Vorimo, Brianna Yarborough, Kevin Xiankun Zeng, and Chris Zugates, with Steering Committee of Y.A., G.M.R, Gwyneth Card, Barry Dickson, Reed George, Wyatt

Korff, and James Truman. We also thank Kelly Ashley, Pria Chang, Tam Dang, Dona Fetter, Guillermo Gonzalez, Donald Hall, Jui-Chun Kao, James McMahon, Monti Mercer, Brenda Perez, Scarlett Pitts, Danielle Ruiz, Brandi Sharp, Viruthika Vallanadu, Grace Zheng, Amanda Cavallaro, Todd Laverty of Janelia Fly facility (https://www.janelia.org/support-team/fly-facility) for husbandry of stocks, and Eric Trautman, Rob Svirskas, Hideo Otsuna, Takashi Kawase and other members of Janelia Scientific Computing (https://www.janelia.org/support-team/scientific-computing-software) for supporting organization and analysis of confocal and EM microscopy images.

## Author contributions

Conceptualization, G.M.R., G.T., L.T. and Y.A.; Formal Analysis and Investigation, Y.S., M.S., G.B.., K.H., C.Y., C.M.., I.S., and Y.A.; Writing, Y.S., G.M.R., G.T., G.S., and Y.A.; Supervision, G.M.R., G.T., T.L., and Y.A..; Funding Acquisition, G.M.R., G.T., T.L. and Y.A.

## Competing interests

The authors declare no competing interests.

## References

Amin H, Apostolopoulou AA, Suárez-Grimalt R, Vrontou E, Lin AC. 2020. Localized inhibition in the Drosophila mushroom body. *Elife* **9**. doi:10.7554/eLife.56954

Aso Y, Hattori D, Yu Y, Johnston RM, Iyer NA, Ngo T-TB, Dionne H, Abbott LF, Axel R, Tanimoto H, Rubin GM. 2014a. The neuronal architecture of the mushroom body provides a logic for associative learning. *Elife* **3**:e04577.

Aso Y, Ray RP, Long X, Bushey D, Cichewicz K, Ngo T-T, Sharp B, Christoforou C, Hu A, Lemire AL, Tillberg P, Hirsh J, Litwin-Kumar A, Rubin GM. 2019. Nitric oxide acts as a cotransmitter in a subset of dopaminergic neurons to diversify memory dynamics. *Elife* **8**. doi:10.7554/eLife.49257

Aso Y, Rubin GM. 2016. Dopaminergic neurons write and update memories with cell-type-specific rules. *Elife* **5**. doi:10.7554/eLife.16135

Aso Y, Sitaraman D, Ichinose T, Kaun KR, Vogt K, Belliart-Guérin G, Plaçais P-Y, Robie AA, Yamagata N, Schnaitmann C, Rowell WJ, Johnston RM, Ngo T-TB, Chen N, Korff W, Nitabach MN, Heberlein U, Preat T, Branson KM, Tanimoto H, Rubin GM. 2014b. Mushroom body output neurons encode valence and guide memory-based action selection in Drosophila. *Elife* **3**:e04580.

Aso Y, Siwanowicz I, Bräcker L, Ito K, Kitamoto T, Tanimoto H. 2010. Specific dopaminergic neurons for the formation of labile aversive memory. *Curr Biol* **20**:1445–1451.

Aso Y, Yamada D, Bushey D, Hibbard KL, Sammons M, Otsuna H, Shuai Y, Hige T. 2023. Neural circuit mechanisms for transforming learned olfactory valences into wind-oriented movement. *Elife* **12**. doi:10.7554/eLife.85756

Awata H, Takakura M, Kimura Y, Iwata I, Masuda T, Hirano Y. 2019. The neural circuit linking mushroom body parallel circuits induces memory consolidation in. *Proc Natl Acad Sci U S A* **116**:16080–16085.

Bates AS, Schlegel P, Roberts RJV, Drummond N, Tamimi IFM, Turnbull R, Zhao X, Marin EC, Popovici PD, Dhawan S, Jamasb A, Javier A, Serratosa Capdevila L, Li F, Rubin GM, Waddell S, Bock DD, Costa M, Jefferis GSXE. 2020. Complete Connectomic Reconstruction of Olfactory Projection Neurons in the Fly Brain. *Curr Biol* **30**:3183–3199.e6.

Berry JA, Phan A, Davis RL. 2018. Dopamine Neurons Mediate Learning and Forgetting through Bidirectional Modulation of a Memory Trace. *Cell Rep* **25**:651–662.e5.

590 Bogovic JA, Otsuna H, Heinrich L, Ito M, Jeter J, Meissner G, Nern A, Colonell J, Malkesman O, Ito K,
591 Saalfeld S. 2020. An unbiased template of the Drosophila brain and ventral nerve cord. *PLoS*
592 *One* **15**:e0236495.
593 Bohra AA, Kallman BR, Reichert H, VijayRaghavan K. 2018. Identification of a Single Pair of
594 Interneurons for Bitter Taste Processing in the Drosophila Brain. *Curr Biol* **28**:847–858.e3.
595 Burke CJ, Huetteroth W, Owald D, Perisse E, Krashes MJ, Das G, Gohl D, Silies M, Certel S, Waddell S.
596 2012. Layered reward signalling through octopamine and dopamine in Drosophila. *Nature*
597 **492**:433–437.
598 Chen H-L, Motevalli D, Stern U, Yang C-H. 2022. A functional division of sweet taste neurons that is
599 value-based and task-specific. *Proc Natl Acad Sci U S A* **119**. doi:10.1073/pnas.2110158119
600 Chiang A-S, Lin C-Y, Chuang C-C, Chang H-M, Hsieh C-H, Yeh C-W, Shih C-T, Wu J-J, Wang G-T, Chen Y-
601 C, Wu C-C, Chen G-Y, Ching Y-T, Lee P-C, Lin C-Y, Lin H-H, Wu C-C, Hsu H-W, Huang Y-A, Chen J-Y,
602 Chiang H-J, Lu C-F, Ni R-F, Yeh C-Y, Hwang J-K. 2011. Three-dimensional reconstruction of brain-
603 wide wiring networks in Drosophila at single-cell resolution. *Curr Biol* **21**:1–11.
604 Claridge-Chang A, Roorda RD, Vrontou E, Sjulson L, Li H, Hirsh J, Miesenböck G. 2009. Writing
605 memories with light-addressable reinforcement circuitry. *Cell* **139**:405–415.
606 Corfas RA, Sharma T, Dickinson MH. 2019. Diverse Food-Sensing Neurons Trigger Idiothetic Local
607 Search in Drosophila. *Curr Biol* **29**:1660–1668.e4.
608 Costa M, Manton JD, Ostrovsky AD, Prohaska S, Jefferis GSXE. 2016. NBLAST: Rapid, Sensitive
609 Comparison of Neuronal Structure and Construction of Neuron Family Databases. *Neuron*
610 **91**:293–311.
611 Dahanukar A, Lei Y-T, Kwon JY, Carlson JR. 2007. Two Gr genes underlie sugar reception in
612 Drosophila. *Neuron* **56**:503–516.
613 Datta SR, Vasconcelos ML, Ruta V, Luo S, Wong A, Demir E, Flores J, Balonze K, Dickson BJ, Axel R.
614 2008. The Drosophila pheromone cVA activates a sexually dimorphic neural circuit. *Nature*
615 **452**:473–477.
616 Davis FP, Nern A, Picard S, Reiser MB, Rubin GM, Eddy SR, Henry GL. 2020. A genetic, genomic, and
617 computational resource for exploring neural circuit function. *Elife* **9**. doi:10.7554/eLife.50901
618 Davis RL. 2023. Learning and memory using Drosophila melanogaster: a focus on advances made in
619 the fifth decade of research. *Genetics*. doi:10.1093/genetics/iyad085
620 de Bivort B, Buchanan S, Skutt-Kakaria K, Gajda E, Ayroles J, O'Leary C, Reimers P, Akhund-Zade J,
621 Senft R, Maloney R, Ho S, Werkhoven Z, Smith MA-Y. 2022. Precise Quantification of Behavioral
622 Individuality From 80 Million Decisions Across 183,000 Flies. *Front Behav Neurosci* **16**:836626.
623 Deere JU, Sarkissian AA, Yang M, Uttley HA, Martinez Santana N, Nguyen L, Ravi K, Devineni AV.
624 2023. Selective integration of diverse taste inputs within a single taste modality. *Elife* **12**.
625 doi:10.7554/eLife.84856
626 Dionne H, Hibbard KL, Cavallaro A, Kao J-C, Rubin GM. 2018. Genetic Reagents for Making Split-GAL4
627 Lines in. *Genetics* **209**:31–35.
628 Dolan M-J, Belliart-Guérin G, Bates AS, Frechter S, Lampin-Saint-Amaux A, Aso Y, Roberts RJV,
629 Schlegel P, Wong A, Hammad A, Bock D, Rubin GM, Preat T, Plaçais P-Y, Jefferis GSXE. 2018.
630 Communication from Learned to Innate Olfactory Processing Centers Is Required for Memory
631 Retrieval in Drosophila. *Neuron* **100**:651–668.e8.
632 Dolan M-J, Frechter S, Bates AS, Dan C, Huoviala P, Roberts RJ, Schlegel P, Dhawan S, Tabano R,
633 Dionne H, Christoforou C, Close K, Sutcliffe B, Giuliani B, Li F, Costa M, Ihrke G, Meissner GW,
634 Bock DD, Aso Y, Rubin GM, Jefferis GS. 2019. Neurogenetic dissection of the Drosophila lateral
635 horn reveals major outputs, diverse behavioural functions, and interactions with the mushroom
636 body. *Elife* **8**. doi:10.7554/eLife.43079
637 Dorkenwald S, Matsliah A, Sterling AR, Schlegel P, Yu S-C, McKellar CE, Lin A, Costa M, Eichler K, Yin
638 Y, Silversmith W, Schneider-Mizell C, Jordan CS, Brittain D, Halageri A, Kuehner K, Ogedengbe O,
639 Morey R, Gager J, Kruk K, Perlman E, Yang R, Deutsch D, Bland D, Sorek M, Lu R, Macrina T, Lee
640 K, Bae JA, Mu S, Nehoran B, Mitchell E, Popovych S, Wu J, Jia Z, Castro M, Kemnitz N, Ih D, Bates

641 AS, Eckstein N, Funke J, Collman F, Bock DD, Jefferis GSXE, Seung HS, Murthy M, FlyWire
642 Consortium. 2023. Neuronal wiring diagram of an adult brain. *bioRxiv*.
643 doi:10.1101/2023.06.27.546656
644 Dunipace L, Meister S, McNealy C, Amrein H. 2001. Spatially restricted expression of candidate taste
645 receptors in the Drosophila gustatory system. *Curr Biol* **11**:822–835.
646 Eckstein N, Bates AS, Champion A, Du M, Yin Y, Schlegel P, Lu AK-Y, Rymer T, Finley-May S, Paterson
647 T, Parekh R, Dorkenwald S, Matsliah A, Yu S-C, McKellar C, Sterling A, Eichler K, Costa M, Seung
648 S, Murthy M, Hartenstein V, Jefferis GSX, Funke J. 2023. Neurotransmitter Classification from
649 Electron Microscopy Images at Synaptic Sites in Drosophila Melanogaster. *bioRxiv*.
650 doi:10.1101/2020.06.12.148775
651 Eichler K, Li F, Litwin-Kumar A, Park Y, Andrade I, Schneider-Mizell CM, Saumweber T, Huser A,
652 Eschbach C, Gerber B, Fetter RD, Truman JW, Priebe CE, Abbott LF, Thum AS, Zlatic M, Cardona
653 A. 2017. The complete connectome of a learning and memory centre in an insect brain. *Nature*
654 **548**:175–182.
655 Enjin A, Zaharieva EE, Frank DD, Mansourian S, Suh GSB, Gallio M, Stensmyr MC. 2016. Humidity
656 Sensing in Drosophila. *Curr Biol* **26**:1352–1358.
657 Eschbach C, Fushiki A, Winding M, Schneider-Mizell CM, Shao M, Arruda R, Eichler K, Valdes-Aleman
658 J, Ohyama T, Thum AS, Gerber B, Fetter RD, Truman JW, Litwin-Kumar A, Cardona A, Zlatic M.
659 2020. Recurrent architecture for adaptive regulation of learning in the insect brain. *Nat*
660 *Neurosci* **23**:544–555.
661 Eyjolfsdottir E, Branson S, Burgos-Artizzu XP, Hoopfer ED, Schor J, Anderson DJ, Perona P. 2014.
662 Detecting Social Actions of Fruit FliesComputer Vision – ECCV 2014. Springer International
663 Publishing. pp. 772–787.
664 Felsenberg J, Barnstedt O, Cognigni P, Lin S, Waddell S. 2017. Re-evaluation of learned information in
665 Drosophila. *Nature* **544**:240–244.
666 Frank DD, Jouandet GC, Kearney PJ, Macpherson LJ, Gallio M. 2015. Temperature representation in
667 the Drosophila brain. *Nature* **519**:358–361.
668 Fujii S, Yavuz A, Slone J, Jagge C, Song X, Amrein H. 2015. Drosophila sugar receptors in sweet taste
669 perception, olfaction, and internal nutrient sensing. *Curr Biol* **25**:621–627.
670 Gallio M, Ofstad TA, Macpherson LJ, Wang JW, Zuker CS. 2011. The coding of temperature in the
671 Drosophila brain. *Cell* **144**:614–624.
672 Gao R, Asano SM, Upadhyayula S, Pisarev I, Milkie DE, Liu T-L, Singh V, Graves A, Huynh GH, Zhao Y,
673 Bogovic J, Colonell J, Ott CM, Zugates C, Tappan S, Rodriguez A, Mosaliganti KR, Sheu S-H,
674 Pasolli HA, Pang S, Xu CS, Megason SG, Hess H, Lippincott-Schwartz J, Hantman A, Rubin GM,
675 Kirchhausen T, Saalfeld S, Aso Y, Boyden ES, Betzig E. 2019. Cortical column and whole-brain
676 imaging with molecular contrast and nanoscale resolution. *Science* **363**.
677 doi:10.1126/science.aau8302
678 Haberkern H, Basnak MA, Ahanonu B, Schauder D, Cohen JD, Bolstad M, Bruns C, Jayaraman V. 2019.
679 Visually Guided Behavior and Optogenetically Induced Learning in Head-Fixed Flies Exploring a
680 Virtual Landscape. *Curr Biol* **29**:1647–1659.e8.
681 Hammer M. 1993. An identified neuron mediates the unconditioned stimulus in associative olfactory
682 learning in honeybees. *Nature* **366**:59–63.
683 Hampel S, Franconville R, Simpson JH, Seeds AM. 2015. A neural command circuit for grooming
684 movement control. *Elife* **4**:e08758.
685 Handler A, Graham TGW, Cohn R, Morantte I, Siliciano AF, Zeng J, Li Y, Ruta V. 2019. Distinct
686 Dopamine Receptor Pathways Underlie the Temporal Sensitivity of Associative Learning. *Cell*.
687 doi:10.1016/j.cell.2019.05.040
688 Harris DT, Kallman BR, Mullaney BC, Scott K. 2015. Representations of Taste Modality in the
689 Drosophila Brain. *Neuron* **86**:1449–1460.
690 Hattori D, Aso Y, Swartz KJ, Rubin GM, Abbott LF, Axel R. 2017. Representations of Novelty and
691 Familiarity in a Mushroom Body Compartment. *Cell* **169**:956–969.e17.

Hige T, Aso Y, Modi MN, Rubin GM, Turner GC. 2015a. Heterosynaptic Plasticity Underlies Aversive Olfactory Learning in Drosophila. *Neuron* **88**:985–998.

Hige T, Aso Y, Rubin GM, Turner GC. 2015b. Plasticity-driven individualization of olfactory coding in mushroom body output neurons. *Nature* **526**:258–262.

Hiroi M, Marion-Poll F, Tanimura T. 2002. Differentiated Response to Sugars among Labellar Chemosensilla in Drosophila. *jzoo* **19**:1009–1018.

Huetteroth W, Perisse E, Lin S, Klappenbach M, Burke C, Waddell S. 2015. Sweet taste and nutrient value subdivide rewarding dopaminergic neurons in Drosophila. *Curr Biol* **25**:751–758.

Hwang RY, Zhong L, Xu Y, Johnson T, Zhang F, Deisseroth K, Tracey WD. 2007. Nociceptive Neurons Protect Drosophila Larvae from Parasitoid Wasps. *Curr Biol* **17**:2105–2116.

Ichinose T, Aso Y, Yamagata N, Abe A, Rubin GM, Tanimoto H. 2015. Reward signal in a recurrent circuit drives appetitive long-term memory formation. *Elife* **4**:e10719.

Jenett A, Rubin GM, Ngo T-TB, Shepherd D, Murphy C, Dionne H, Pfeiffer BD, Cavallaro A, Hall D, Jeter J, Iyer N, Fetter D, Hausenfluck JH, Peng H, Trautman ET, Svirskas RR, Myers EW, Iwinski ZR, Aso Y, DePasquale GM, Enos A, Hulamm P, Lam SCB, Li H-H, Laverty TR, Long F, Qu L, Murphy SD, Rokicki K, Safford T, Shaw K, Simpson JH, Sowell A, Tae S, Yu Y, Zugates CT. 2012. A GAL4-driver line resource for Drosophila neurobiology. *Cell Rep* **2**:991–1001.

Jiang L, Litwin-Kumar A. 2021. Models of heterogeneous dopamine signaling in an insect learning and memory center. *PLoS Comput Biol* **17**:e1009205.

Joseph RM, Heberlein U. 2012. Tissue-specific activation of a single gustatory receptor produces opposing behavioral responses in Drosophila. *Genetics* **192**:521–532.

Kabra M, Lee A, Robie A, Egnor R, Huston S, Rodriguez IF, Edwards A, Branson K. 2022. APT: Animal Part Tracker v0.3.4. Zenodo. doi:10.5281/ZENODO.6366082

Kanzaki R, Ikeda A, Shibuya T. 1994. [引用] Morphology and physiology of pheromone-triggered flip-flop descending interneurons of the male silkworm moth, Bombyx mori. *J Comp Physiol A*.

Kim H, Kirkhart C, Scott K. 2017. Long-range projection neurons in the taste circuit of Drosophila. *Elife* **6**. doi:10.7554/eLife.23386

Kirkhart C, Scott K. 2015. Gustatory learning and processing in the Drosophila mushroom bodies. *J Neurosci* **35**:5950–5958.

Klapoetke NC, Murata Y, Kim SS, Pulver SR, Birdsey-Benson A, Cho YK, Morimoto TK, Chuong AS, Carpenter EJ, Tian Z, Wang J, Xie Y, Yan Z, Zhang Y, Chow BY, Surek B, Melkonian M, Jayaraman V, Constantine-Paton M, Wong GK-S, Boyden ES. 2014. Independent optical excitation of distinct neural populations. *Nat Methods* **11**:338–346.

König C, Khalili A, Niewalda T, Gao S, Gerber B. 2019. An optogenetic analogue of second-order reinforcement in Drosophila. *Biol Lett* **15**:20190084.

Li F, Lindsey JW, Marin EC, Otto N, Dreher M, Dempsey G, Stark I, Bates AS, Pleijzier MW, Schlegel P, Nern A, Takemura S-Y, Eckstein N, Yang T, Francis A, Braun A, Parekh R, Costa M, Scheffer LK, Aso Y, Jefferis GS, Abbott LF, Litwin-Kumar A, Waddell S, Rubin GM. 2020. The connectome of the adult Drosophila mushroom body provides insights into function. *Elife* **9**. doi:10.7554/eLife.62576

Lin H-H, Chu L-A, Fu T-F, Dickson BJ, Chiang A-S. 2013. Parallel neural pathways mediate CO2 avoidance responses in Drosophila. *Science* **340**:1338–1341.

Lin H-H, Lai JS-Y, Chin A-L, Chen Y-C, Chiang A-S. 2007. A Map of Olfactory Representation in the Drosophila Mushroom Body. *Cell* **128**:1205–1217.

Liu C, Plaçais P-Y, Yamagata N, Pfeiffer BD, Aso Y, Friedrich AB, Siwanowicz I, Rubin GM, Preat T, Tanimoto H. 2012. A subset of dopamine neurons signals reward for odour memory in Drosophila. *Nature*. doi:10.1038/nature11304

Liu WW, Mazor O, Wilson RI. 2015. Thermosensory processing in the Drosophila brain. *Nature* **519**:353–357.

Luan H, Diao F, Scott RL, White BH. 2020. The Drosophila Split Gal4 System for Neural Circuit Mapping. *Frontiers in Neural Circuits*. doi:10.3389/fncir.2020.603397

Luan H, Peabody NC, Vinson CR, White BH. 2006. Refined spatial manipulation of neuronal function by combinatorial restriction of transgene expression. *Neuron* **52**:425–436.
Mao Z, Davis RL. 2009. Eight different types of dopaminergic neurons innervate the Drosophila mushroom body neuropil: anatomical and physiological heterogeneity. *Front Neural Circuits* **3**:612.
Marin EC, Büld L, Theiss M, Sarkissian T, Roberts RJV, Turnbull R, Tamimi IFM, Pleijzier MW, Laursen WJ, Drummond N, Schlegel P, Bates AS, Li F, Landgraf M, Costa M, Bock DD, Garrity PA, Jefferis GSXE. 2020. Connectomics Analysis Reveals First-, Second-, and Third-Order Thermosensory and Hygrosensory Neurons in the Adult Drosophila Brain. *Curr Biol* **30**:3167–3182.e4.
Martinez-Cervantes J, Shah P, Phan A, Cervantes-Sandoval I. 2022. Higher-order unimodal olfactory sensory preconditioning in. *Elife* **11**. doi:10.7554/eLife.79107
Masek P, Worden K, Aso Y, Rubin GM, Keene AC. 2015. A dopamine-modulated neural circuit regulating aversive taste memory in Drosophila. *Curr Biol* **25**:1535–1541.
Masse NY, Cachero S, Ostrovsky AD, Jefferis GSXE. 2012. A mutual information approach to automate identification of neuronal clusters in Drosophila brain images. *Front Neuroinform* **6**:21.
Matheson AMM, Lanz AJ, Medina AM, Licata AM, Currier TA, Syed MH, Nagel KI. 2022. A neural circuit for wind-guided olfactory navigation. *Nat Commun* **13**:1–21.
McCurdy LY, Sareen P, Davoudian PA, Nitabach MN. 2021. Dopaminergic mechanism underlying reward-encoding of punishment omission during reversal learning in Drosophila. *Nat Commun* **12**:1115.
McKellar CE, Siwanowicz I, Dickson BJ, Simpson JH. 2020. Controlling motor neurons of every muscle for fly proboscis reaching. *Elife* **9**:e54978.
Meissner GW, Nern A, Dorman Z, DePasquale GM, Forster K, Gibney T, Hausenfluck JH, He Y, Iyer NA, Jeter J, Johnson L, Johnston RM, Lee K, Melton B, Yarbrough B, Zugates CT, Clements J, Goina C, Otsuna H, Rokicki K, Svirskas RR, Aso Y, Card GM, Dickson BJ, Ehrhardt E, Goldammer J, Ito M, Kainmueller D, Korff W, Mais L, Minegishi R, Namiki S, Rubin GM, Sterne GR, Wolff T, Malkesman O. 2023. A searchable image resource of Drosophila GAL4 driver expression patterns with single neuron resolution. doi:10.7554/eLife.80660
Miyamoto T, Slone J, Song X, Amrein H. 2012. A fructose receptor functions as a nutrient sensor in the Drosophila brain. *Cell* **151**:1113–1125.
Miyazaki T, Lin T-Y, Ito K, Lee C-H, Stopfer M. 2015. A gustatory second-order neuron that connects sucrose-sensitive primary neurons and a distinct region of the gnathal ganglion in the Drosophila brain. *J Neurogenet* **29**:144–155.
Modi MN, Shuai Y, Turner GC. 2020. The Drosophila Mushroom Body: From Architecture to Algorithm in a Learning Circuit. *Annu Rev Neurosci* **43**:465–484.
Namiki S, Dickinson MH, Wong AM, Korff W, Card GM. 2018. The functional organization of descending sensory-motor pathways in Drosophila. doi:10.7554/eLife.34272
Nern A, Pfeiffer BD, Rubin GM. 2015. Optimized tools for multicolor stochastic labeling reveal diverse stereotyped cell arrangements in the fly visual system. *Proc Natl Acad Sci U S A* **112**:E2967–76.
Ohyama T, Schneider-Mizell CM, Fetter RD, Aleman JV, Franconville R, Rivera-Alba M, Mensh BD, Branson KM, Simpson JH, Truman JW, Cardona A, Zlatic M. 2015. A multilevel multimodal circuit enhances action selection in Drosophila. *Nature* **520**:633–639.
Otsuna H, Ito M, Kawase T. 2018. Color depth MIP mask search: a new tool to expedite Split-GAL4 creation. *bioRxiv*. doi:10.1101/318006
Otto N, Pleijzier MW, Morgan IC, Edmondson-Stait AJ, Heinz KJ, Stark I, Dempsey G, Ito M, Kapoor I, Hsu J, Schlegel PM, Bates AS, Feng L, Costa M, Ito K, Bock DD, Rubin GM, Jefferis GSXE, Waddell S. 2020. Input Connectivity Reveals Additional Heterogeneity of Dopaminergic Reinforcement in Drosophila. *Curr Biol* **30**:3200–3211.e8.
Owald D, Felsenberg J, Talbot CB, Das G, Perisse E, Huetteroth W, Waddell S. 2015. Activity of

defined mushroom body output neurons underlies learned olfactory behavior in Drosophila. *Neuron* **86**:417–427.
Park J-H, Kwon JY. 2011. A systematic analysis of Drosophila gustatory receptor gene expression in abdominal neurons which project to the central nervous system. *Mol Cells* **32**:375–381.
Pavlowsky A, Schor J, Plaçais P-Y, Preat T. 2018. A GABAergic Feedback Shapes Dopaminergic Input on the Drosophila Mushroom Body to Promote Appetitive Long-Term Memory. *Curr Biol* **28**:1783–1793.e4.
Perez-Orive J, Mazor O, Turner GC, Cassenaer S, Wilson RI, Laurent G. 2002. Oscillations and sparsening of odor representations in the mushroom body. *Science* **297**:359–365.
Pettersson J. 1970. An Aphid Sex Attractant. *Insect Syst Evol* **1**:63–73.
Pfeiffer BD, Jenett A, Hammonds AS, Ngo T-TB, Misra S, Murphy C, Scully A, Carlson JW, Wan KH, Laverty TR, Mungall C, Svirskas R, Kadonaga JT, Doe CQ, Eisen MB, Celniker SE, Rubin GM. 2008. Tools for neuroanatomy and neurogenetics in Drosophila. *Proc Natl Acad Sci U S A* **105**:9715–9720.
Pfeiffer BD, Ngo T-TB, Hibbard KL, Murphy C, Jenett A, Truman JW, Rubin GM. 2010. Refinement of tools for targeted gene expression in Drosophila. *Genetics* **186**:735–755.
Pfeiffer BD, Truman JW, Rubin GM. 2012. Using translational enhancers to increase transgene expression in Drosophila. *Proc Natl Acad Sci U S A* **109**:6626–6631.
Plaçais P-Y, de Tredern É, Scheunemann L, Trannoy S, Goguel V, Han K-A, Isabel G, Preat T. 2017. Upregulated energy metabolism in the Drosophila mushroom body is the trigger for long-term memory. *Nat Commun* **8**:15510.
Plaza SM, Clements J, Dolafi T, Umayam L, Neubarth NN, Scheffer LK, Berg S. 2022. neuPrint: An open access tool for EM connectomics. *Front Neuroinform* **16**:896292.
Rajagopalan AE, Darshan R, Fitzgerald JE, Turner GC. 2022. Expectation-based learning rules underlie dynamic foraging in Drosophila. *bioRxiv*. doi:10.1101/2022.05.24.493252
Rodrigues V, Siddiqi O. 1978. Genetic analysis of chemosensory pathway. *Proceedings / Indian Academy of Sciences* **87**:147–160.
Rubin GM, Aso Y. 2023. New genetic tools for mushroom body output neurons in Drosophila. *bioRxiv*. doi:10.1101/2023.06.23.546330
Saumweber T, Rohwedder A, Schleyer M, Eichler K, Chen Y-C, Aso Y, Cardona A, Eschbach C, Kobler O, Voigt A, Durairaja A, Mancini N, Zlatic M, Truman JW, Thum AS, Gerber B. 2018. Functional architecture of reward learning in mushroom body extrinsic neurons of larval Drosophila. *Nat Commun* **9**:1104.
Sayin S, De Backer J-F, Siju KP, Wosniack ME, Lewis LP, Frisch L-M, Gansen B, Schlegel P, Edmondson-Stait A, Sharifi N, Fisher CB, Calle-Schuler SA, Lauritzen JS, Bock DD, Costa M, Jefferis GSXE, Gjorgjieva J, Grunwald Kadow IC. 2019. A Neural Circuit Arbitrates between Persistence and Withdrawal in Hungry Drosophila. *Neuron* **104**:544–558.e6.
Scaplen KM, Talay M, Fisher JD, Cohn R, Sorkaç A, Aso Y, Barnea G, Kaun KR. 2021. Transsynaptic mapping of Drosophila mushroom body output neurons. *Elife* **10**. doi:10.7554/eLife.63379
Scheffer LK, Xu CS, Januszewski M, Lu Z, Takemura S-Y, Hayworth KJ, Huang GB, Shinomiya K, Maitlin-Shepard J, Berg S, Clements J, Hubbard PM, Katz WT, Umayam L, Zhao T, Ackerman D, Blakely T, Bogovic J, Dolafi T, Kainmueller D, Kawase T, Khairy KA, Leavitt L, Li PH, Lindsey L, Neubarth N, Olbris DJ, Otsuna H, Trautman ET, Ito M, Bates AS, Goldammer J, Wolff T, Svirskas R, Schlegel P, Neace E, Knecht CJ, Alvarado CX, Bailey DA, Ballinger S, Borycz JA, Canino BS, Cheatham N, Cook M, Dreher M, Duclos O, Eubanks B, Fairbanks K, Finley S, Forknall N, Francis A, Hopkins GP, Joyce EM, Kim S, Kirk NA, Kovalyak J, Lauchie SA, Lohff A, Maldonado C, Manley EA, McLin S, Mooney C, Ndama M, Ogundeyi O, Okeoma N, Ordish C, Padilla N, Patrick CM, Paterson T, Phillips EE, Phillips EM, Rampally N, Ribeiro C, Robertson MK, Rymer JT, Ryan SM, Sammons M, Scott AK, Scott AL, Shinomiya A, Smith C, Smith K, Smith NL, Sobeski MA, Suleiman A, Swift J, Takemura S, Talebi I, Tarnogorska D, Tenshaw E, Tokhi T, Walsh JJ, Yang T, Horne JA, Li F, Parekh R, Rivlin PK, Jayaraman V, Costa M, Jefferis GS, Ito K, Saalfeld S, George R,

845 Meinertzhagen IA, Rubin GM, Hess HF, Jain V, Plaza SM. 2020. A connectome and analysis of
846 the adult central brain. *Elife* **9**. doi:10.7554/eLife.57443
847 Schindelin J, Arganda-Carreras I, Frise E, Kaynig V, Longair M, Pietzsch T, Preibisch S, Rueden C,
848 Saalfeld S, Schmid B, Tinevez J-Y, White DJ, Hartenstein V, Eliceiri K, Tomancak P, Cardona A.
849 2012. Fiji: an open-source platform for biological-image analysis. *Nat Methods* **9**:676–682.
850 Schlegel P, Yin Y, Bates AS, Dorkenwald S, Eichler K, Brooks P, Han DS, Gkantia M, Dos Santos M,
851 Munnelly EJ, Badalamente G, Capdevila LS, Sane VA, Pleijzier MW, Tamimi IFM, Dunne CR,
852 Salgarella I, Javier A, Fang S, Perlman E, Kazimiers T, Jagannathan SR, Matsliah A, Sterling AR, Yu
853 S-C, McKellar CE, FlyWire Consortium, Costa M, Seung HS, Murthy M, Hartenstein V, Bock DD,
854 Jefferis GSXE. 2023. Whole-brain annotation and multi-connectome cell typing quantifies circuit
855 stereotypy in Drosophila. *bioRxiv*. doi:10.1101/2023.06.27.546055
856 Schretter CE, Aso Y, Robie AA, Dreher M, Dolan M-J, Chen N, Ito M, Yang T, Parekh R, Branson KM,
857 Rubin GM. 2020. Cell types and neuronal circuitry underlying female aggression in Drosophila.
858 *eLife*. doi:10.7554/elife.58942
859 Schroll C, Riemensperger T, Bucher D, Ehmer J, Völler T, Erbguth K, Gerber B, Hendel T, Nagel G,
860 Buchner E, Fiala A. 2006. Light-induced activation of distinct modulatory neurons triggers
861 appetitive or aversive learning in Drosophila larvae. *Curr Biol* **16**:1741–1747.
862 Schwaerzel M, Monastirioti M, Scholz H, Friggi-Grelin F, Birman S, Heisenberg M. 2003. Dopamine
863 and octopamine differentiate between aversive and appetitive olfactory memories in
864 Drosophila. *J Neurosci* **23**:10495–10502.
865 Shannon P, Markiel A, Ozier O, Baliga NS, Wang JT, Ramage D, Amin N, Schwikowski B, Ideker T.
866 2003. Cytoscape: a software environment for integrated models of biomolecular interaction
867 networks. *Genome Res* **13**:2498–2504.
868 Shimono K, Fujimoto A, Tsuyama T, Yamamoto-Kochi M, Sato M, Hattori Y, Sugimura K, Usui T,
869 Kimura K-I, Uemura T. 2009. Multidendritic sensory neurons in the adult Drosophila abdomen:
870 origins, dendritic morphology, and segment- and age-dependent programmed cell death.
871 *Neural Dev* **4**:37.
872 Shuai Y, Hirokawa A, Ai Y, Zhang M, Li W, Zhong Y. 2015. Dissecting neural pathways for forgetting in
873 Drosophila olfactory aversive memory. *Proc Natl Acad Sci U S A* **112**:E6663–72.
874 Shyu W-H, Chiu T-H, Chiang M-H, Cheng Y-C, Tsai Y-L, Fu T-F, Wu T, Wu C-L. 2017. Neural circuits for
875 long-term water-reward memory processing in thirsty Drosophila. *Nat Commun* **8**:15230.
876 Smith MA-Y, Honegger KS, Turner G, de Bivort B. 2022. Idiosyncratic learning performance in flies.
877 *Biol Lett* **18**:20210424.
878 Sterne GR, Otsuna H, Dickson BJ, Scott K. 2021. Classification and genetic targeting of cell types in
879 the primary taste and premotor center of the adult brain. *Elife* **10**. doi:10.7554/eLife.71679
880 Stocker RF, Lienhard MC, Borst A, Fischbach KF. 1990. Neuronal architecture of the antennal lobe in
881 Drosophila melanogaster. *Cell Tissue Res* **262**:9–34.
882 Strother JA, Wu S-T, Wong AM, Nern A, Rogers EM, Le JQ, Rubin GM, Reiser MB. 2017. The
883 Emergence of Directional Selectivity in the Visual Motion Pathway of Drosophila. *Neuron*
884 **94**:168–182.e10.
885 Suh GSB, Wong AM, Hergarden AC, Wang JW, Simon AF, Benzer S, Axel R, Anderson DJ. 2004. A
886 single population of olfactory sensory neurons mediates an innate avoidance behaviour in
887 Drosophila. *Nature* **431**:854–859.
888 Takagi S, Cocanougher BT, Niki S, Miyamoto D, Kohsaka H, Kazama H, Fetter RD, Truman JW, Zlatic
889 M, Cardona A, Nose A. 2017. Divergent Connectivity of Homologous Command-like Neurons
890 Mediates Segment-Specific Touch Responses in Drosophila. *Neuron* **96**:1373–1387.e6.
891 Tanaka NK, Awasaki T, Shimada T, Ito K. 2004. Integration of chemosensory pathways in the
892 Drosophila second-order olfactory centers. *Curr Biol* **14**:449–457.
893 Tanaka NK, Endo K, Ito K. 2012. Organization of antennal lobe-associated neurons in adult
894 Drosophila melanogaster brain. *J Comp Neurol* **520**:4067–4130.
895 Tanaka NK, Tanimoto H, Ito K. 2008. Neuronal assemblies of the Drosophila mushroom body. *J Comp*

*Neurol* **508**:711–755.
Thoma V, Knapek S, Arai S, Hartl M, Kohsaka H, Sirigrivatanawong P, Abe A, Hashimoto K, Tanimoto H. 2016. Functional dissociation in sweet taste receptor neurons between and within taste organs of Drosophila. *Nat Commun* **7**:10678.
Ting C-Y, Gu S, Guttikonda S, Lin T-Y, White BH, Lee C-H. 2011. Focusing transgene expression in Drosophila by coupling Gal4 with a novel split-LexA expression system. *Genetics* **188**:229–233.
Tirian L, Dickson BJ. 2017. The VT GAL4, LexA, and split-GAL4 driver line collections for targeted expression in the Drosophila nervous system. *bioRxiv*. doi:10.1101/198648
Truman JW, Price J, Miyares RL, Lee T. 2023. Metamorphosis of memory circuits in Drosophila reveals a strategy for evolving a larval brain. doi:10.7554/eLife.80594
Tsao C-H, Chen C-C, Lin C-H, Yang H-Y, Lin S. 2018. mushroom bodies integrate hunger and satiety signals to control innate food-seeking behavior. *Elife* **7**. doi:10.7554/eLife.35264
Turner GC, Bazhenov M, Laurent G. 2008. Olfactory Representations by Drosophila Mushroom Body Neurons. *J Neurophysiol*. doi:10.1152/jn.01283.2007
Tuthill JC, Nern A, Holtz SL, Rubin GM, Reiser MB. 2013. Contributions of the 12 neuron classes in the fly lamina to motion vision. *Neuron* **79**:128–140.
Vogt K, Aso Y, Hige T, Knapek S, Ichinose T, Friedrich AB, Turner GC, Rubin GM, Tanimoto H. 2016. Direct neural pathways convey distinct visual information to Drosophila mushroom bodies. *Elife* **5**. doi:10.7554/eLife.14009
Wang K, Wang F, Forknall N, Yang T, Patrick C, Parekh R, Dickson BJ. 2021. Neural circuit mechanisms of sexual receptivity in Drosophila females. *Nature* **589**:577–581.
Wang Z, Singhvi A, Kong P, Scott K. 2004. Taste representations in the Drosophila brain. *Cell* **117**:981–991.
Wan Y, Otsuna H, Chien C-B, Hansen C. 2012. FluoRender: An Application of 2D Image Space Methods for 3D and 4D Confocal Microscopy Data Visualization in Neurobiology Research. *IEEE Pac Vis Symp* 201–208.
Winding M, Pedigo BD, Barnes CL, Patsolic HG, Park Y, Kazimiers T, Fushiki A, Andrade IV, Khandelwal A, Valdes-Aleman J, Li F, Randel N, Barsotti E, Correia A, Fetter RD, Hartenstein V, Priebe CE, Vogelstein JT, Cardona A, Zlatic M. 2023. The connectome of an insect brain. *Science* **379**:eadd9330.
Wolff T, Rubin GM. 2018. Neuroarchitecture of the Drosophila central complex: A catalog of nodulus and asymmetrical body neurons and a revision of the protocerebral bridge catalog. *J Comp Neurol* **526**:2585–2611.
Wu J-K, Tai C-Y, Feng K-L, Chen S-L, Chen C-C, Chiang A-S. 2017. Long-term memory requires sequential protein synthesis in three subsets of mushroom body output neurons in Drosophila. *Sci Rep* **7**:7112.
Wu M, Nern A, Williamson WR, Morimoto MM, Reiser MB, Card GM, Rubin GM. 2016. Visual projection neurons in the lobula link feature detection to distinct behavioral programs. *Elife* **5**. doi:10.7554/eLife.21022
Xie Q, Brbic M, Horns F, Kolluru SS, Jones RC, Li J, Reddy AR, Xie A, Kohani S, Li Z, McLaughlin CN, Li T, Xu C, Vacek D, Luginbuhl DJ, Leskovec J, Quake SR, Luo L, Li H. 2021. Temporal evolution of single-cell transcriptomes of olfactory projection neurons. *Elife* **10**. doi:10.7554/eLife.63450
Yamada D, Bushey D, Li F, Hibbard KL, Sammons M, Funke J, Litwin-Kumar A, Hige T, Aso Y. 2023. Hierarchical architecture of dopaminergic circuits enables second-order conditioning in Drosophila. *Elife* **12**. doi:10.7554/eLife.79042
Yamagata N, Ichinose T, Aso Y, Plaçais P-Y, Friedrich AB, Sima RJ, Preat T, Rubin GM, Tanimoto H. 2015. Distinct dopamine neurons mediate reward signals for short- and long-term memories. *Proc Natl Acad Sci U S A* **112**:578–583.
Yavuz A, Jagge C, Slone J, Amrein H. 2014. A genetic tool kit for cellular and behavioral analyses of insect sugar receptors. *Fly* **8**:189–196.
Zhang X, Noyes NC, Zeng J, Li Y, Davis RL. 2019. Aversive Training Induces Both Presynaptic and

Postsynaptic Suppression in. *J Neurosci* **39**:9164–9172.
Zheng Z, Lauritzen JS, Perlman E, Robinson CG, Nichols M, Milkie D, Torrens O, Price J, Fisher CB, Sharifi N, Calle-Schuler SA, Kmecova L, Ali IJ, Karsh B, Trautman ET, Bogovic JA, Hanslovsky P, Jefferis GSXE, Kazhdan M, Khairy K, Saalfeld S, Fetter RD, Bock DD. 2018. A Complete Electron Microscopy Volume of the Brain of Adult Drosophila melanogaster. *Cell* **174**:730–743.e22.
Zheng Z, Li F, Fisher C, Ali IJ, Sharifi N, Calle-Schuler S, Hsu J, Masoodpanah N, Kmecova L, Kazimiers T, Perlman E, Nichols M, Li PH, Jain V, Bock DD. 2022. Structured sampling of olfactory input by the fly mushroom body. *Curr Biol* **32**:3334–3349.e6.

## Figures and figure legends

**Figure 1 Generation and annotation of split-GAL4 lines**

(A) In associative learning, flies adjust their behavioral responses to conditioned stimuli (CS), such as odors and colors, based on the contingency with innately rewarding or punishing unconditioned stimuli (US), such as sugar, bitter, shock and heat. A schematic of *Drosophila* melanogaster is from (Namiki et al., 2018).

(B) An image of the right half of an adult fly brain showing the mushroom bodies (MB). Projections neurons (PN) convey information from the antennal lobes (AL) to the calyx of the MB and the lateral horn (LH).

(C) A simplified diagram of the mushroom body circuit. The identity of sensory stimuli is represented by sparse activity patterns of Kenyon cells (KCs). A subset of dopaminergic neurons (DANs) respond to punishment/reward. Dopamine modulates weights of synapses between KCs and MB output neurons (MBONs) depending on the activity status of KCs. The skewed activity patterns of MBONs across compartments in response to the learned stimulus drive memory-based actions and feedback pathways to DANs.

(D) A summary of the workflow to generate split-GAL4 lines.

(E) Coverage of the collection. The crepine (CRE), the superior medial protocerebrum (SMP), the superior intermediate protocerebrum (SIP) and the superior lateral protocerebrum (SLP) are MB adjacent brain areas where MBONs and DANs most often have arborizations. CX, central complex. LAL, lateral accessory lobes.

(F) Examples of cell types covered by the collection. Expression patterns of CsChrimson-mVenus (green) are shown with neuropil counterstaining of Bruchpilot (Brp) with nc82 antibody (magenta). The whole body image came from Gr64f-Gal4 with muscle counterstaining (magenta). Putative cell types are bracketed.

**Figure 1-figure supplement 1 Examples of cell types covered by the split-GAL4 lines in this collection**

Additional examples of cell types covered by the collection. Expression patterns of CsChrimson-mVenus (green) are shown with neuropil counterstaining of Brp (magenta). Only one brain hemisphere is shown.

**Figure 2 LM-EM match of CRE011 driver**

(A) Expression pattern of SS45245-split-GAL4 in a brain.

(B) MCFO image of SS45245 showing individual labeled neurons.

(C) Frontal and ventral views of segmented light microscopy (LM) images of an exemplary split-Gal4 line (SS45245) visualized with a membrane reporter (myr-smGFP-FLAG) that was aligned to the JRC2018 standard brain. Frontal (top) and dorsal (bottom) projections are shown with outline of relevant neuropils.

(D) The skeleton reconstructed from electron microscopy (EM) data of the matched cell type CRE011 in the hemibrain connectome. The CRE011 cell on the right hemisphere is shown.

(E) Synaptic connectivity of CRE011 with MBONs and DANs in the MB derived from the hemibrain connectome.

1001
1002
1003 **Figure 2-figure supplement 1 LM-EM match of SS00460**
1004 (A) Frontal and ventral views of segmented light microscopy (LM) images of SS00460 in the JRC2018
1005 standard brain. Projections are shown with the outline of relevant neuropils. A' (ventral) is a rotated
1006 view of A (frontal) with the reference axis indicated.
1007 (B) The skeleton reconstructed from electron microscopy (EM) data in the hemibrain volume of the
1008 matched cell type I2LN44.
1009 (C) EM images of neurons with the most input connections (upstream) to I2LN44 in the hemibrain
1010 connectome. The number after "#" indicates the number of connections between the matched cell
1011 type (i.e. v2LN44) and its synaptic partners. The color code and EM BodyId for each EM-reconstructed
1012 neuron are also listed.
1013 (D) EM images of neurons with the most output connections (downstream) from I2LN44 in the
1014 hemibrain connectome. In Figure 2-figure supplement 1-20, sensory neurons and KCs are not
1015 displayed as top upstream or downstream neurons.
1016
1017 **Figure 2-figure supplement 2 LM-EM match of SS34963**
1018 **Figure 2-figure supplement 3 LM-EM match of SS33915**
1019 **Figure 2-figure supplement 4 LM-EM match of SS35020**
1020 **Figure 2-figure supplement 5 LM-EM match of SS34979**
1021 **Figure 2-figure supplement 6 LM-EM match of SS34947**
1022 **Figure 2-figure supplement 7 LM-EM match of SS00486**
1023 **Figure 2-figure supplement 8 LM-EM match of SS49308**
1024 **Figure 2-figure supplement 9 LM-EM match of SS49361**
1025 **Figure 2-figure supplement 10 LM-EM match of SS49868**
1026 **Figure 2-figure supplement 11 LM-EM match of SS49352**
1027 **Figure 2-figure supplement 12 LM-EM match of SS32228**
1028 **Figure 2-figure supplement 13 LM-EM match of SS32219**
1029 **Figure 2-figure supplement 14 LM-EM match of SS48890**
1030 **Figure 2-figure supplement 15 LM-EM match of SS48799**
1031 **Figure 2-figure supplement 16 LM-EM match of SS32259**
1032 **Figure 2-figure supplement 17 LM-EM match of SS48341**
1033 **Figure 2-figure supplement 18 LM-EM match of SS35040**
1034 **Figure 2-figure supplement 19 LM-EM match of SS33905**
1035 **Figure 2-figure supplement 20 LM-EM match of SS39538**
1036
1037 **Figure 3 Drivers for MBON downstream and DAN upstream neurons.**
1038 (A) Examples of confocal microscopy images of split-GAL4 lines (bottom) and their matching cell types
1039 in the hemibrain connectome (top). CsChrimson-mVenus (green); Brp (magenta).
1040 (B) The number of cell types that receive synaptic output from MBONs and supply synaptic input to
1041 DANs. Only cell types with connection (conn) over the indicated thresholds (i.e., more than 4 synapses
1042 for DAN upstream and more than 9 synapses for MBON downstream) were considered. The number
1043 of covered cell types are indicated in the brackets.
1044 (C) A scatter plot of MB interneuron cell types connected with DANs and MBONs. Cell types covered
1045 by Split-GAL4 lines are highlighted in red.

1046
1047 **Figure 3-figure supplement 1 New or improved drivers for MB cell types**
1048 (A) Confocal images and matched EM cell types. CsChrimson-mVenus (green); Brp (magenta).
1049 (B) Summary of within-MB split-GAL4 coverage. See Supplementary File 4 for details.
1050
1051 **Figure 4 Driver lines for uni-glomerular projection neurons**
1052 (A) Examples of covered uni-glomerular PN (uPN) cell types.
1053 (B) Coverage of the 51 antennal lobe glomeruli. The new collection of split-GAL4 covers uPN in the
1054 colored glomeruli.
1055 (C) Split-GAL4 coverage summary.
1056
1057 **Figure 5 Driver lines for multi-glomerular projection neurons**
1058 Examples of multi-glomerular projection neurons (mPN) types. M_l2PN3t18 [VC5++ l2PN1],
1059 M_lPNm11A [VP4++ lPN], and M_smPNm1 [VP3+ smPN] are predicted to receive majority non-
1060 olfactory input (Marin et al., 2020).
1061
1062 **Figure 6 Driver lines for non-olfactory projection neurons and sensory neurons**
1063 Examples of thermo-/hygro-sensory PN types and sensory neurons covered by this collection
1064
1065 **Figure 7 Driver lines for gustatory sensory neurons**
1066 (A) A summary of new transgenic lines generated by this study. In addition to Gr64f promoters,
1067 LexADBD lines were generated with Gr64f, Gr43a, Gr66a, Gr28b promoters and other GMR or VT
1068 promoters.
1069 (B) Schematic of the screening strategy used here to subdivide the Gr64f-DBD pattern by intersecting
1070 it with GMR and VT AD lines.
1071 (C) A schematic of the sensory neuron projection types that compose the Gr64f-DBD pattern.
1072 (D) A summary of expression patterns of 6 of the Gr64f split-GAL4 lines derived from the screening
1073 strategy in (B), using the anatomical notation described in (C).
1074 (E) Expression pattern of SS87269 in the brain and VNC. The arrow indicates an ascending projection
1075 of atGRN.
1076 (F) Expression of SS87269 in the labellum.
1077 (G) Expression of SS87269 in tarsi of fore (f), middle (m) and hind (h) legs.
1078 (H) Expression of SS87272 in the labral sense organ (LSO).
1079 (I) Expression of SS88801 in tarsi.
1080 (J) Expression of SS87278 in the abdominal body wall.
1081 (K-Q) Expression patterns of designated driver lines in the Gnathal Ganglia (GNG) and VNC. The arrow
1082 in K indicates the absence of ascending projections from stGRN.
1083 Magenta in F-J indicates muscle counterstaining with phalloidin (actin filaments); magenta in other
1084 panels indicates neuropil counterstaining of Brp.
1085
1086 **Figure 7-figure supplement 1 Expression pattern of Gr64f-Gal4**
1087 Expression pattern of Gr64f-GAL4 driving 5xUAS-myr-smFLAG in VK0005 in the brain and VNC (green)
1088 with neuropil counterstaining of Brp (magenta). The line used contains two copies of Gr64f-Gal4, with
1089 one copy on the second and one copy on the third chromosome. The insert on the left shows a

magnified view of each cell type in different colors. The insert on the right shows a sagittal view of the VNC.

**Figure 8 Behaviors with Gr64f-split-GAL4 lines**

(A) In the optogenetic olfactory arena, odors are delivered from the periphery and sucked out from the central vacuum port to deliver odors only to defined quadrants. Red LEDs (627nm peak) enable programmed optogenetic activation of neurons expressing CsChrimson.

(B) Training and testing protocol for experiments shown in (E). The training protocol consisted of 3 x 20s optogenetic activation training followed by the first preference test, 1x 1 min training followed by the 2nd test, and additional 2x 1 min training followed by the last test. Odors delivered to the two zones and odor durations in each period are indicated. LED intensities were 4.3 µW/mm2 in early 20s training and 34.9 µW/mm2 in later training. Activation LED was applied with 1s ON and 1s OFF during pairing with odor A. Odors were trained reciprocally. Pentyl acetate and Ethyl lactate were used as odor A and B, respectively, in half of the experiments. The two odors were swapped in the other half of experiments.

(C) Protocol to characterize Gr64f split-GAL4 activation phenotypes in the absence of an odor. During each trial, flies were illuminated with a red LED light continuously for 10 seconds.

(D) Summary diagram of the expression patterns of the original Gr64f-GAL4 (far left) and 6 Gr64f-split-GAL4s. The expression of the original Gr64f-GAL4 in olfactory sensory neurons is not depicted here.

(E) Associative memory scores after the training protocol in (B). Mean, standard error of the mean (SEM), and the number of groups are shown.

(F) The kinematic parameters of trajectories measured with Caltech FlyTracker during split-GAL4 activation in the absence of odor as shown in (C). Each group of flies received 6 activation trials. Summarization was based on the trial average of each group. The number of groups is indicated. The thick lines and shadows are mean and SEM. Gray lines are Empty-split-GAL4 control. Dashed lines are time bins for data summary in Figure 8-figure supplement 1.

(G) Average walking speed in each of 6 trials.

(H) An image of a tethered fly on a floating ball. Flies were tracked for proboscis extension (PE) activity with the Animal Part Tracker (Kabra et al., 2022). The annotated points, in the order of numbers, consisted of the tip of the abdomen (1), the highest point on the thorax (2), the midpoint between the root of the antennae (3), the base of the proboscis (4) and the tip of the proboscis (5). PE activity was quantified as the change of proboscis length, i.e., the distance from the tip to the base of the proboscis, or the distance between points 4 and 5.

(I) SS87269 and SS88801 activation and proboscis extension. Each fly was recorded over 6 activation trials in which the 624 nm LED was turned on for 1 second. LED intensity for SS87269 and SS88801, 11 µW/mm2; for empty Gal4 (pBDPGal4), 50 µW/mm2. Less saturated traces indicate behavior during LED off trials, while more saturated traces indicate behavior during LED on trials.

**Figure 8-figure supplement 1 Olfactory arena learning experiment, fly tracking and data analysis**

(A) To test associative learning in the olfactory circular arena, two different odors (A and B) were delivered to interleaved quadrants, defined as Zone 1 and Zone 2. The trajectory of an example fly during the odor choice period after automatic tracking of the experiment movies is shown.

1134 (B) Experiment protocol for learning as in Figure 8B. Odors (green-A, purple-B) and LED delivered to
1135 the two zones are indicated. The transition between sessions that were not video-recorded are
1136 masked by gray. In the example data, the odor ethyl lactate (EL) served as CS+ and was paired with
1137 CsChrimson-activation of SS87269, while the other odor pentyl acetate (PA) served as CS- and was
1138 unpaired. The full data set included an additional reciprocal group with PA as CS+ and EL as CS-.
1139 (C) Upwind displacement towards CS+ and CS- during the experiment was quantified by a change in
1140 the mean distance-to-wall for all flies (airflow came from the periphery of the arena and was drawn
1141 out in the center). In addition to the three testing periods (0-20 second after odor onset), the mean
1142 distance-to-wall during training in the odor periods before LED onset (0-10 second after odor onset)
1143 were also quantified. "CS+" and "CS-" groups were compared with a multi-comparison t-test with
1144 Bonferroni-Dunn's correction. *, P<0.05; ***, P<0.001.
1145
1146 **Figure 8-figure supplement 2 Summary data of Gr64f-split-Gal4 activation phenotypes**
1147 The data points during the time bin shown in Figure 8F.
1148 (A) Probability of return during the post-activation period.
1149 (B) Change of walking speed during the onset of activation period.
1150 (C) Change of curvature during the onset of activation period.
1151 (D) Change of curvature during the post-activation period.
1152 One-way ANOVA followed by Dunnett's multiple comparisons test. ***, P<0.001. Individual data
1153 points are shown with minimum, maximum, median, and interquartile ranges.
1154
1155 **Figure 8-figure supplement 3 Examples of covered SEZ neurons.**
1156 (Top two rows) New or improved split-GAL4 drivers for cell types already covered by the SEZ Split-
1157 GAL4 Collection (Sterne et al., 2021). (Bottom row) Split-GAL4 drivers for cell types not included in the
1158 SEZ Split-GAL4 Collection. Cell types are from Hemibrain 1.2.1, Sterne 2021 or mn2V (McKellar et al.,
1159 2020).
1160
1161 **Figure 9 Examples of covered ascending neurons**
1162 (A) Activation preference screen of 581 split-GAL4 lines (342 lines from this study). SS01159 (blue
1163 arrow) is one of the lines that flies showed strong avoidance at optogenetic activation.
1164 (B) Time course of flies' preference to quadrants with red LED light by SS01159>CsChrimson (blue) or
1165 empty-GAL4>CsChrimson (gray). A preference score to red LED quadrants was quantified from the
1166 distribution during the last 5s of two 30s activation periods. n = 8 groups for SS01159, n = 15 for empty
1167 Gal4. Mean (thick lines) and SEM (shadow) are plotted.
1168 (C) The mean normalized movement speed at the LED onset for flies in the LED quadrants. The 3-s
1169 period before LED onset was used as the baseline for normalization.
1170 (D) The mean cumulative turning angles in 5 movie frames (total elapsed time of 167 ms) when flies
1171 encountered the LED boundary. The boundary was defined as a 4-mm zone in between the LED and
1172 dark quadrants. Trajectories too close to the center (< 0.2*radius) or the wall (> 0.6*radius) of the
1173 arena were not analyzed.
1174 (E) Examples of split-GAL4 lines for ascending neurons. SS35227 and SS35256 shared a split half
1175 (R41C05-AD) with SS01159. SS32217 matched with TPN1 (Kim et al., 2017). No cell types were
1176 assigned to the other lines shown due to missing information in the hemibrain volume.
1177

1178 **Figure 10 Stereotypy and erroneous projections**
1179 (A) V_l2PN from both hemispheres send axonal projections to the right hemisphere in an atypical case
1180 (arrowhead).
1181 (B) In this atypical case, there are two MB-DPM neurons in one hemisphere (arrowhead) and the
1182 arborizations extend beyond the pedunculus into the calyx.
1183 (C) MBON-α1 occasionally has additional arborizations in the ellipsoid body (arrowhead)
1184 (D) The localization of MBON-α3 soma widely varied along the dorso-ventral axis. It occasionally had
1185 an additional axonal branch (arrowhead).
1186 (E) A table to summarize normal and erroneous projections of MBONs and MB-DPM. In all the cases
1187 except for the DPM, "different number of cells" was likely due to stochastic expression of the drivers
1188 (i.e., lack of labeling) rather than biological difference. We defined "mislocalization" when axons or
1189 dendrites projected to outside of the normally targeted brain regions. For instance, dendrites of
1190 typical MBON07 are usually confined inside the α1, but were extended to outside the MB lobes in
1191 22.9% of samples. Variable branching patterns inside the normally targeted brain regions were not
1192 counted as mislocalization here. In some MB310C-split-GAL4 samples, we observed a third soma
1193 attached to MBON-α1 but they lacked any neurites. We did not observe obvious mislocalization of
1194 dendrites or axons for MBON03, 5, 6, 12, 18 and 19. See Figure 11 for variability of MBON08/09 in
1195 MB083C.
1196
1197 **Figure 11 Individuality and asymmetry of MBON08 and MBON09**
1198 (A) A typical image of two MBONs in MB083C-split-GAL4 driver.
1199 (B) Abnormal axonal projection of MBON08/09 observed in one of 169 samples.
1200 (C-D) MCFO images of MB083C driver from different flies show that the two cells can either be both
1201 MBON09-γ3β'1 (C) or one MBON09-γ3β'1 and one MBON08-γ3 (D).
1202 (E-G) An example of MCFO image of MB083C, which visualized one MBON08 and two MBON09 in the
1203 same brain. The projection (E) and image sections at the γ3 (F) or β'1 (G) are shown.
1204 (H) Diagrams of the three MBONs shown in E-G.
1205 (I) A summary table for observation of MBON08 and MBON09 in male and female brains.
1206 (J) All possible variations of 4 MBONs in MB083C driver, and estimated probability for each case.
1207 Panel (A) and (C) were adapted from Figure 8 of (Aso et al., 2014a).
1208
1209 **Figure 11-figure supplement 1 MB083C invariantly label two MBONs**
1210 Maximum intensity projection images of individual samples are shown. Note that two somas in each
1211 hemisphere are labeled in all samples. Reporters used are indicated in each panel.
1212
1213 **Figure 11-figure supplement 2 Subdivisions of medial and lateral γ3 compartments**
1214 (A) Overlay between the dendrites of MBON08/09 and axons of PAM-γ4 DANs.
1215 (B) Overlay between the dendrites of MBON08/09 and axons of PAM-γ3 DANs.
1216 (C) A subset of PAM-γ3 arborizes in the medial part of the γ3 compartment. Asterisk indicates the
1217 position of the lateral γ3 that is not labeled in this line.
1218
1219 **Figure 12 Examples of split-LexA conversion**
1220 Split-LexA shares the same enhancers with split-GAL4 but with the Gal4DBD replaced by LexADBD.
1221 Among 34 conversions tested, 22 were successful, with the split-LexA showing identical or similar
1222 expression patterns as the split-GAL4. The remaining 12 had weak/no expression or showed

1223 unintended intersectional patterns. See Supplementary File 2 for the hemidriver lines with p10
1224 translational enhancers to enhance expression level.

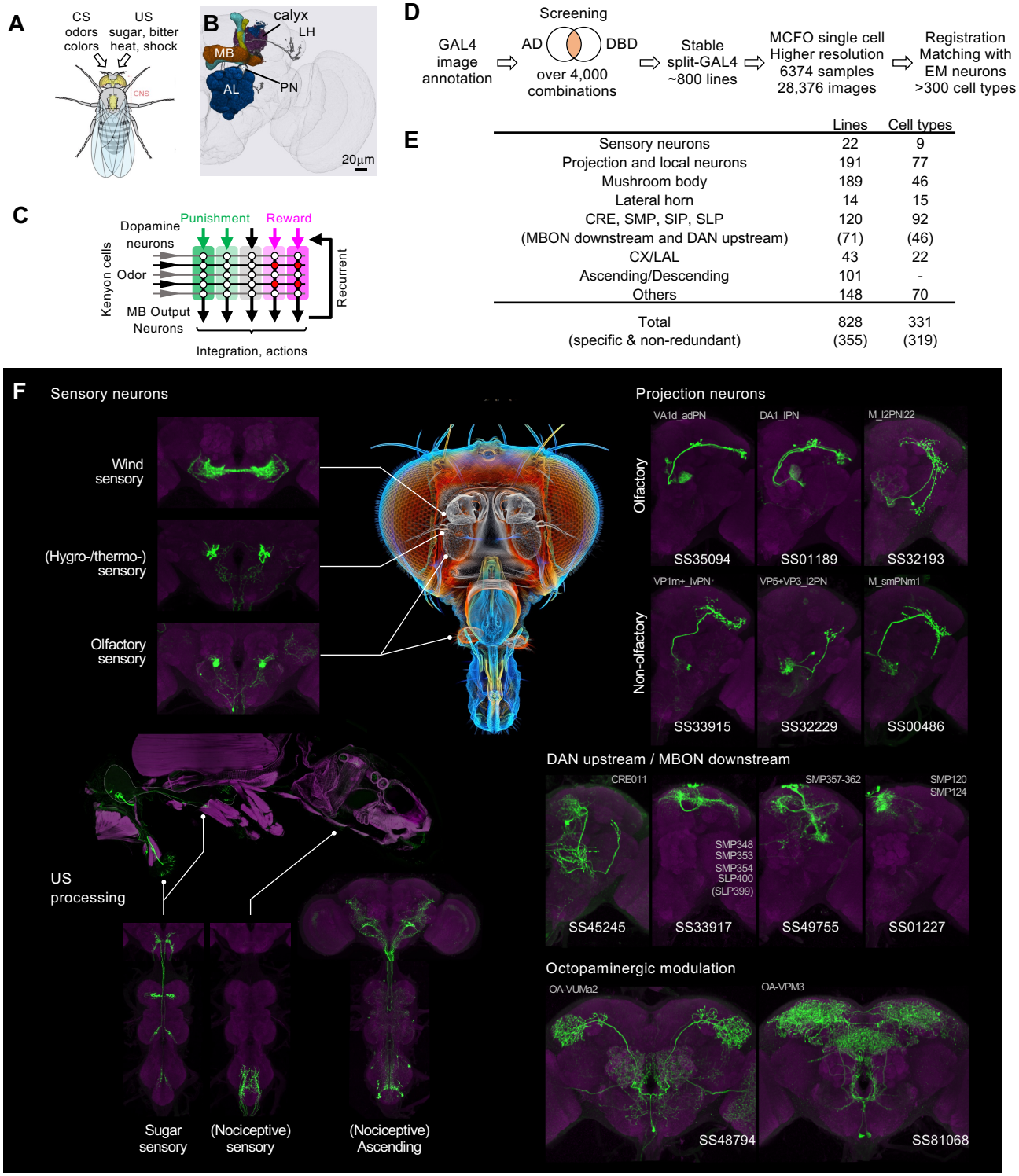


| | Lines | Cell types |
|---|---|---|
| Sensory neurons | 22 | 9 |
| Projection and local neurons | 191 | 77 |
| Mushroom body | 189 | 46 |
| Lateral horn | 14 | 15 |
| CRE, SMP, SIP, SLP | 120 | 92 |
| (MBON downstream and DAN upstream) | (71) | (46) |
| CX/LAL | 43 | 22 |
| Ascending/Descending | 101 | - |
| Others | 148 | 70 |
| Total | 828 | 331 |
| (specific & non-redundant) | (355) | (319) |

**Figure 1 Generation and annotation of split-GAL4 lines**

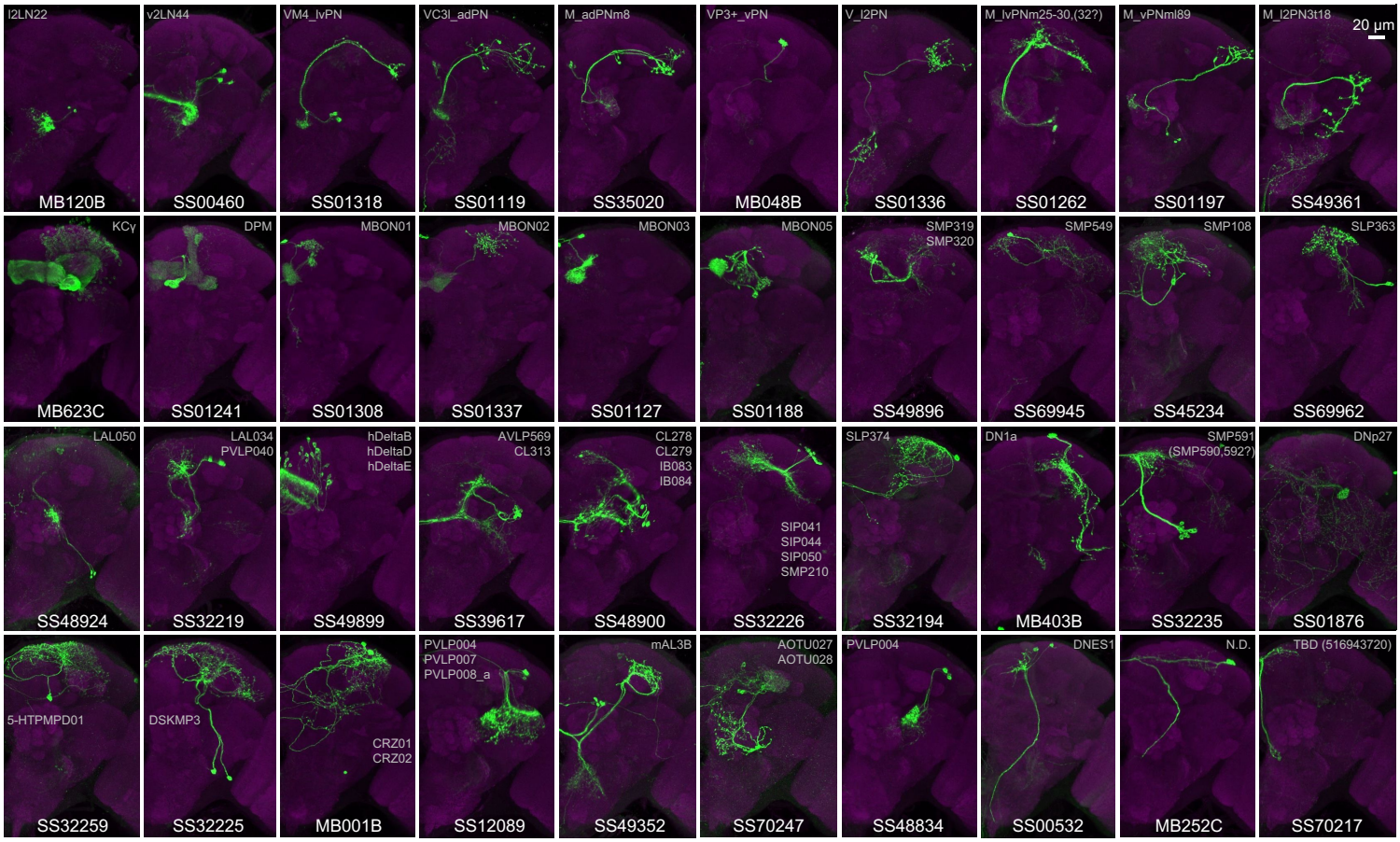


**Figure 1-figure supplement 1 Examples of cell types covered by the split-GAL4 lines in this collection**

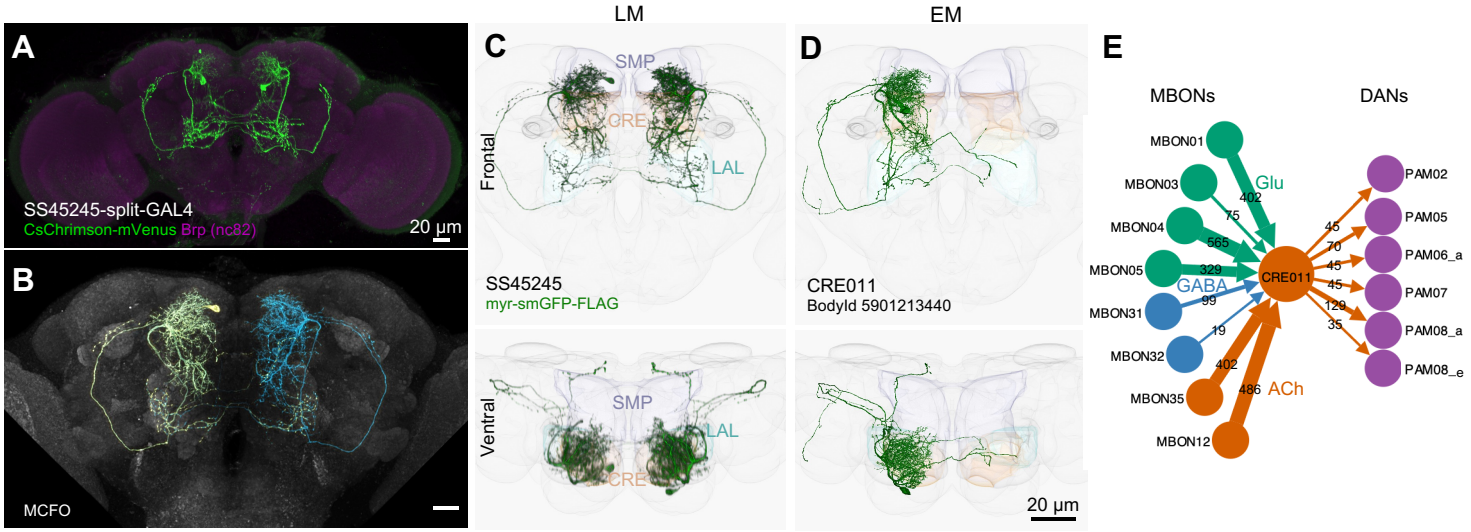


**Figure 2 LM-EM match of CRE011 driver**

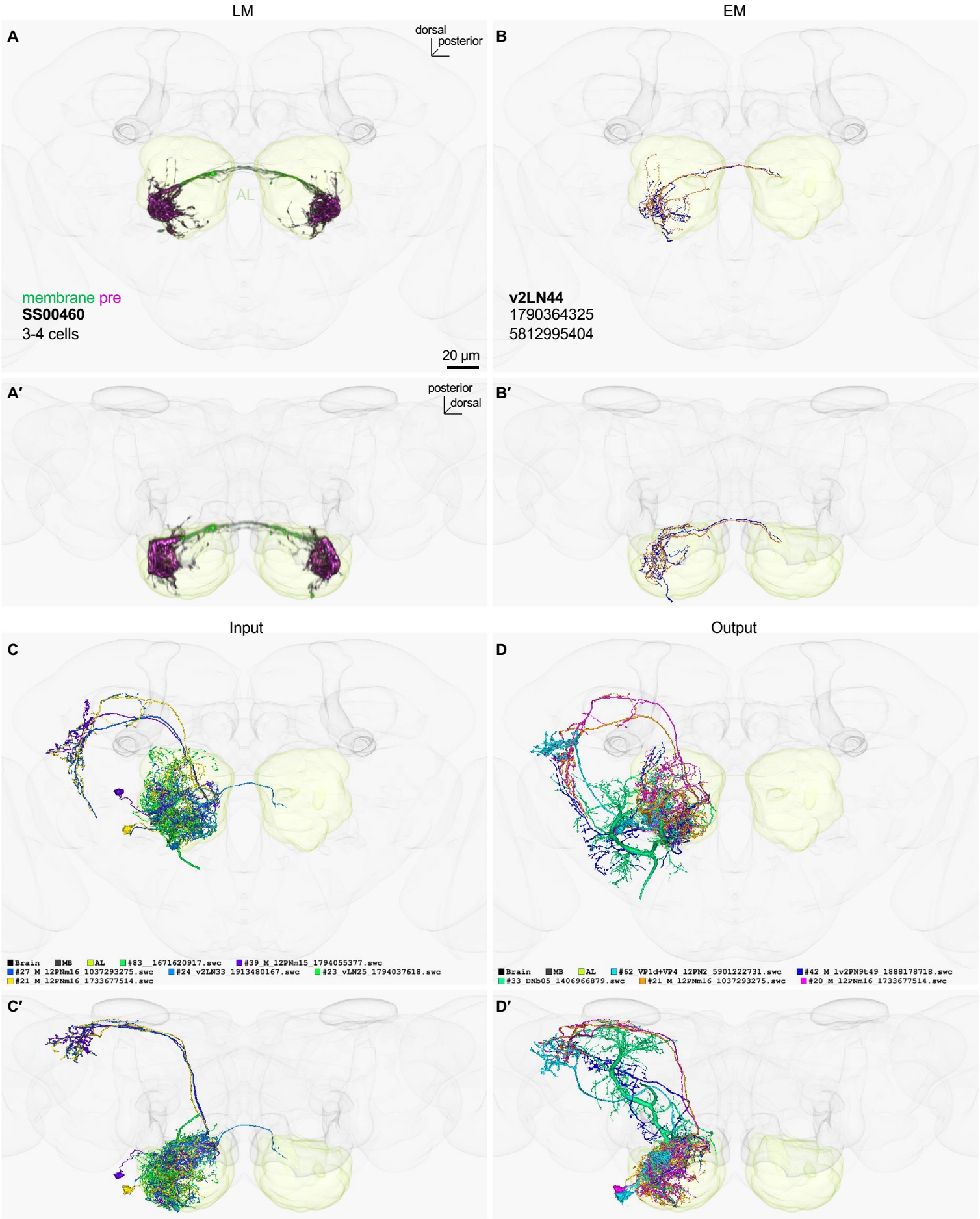


**Figure 2 – figure supplement 1**

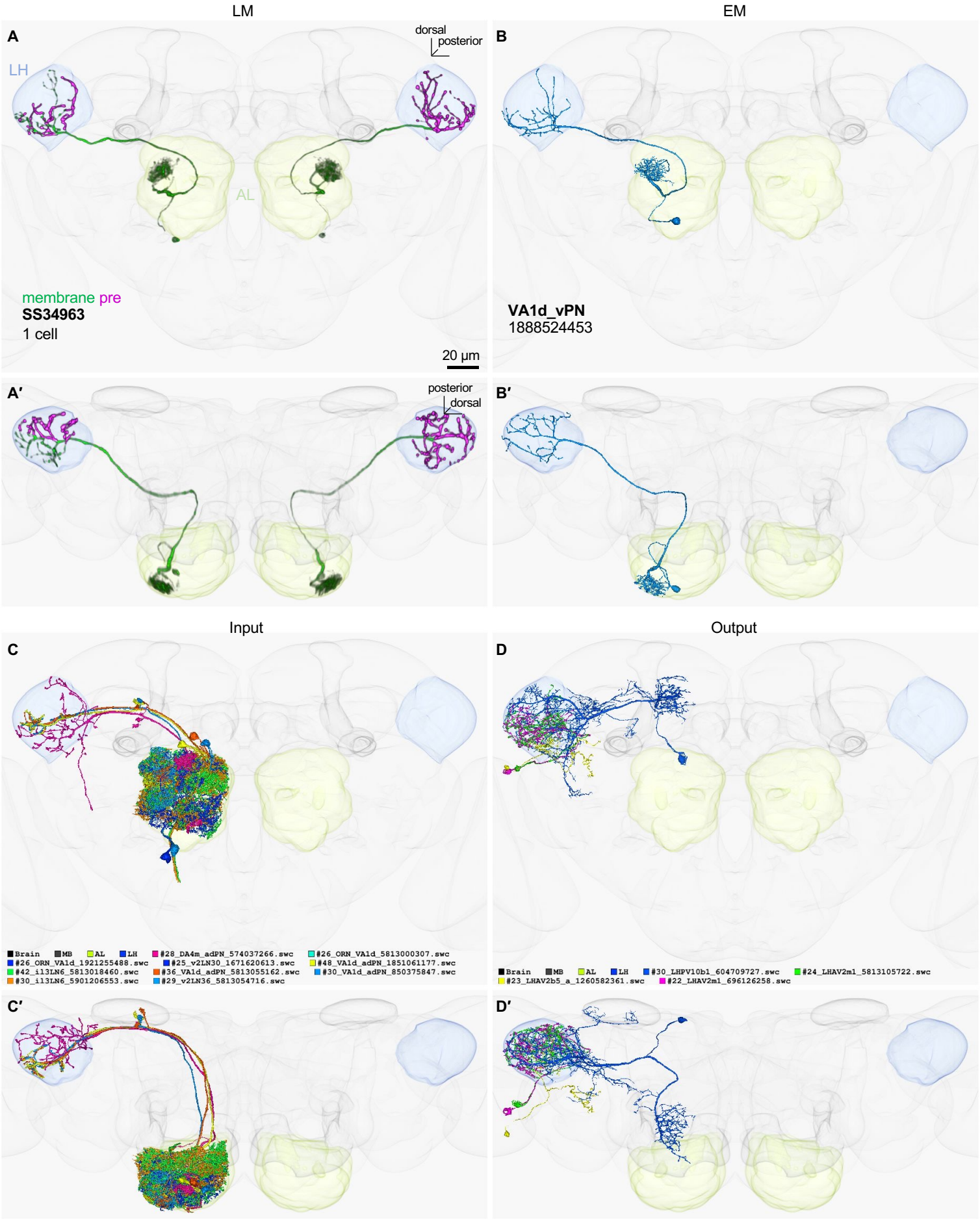


**Figure 2 – figure supplement 2**

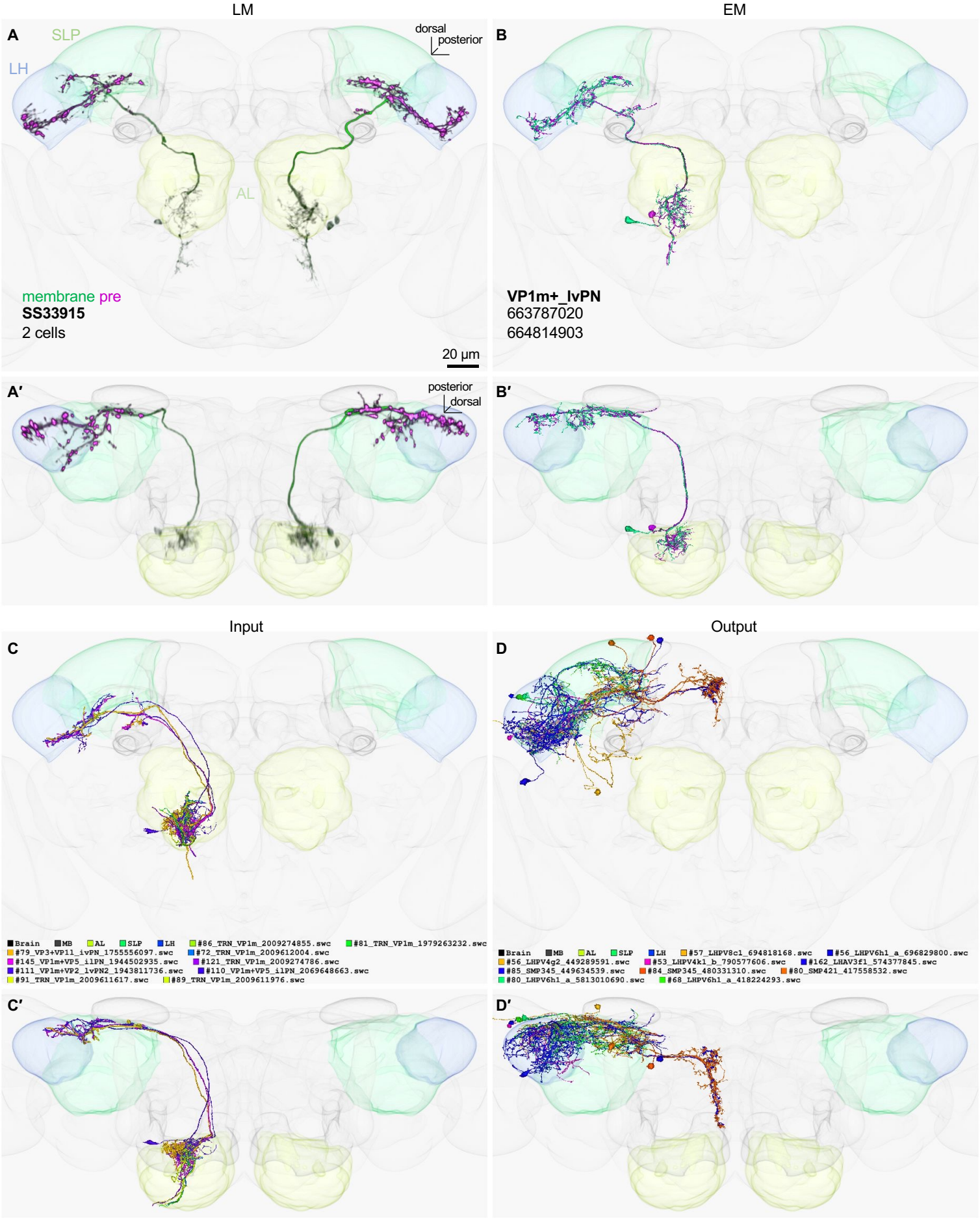


**Figure 2 – figure supplement 3**

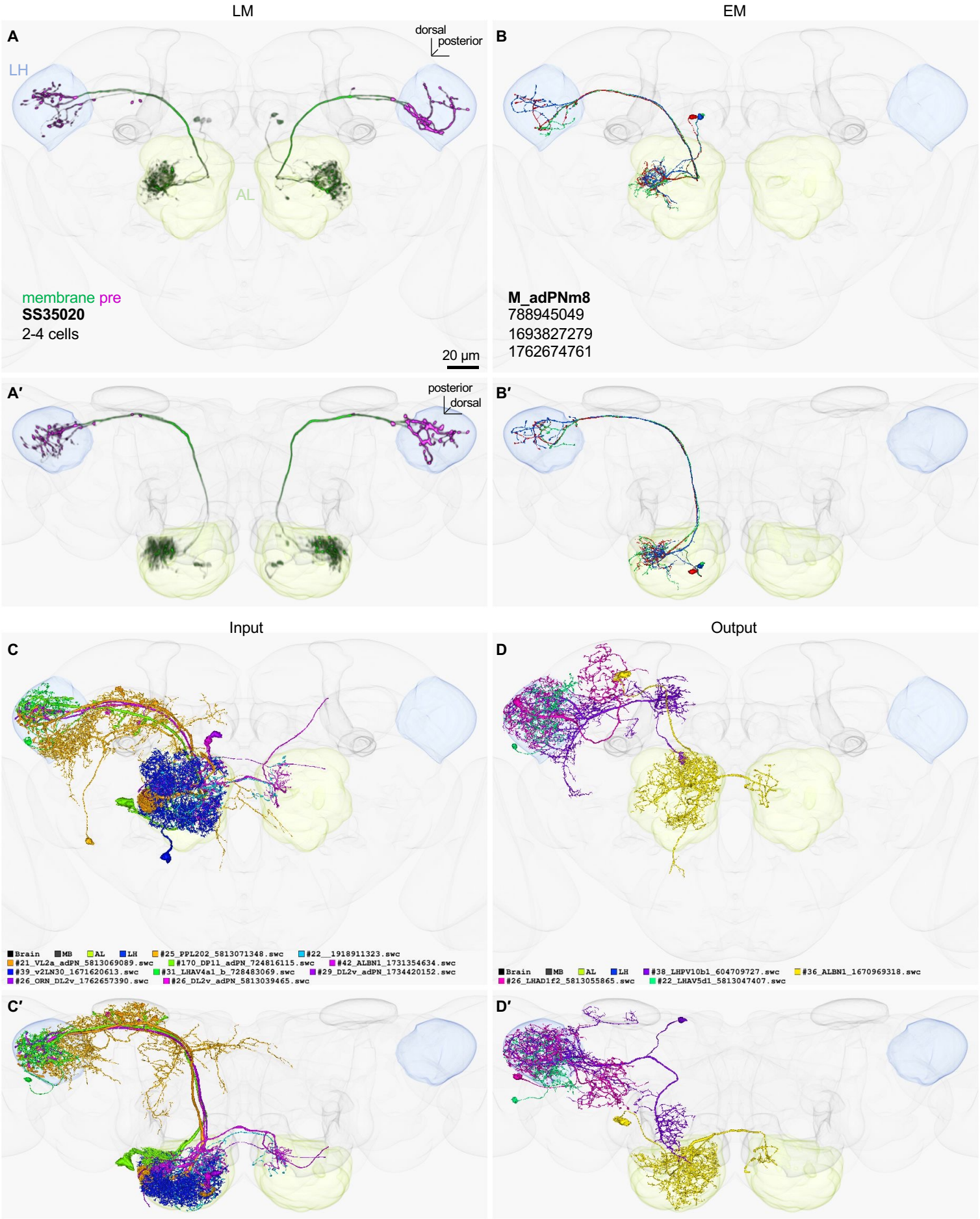


**Figure 2 – figure supplement 4**

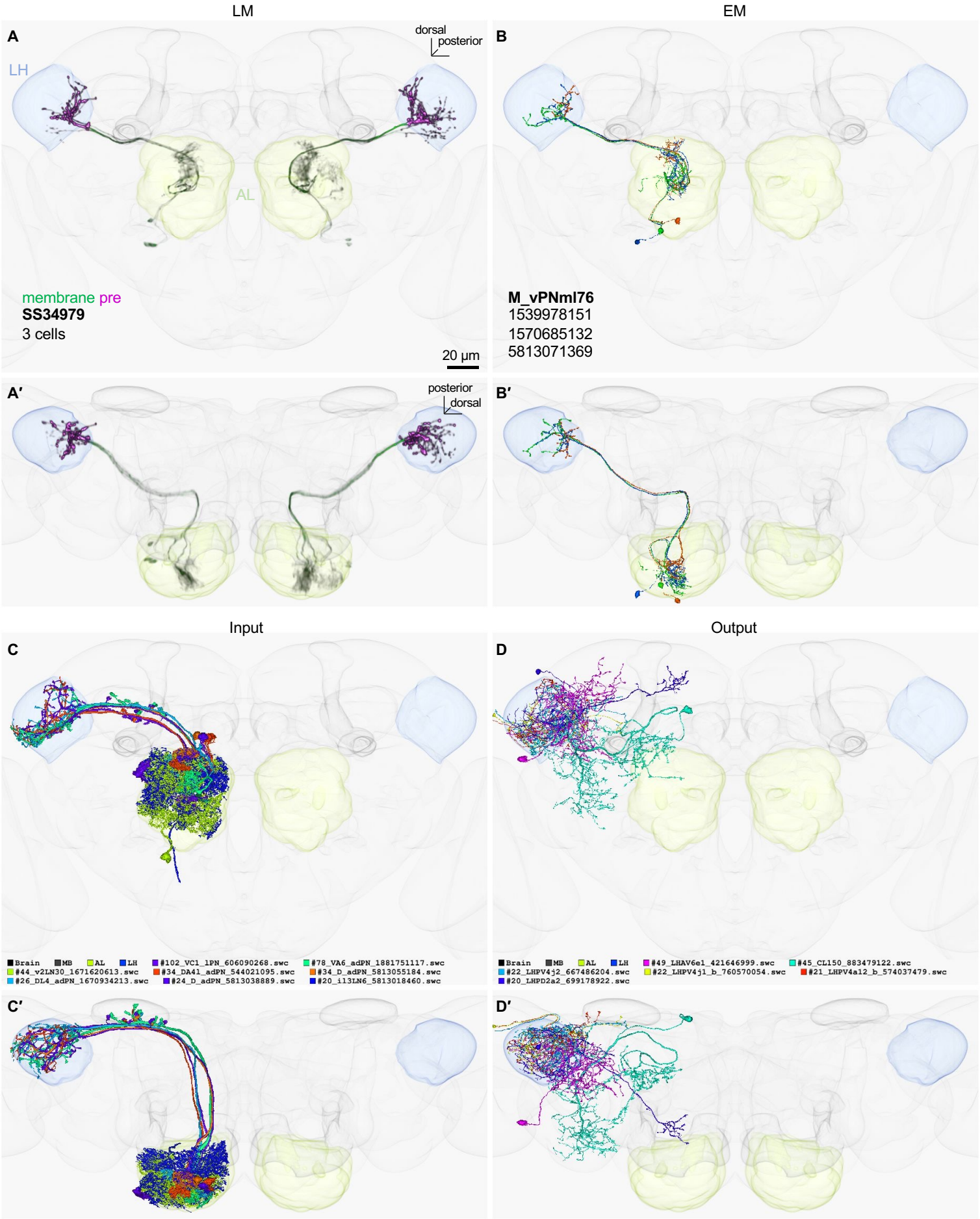


**Figure 2 – figure supplement 5**

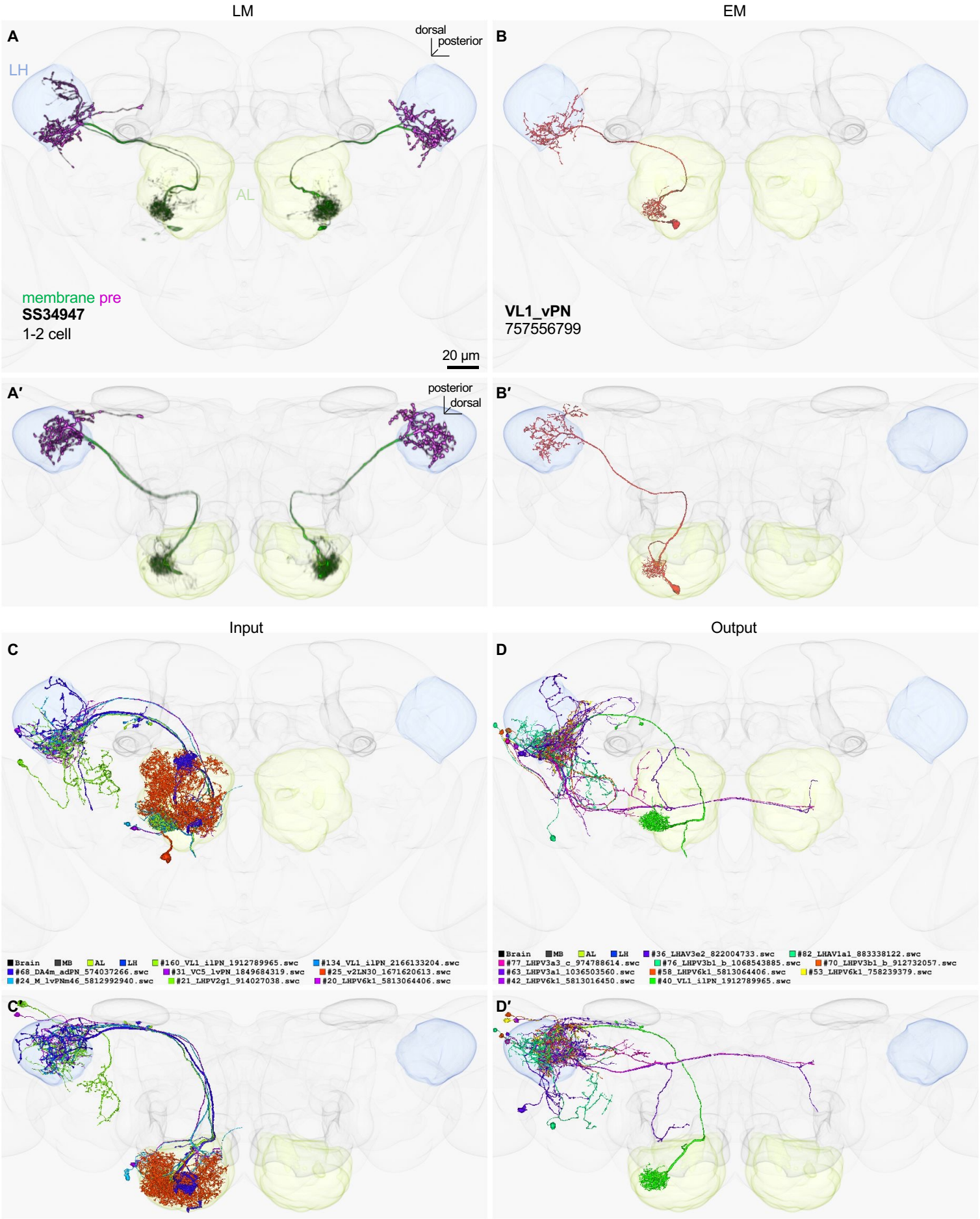


**Figure 2 – figure supplement 6**

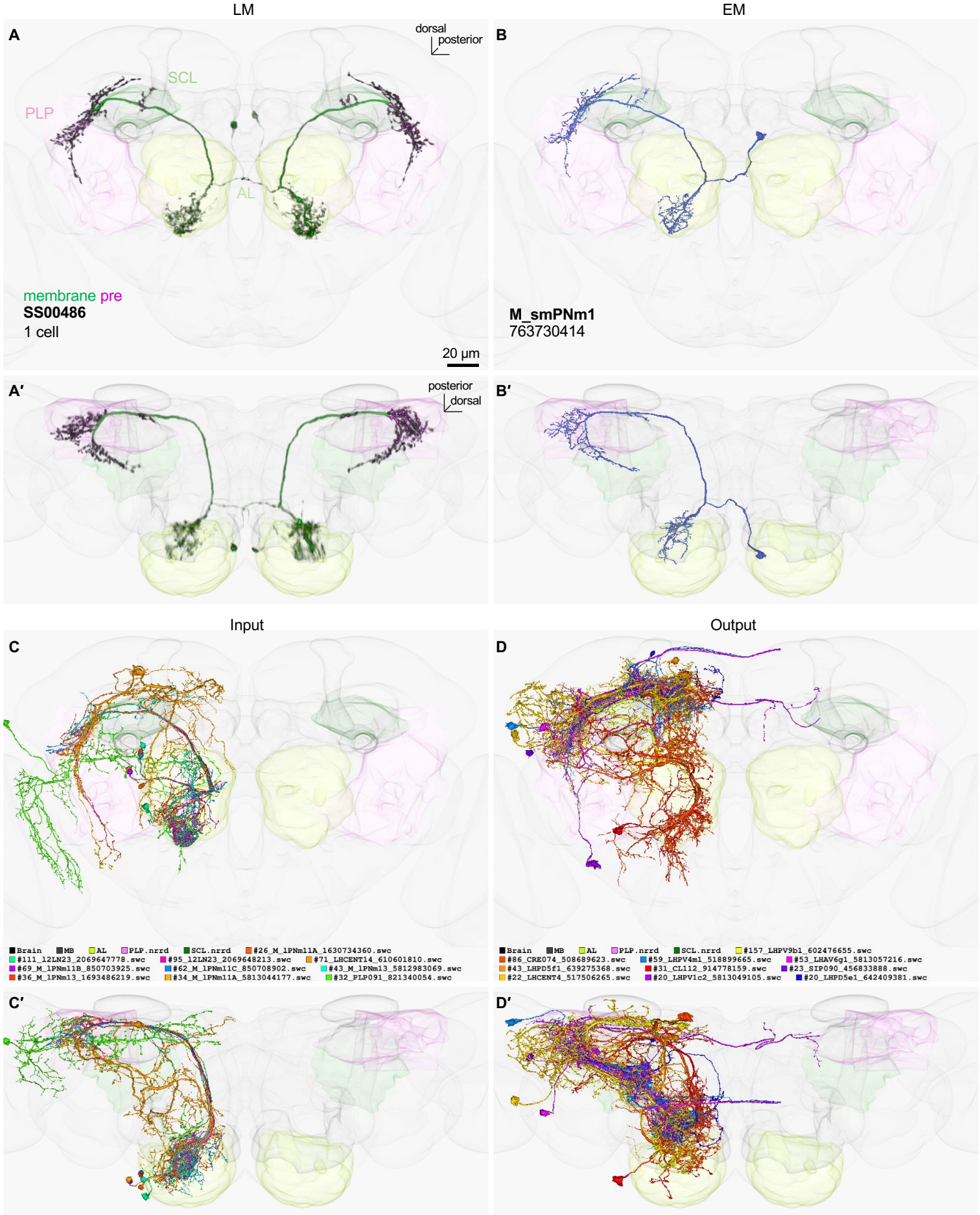


**Figure 2 – figure supplement 7**

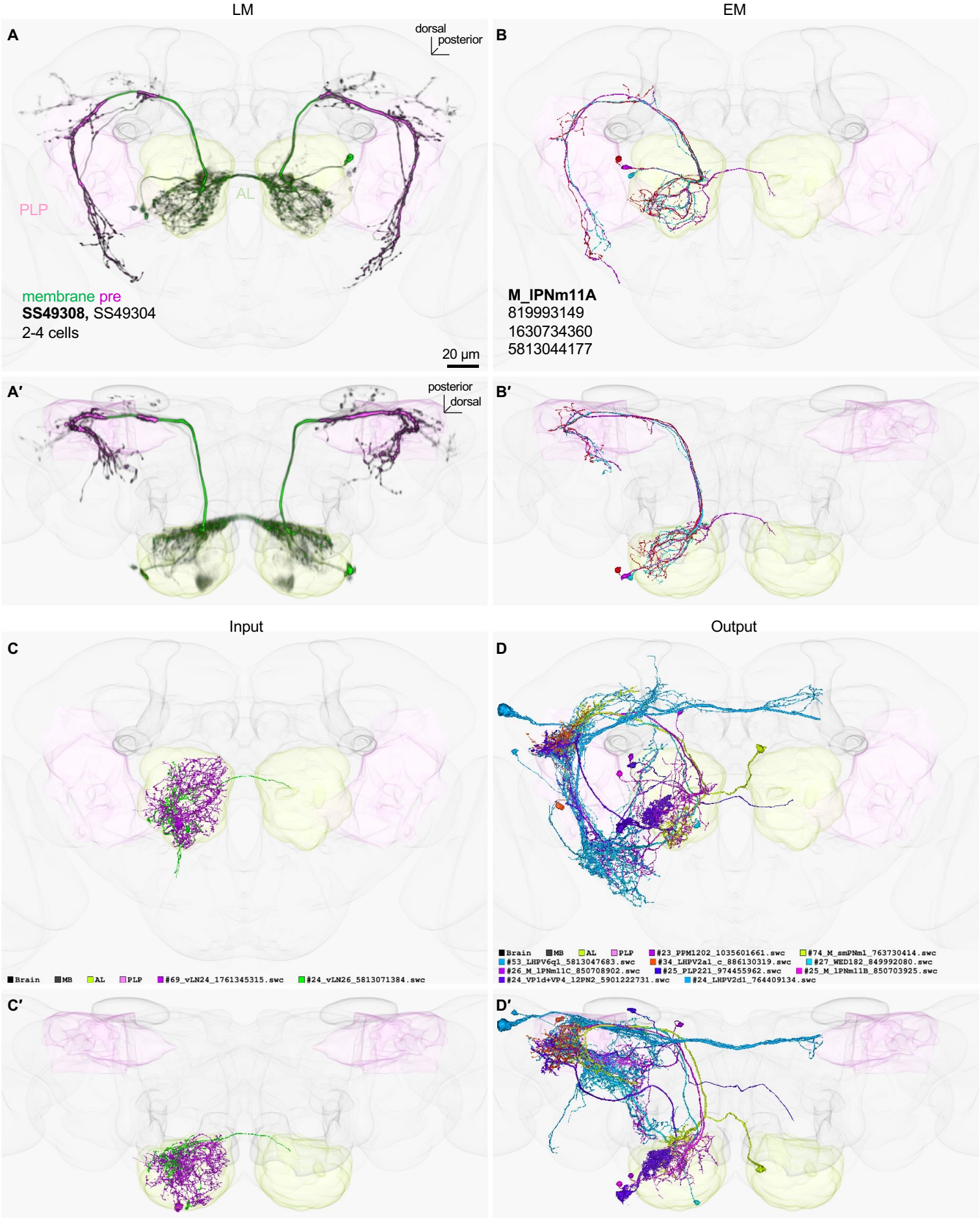


**Figure 2 – figure supplement 8**

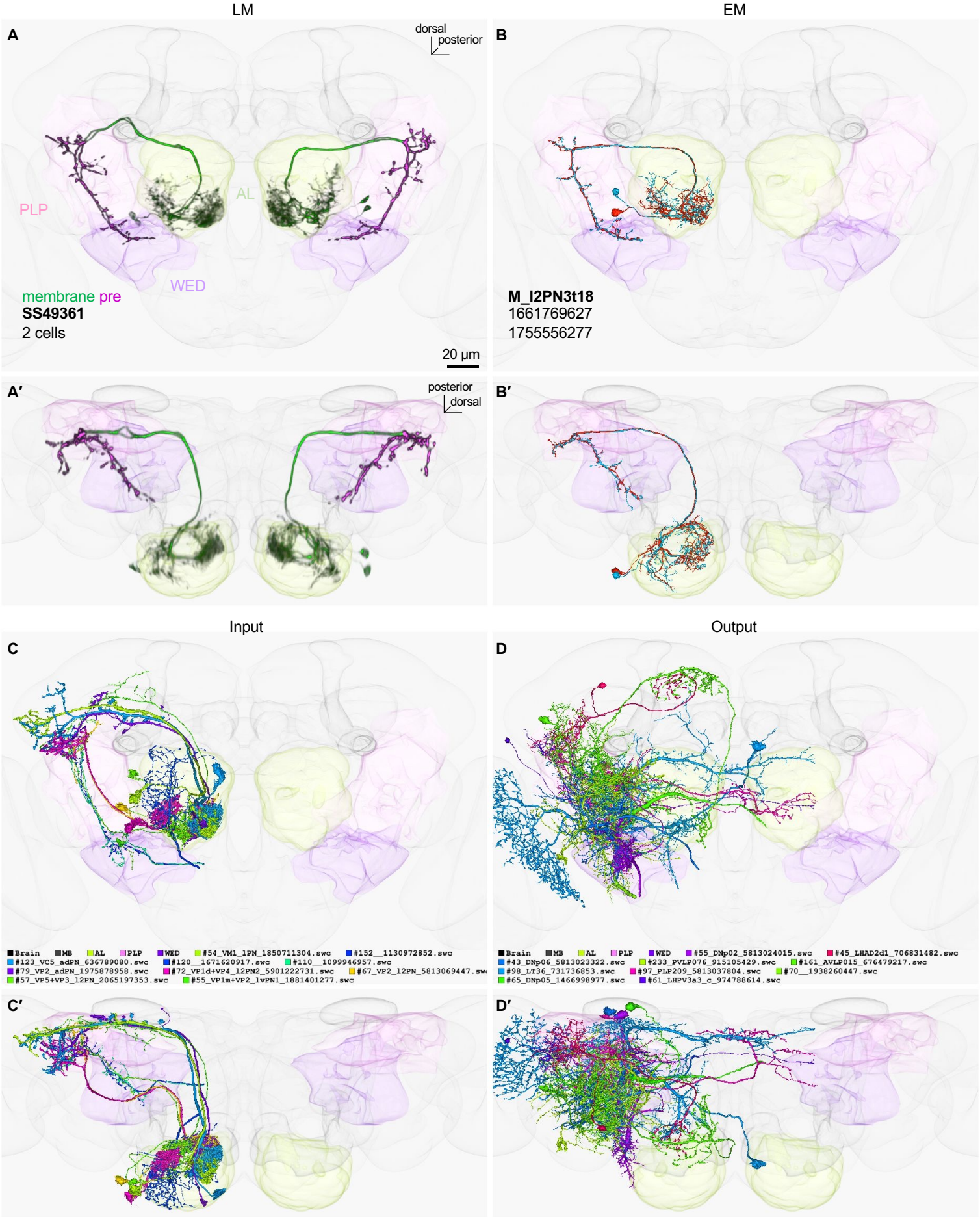


**Figure 2 – figure supplement 9**

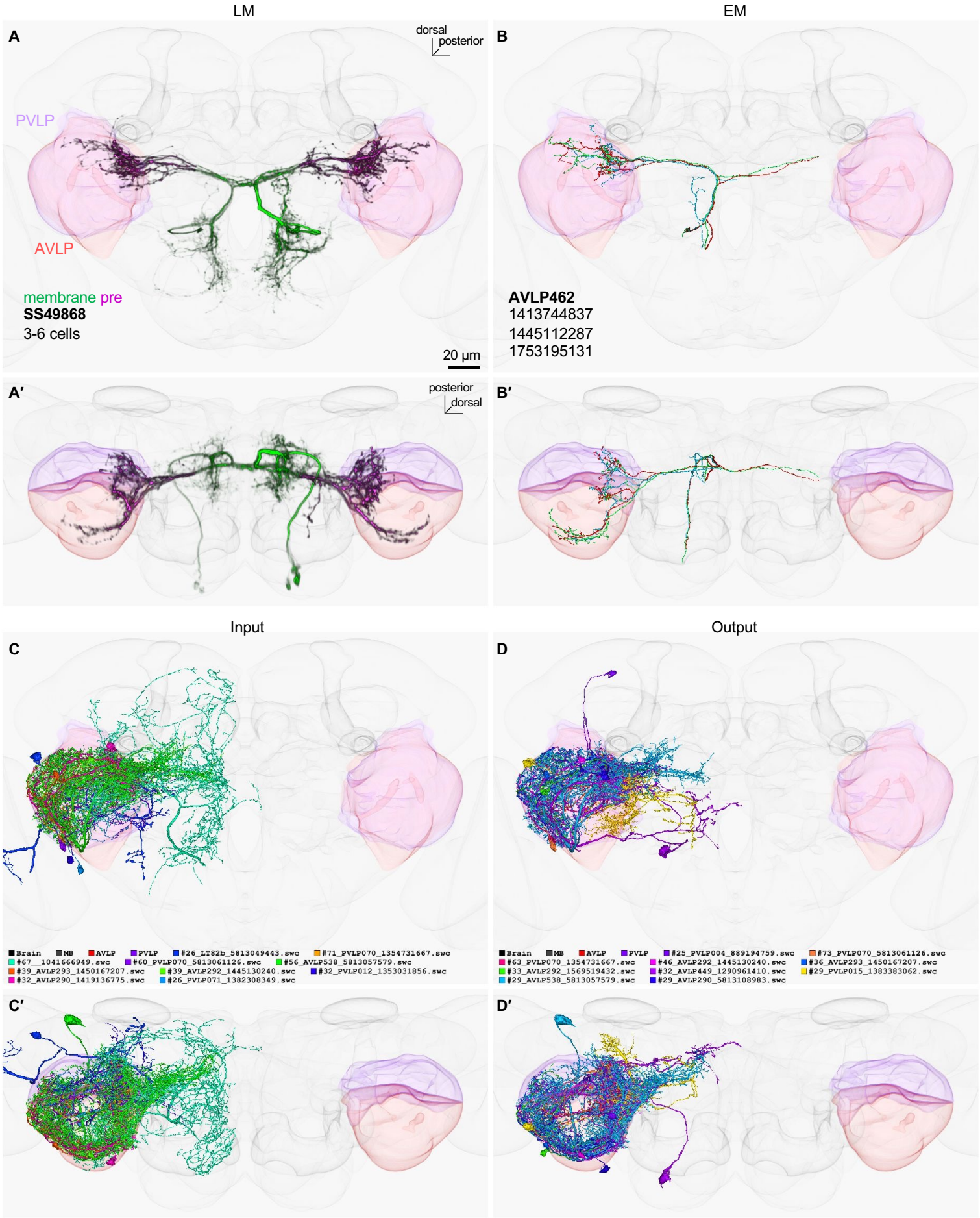


**Figure 2 – figure supplement 10**

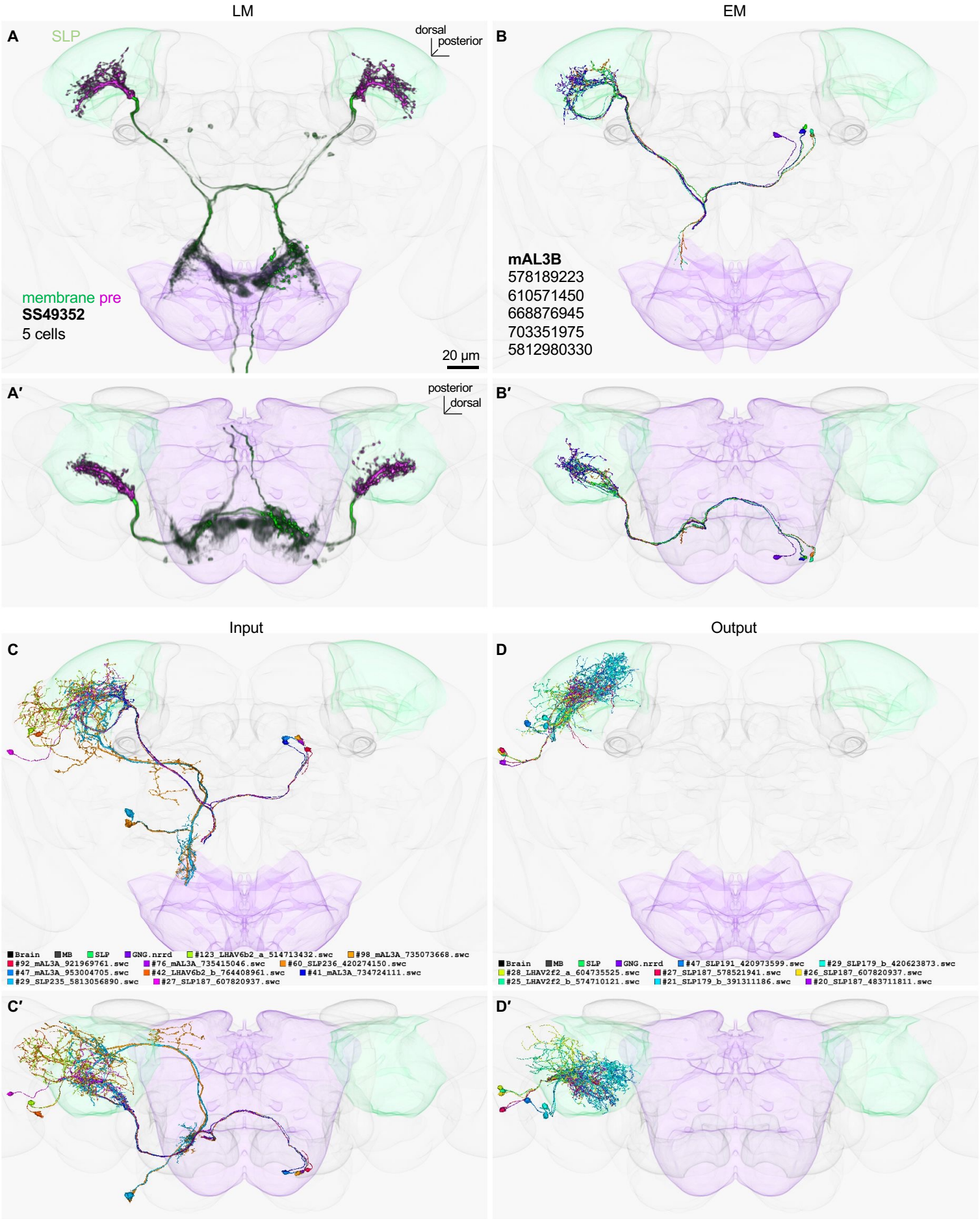


**Figure 2 – figure supplement 11**

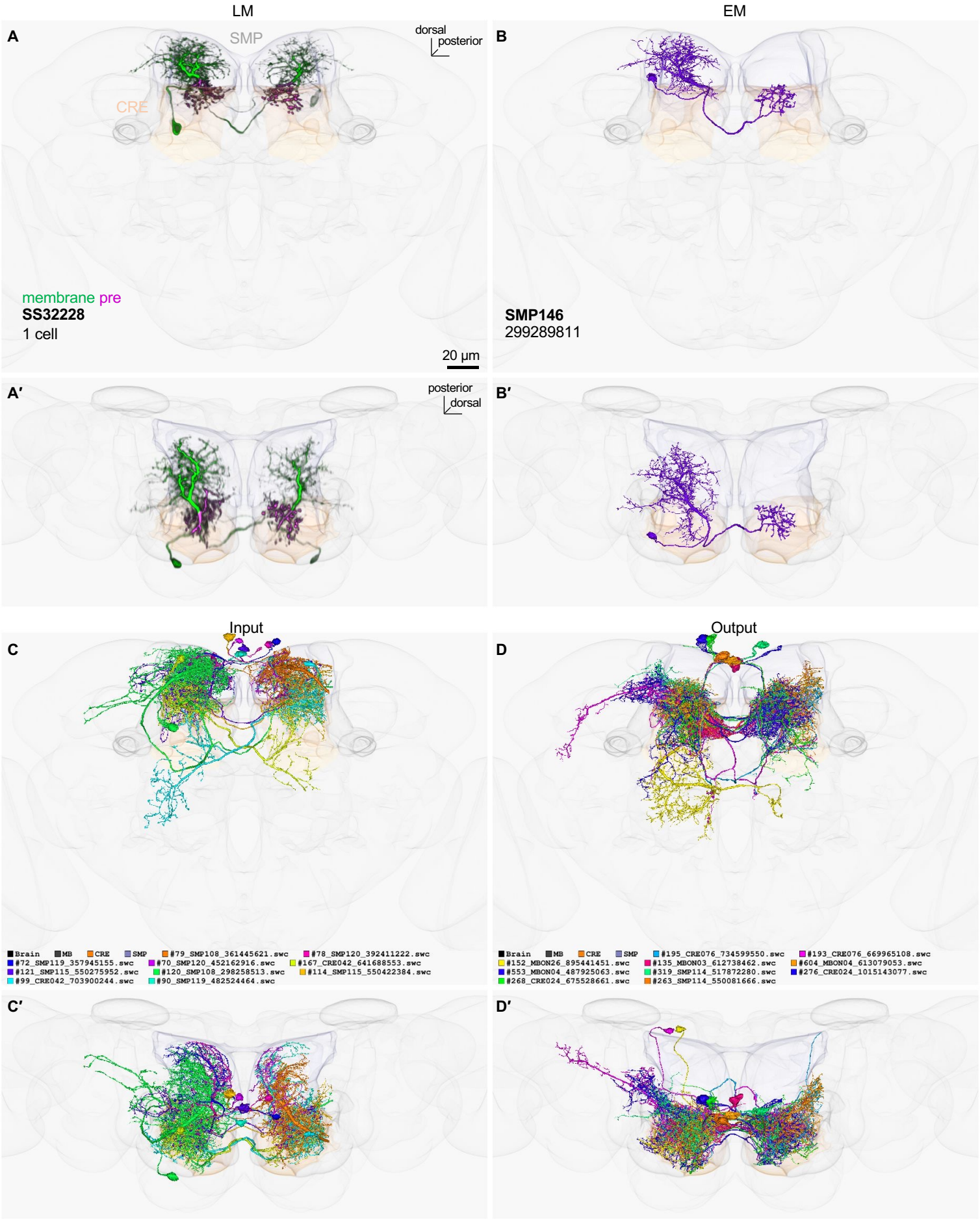


**Figure 2 – figure supplement 12**

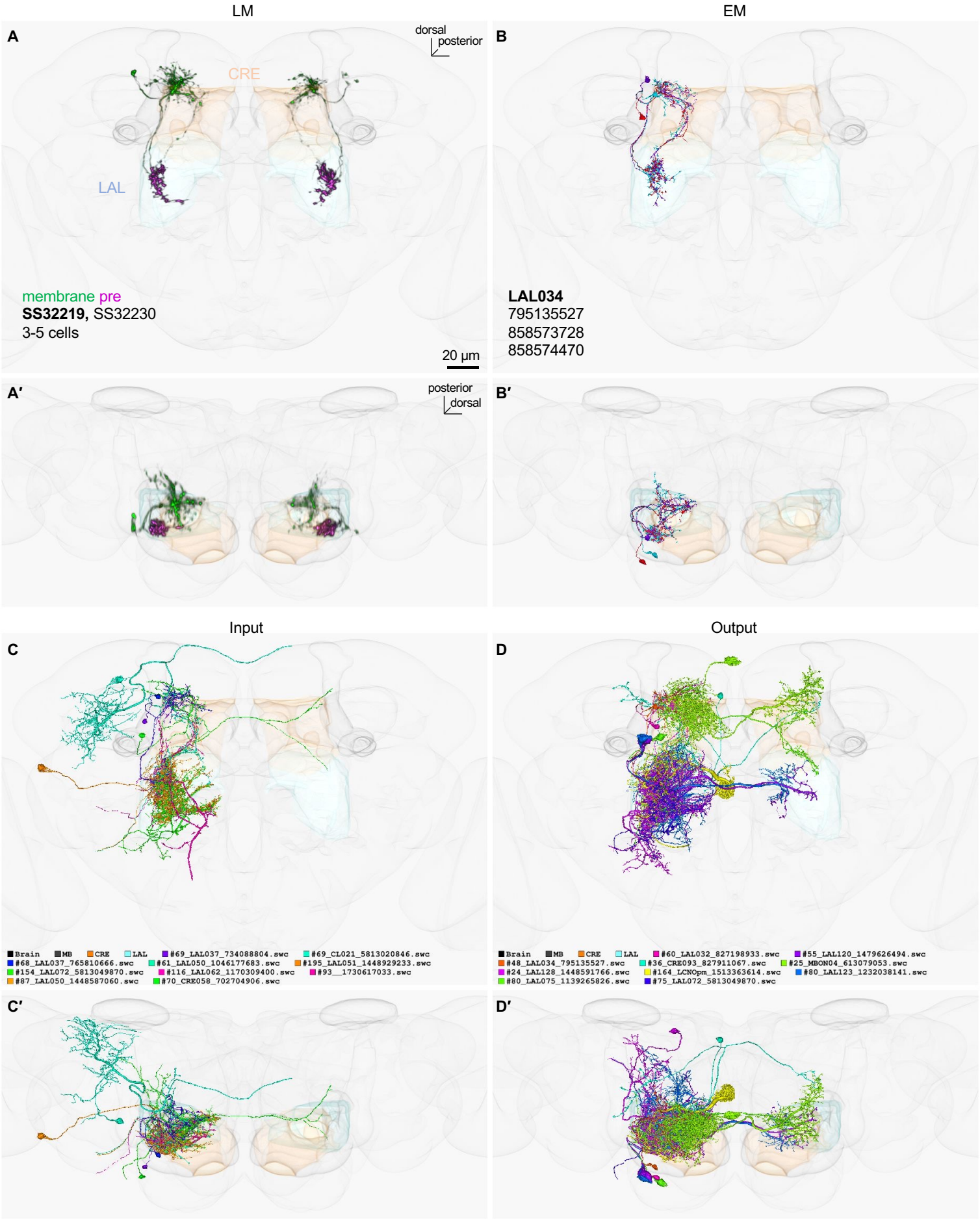


**Figure 2 – figure supplement 13**

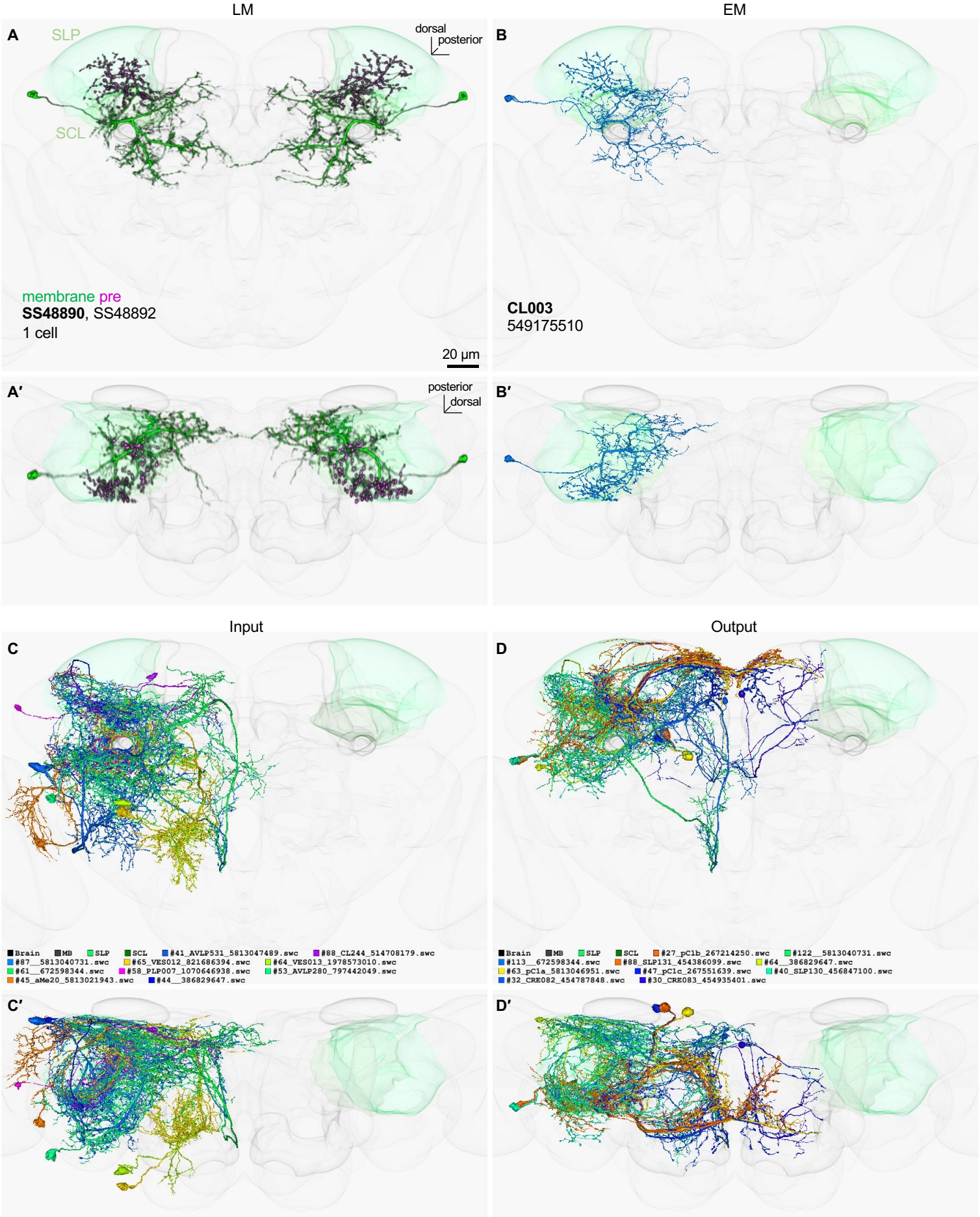


**Figure 2 – figure supplement 14**

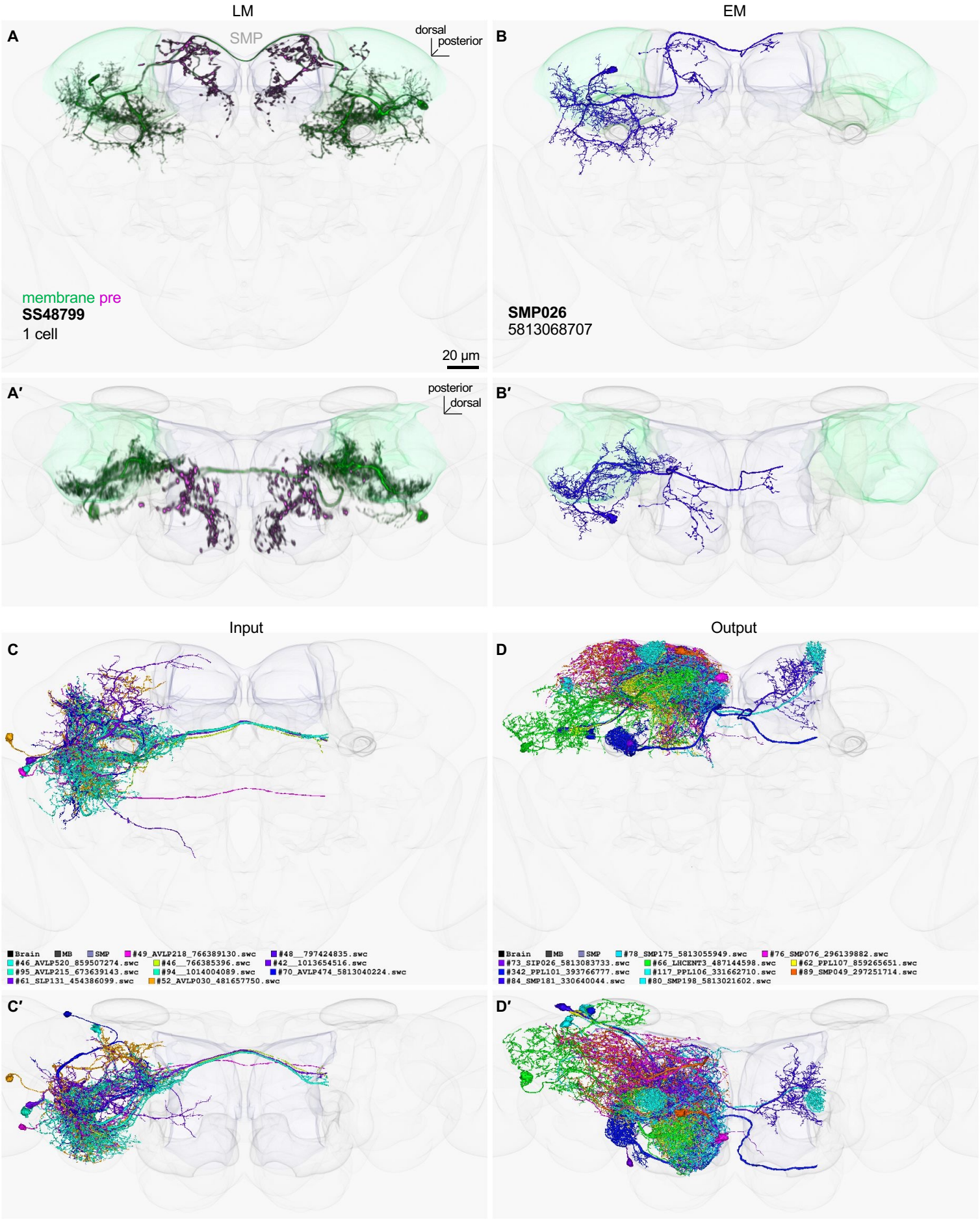


**Figure 2 – figure supplement 15**

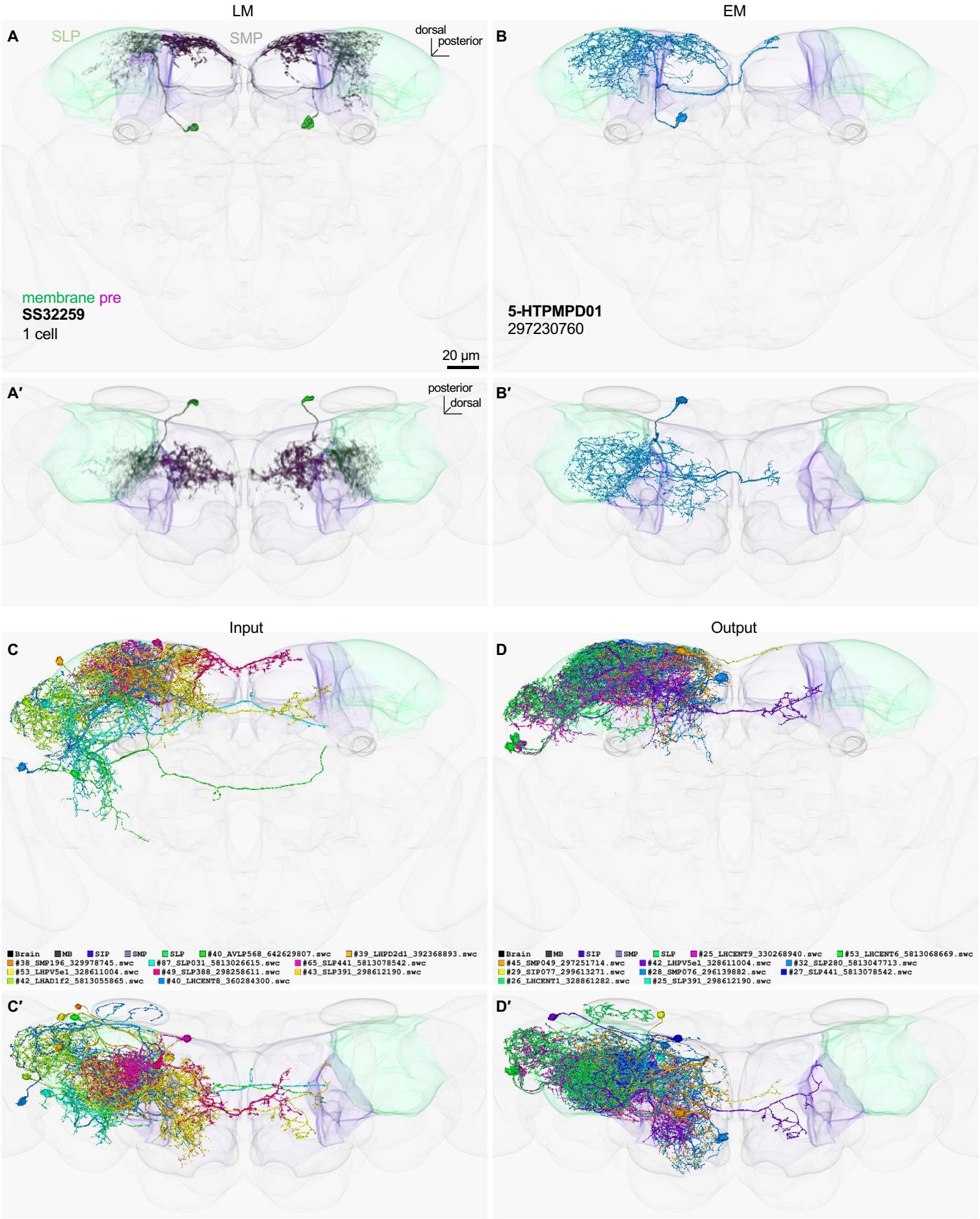


**Figure 2 – figure supplement 16**

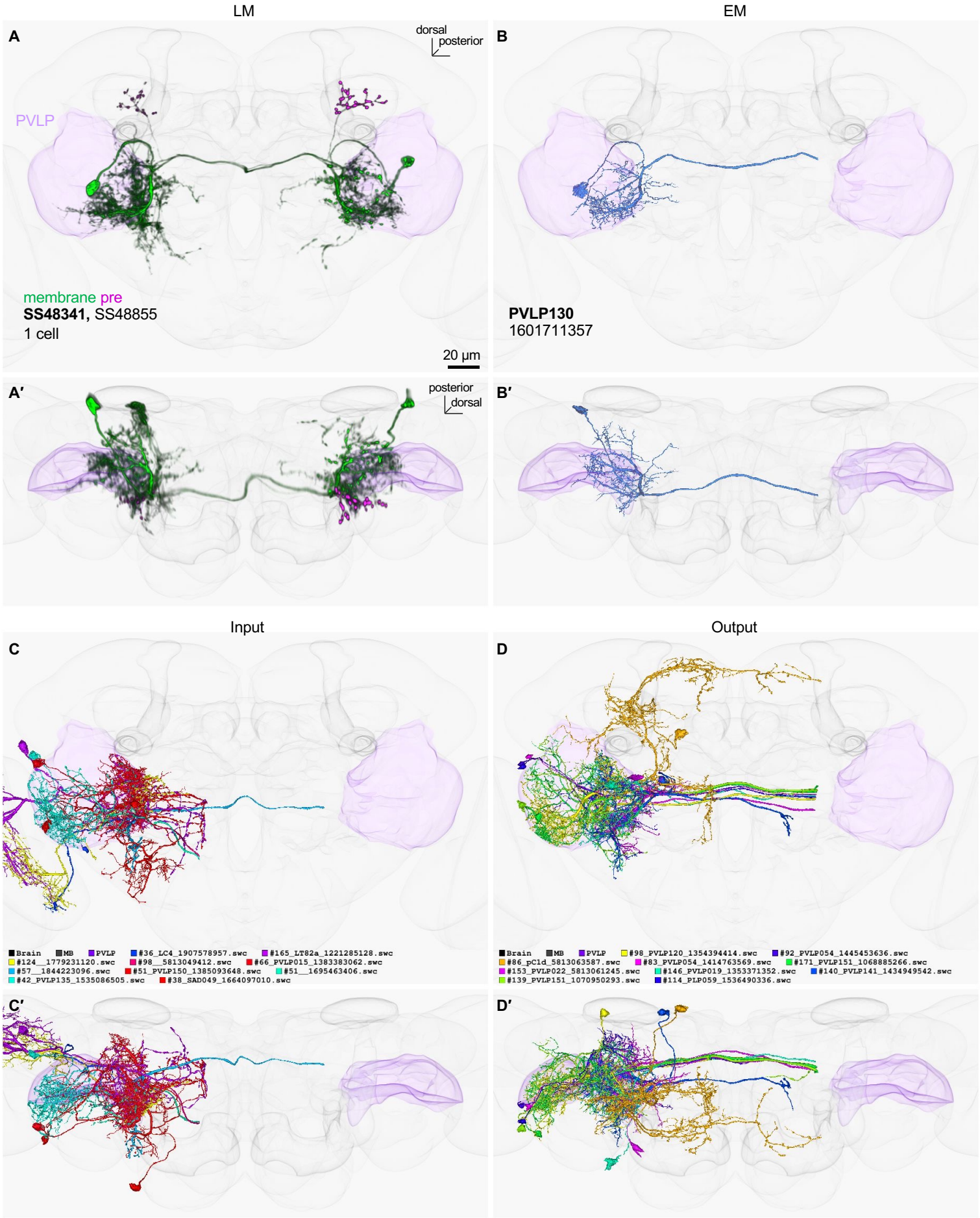


**Figure 2 – figure supplement 17**

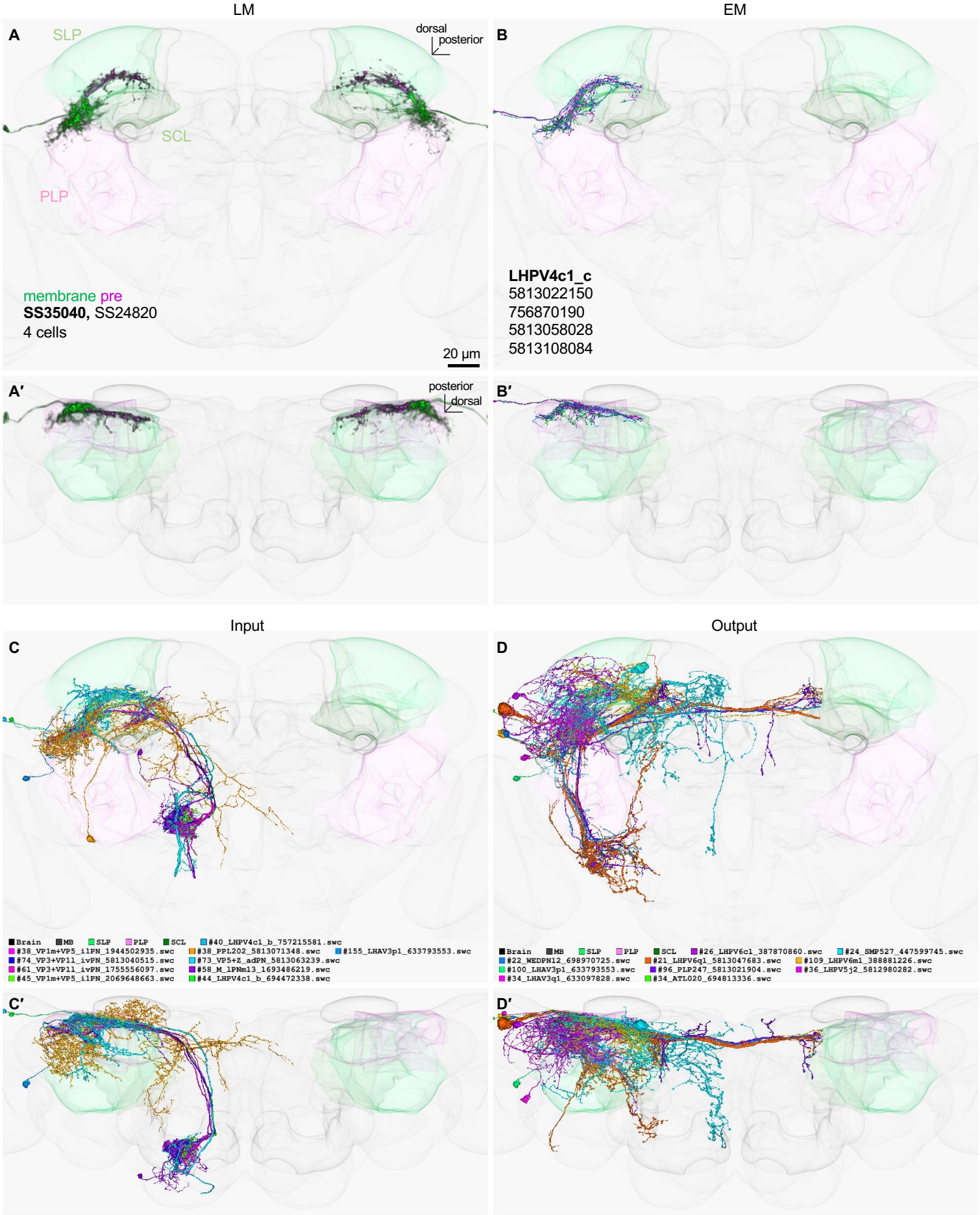


**Figure 2 – figure supplement 18**

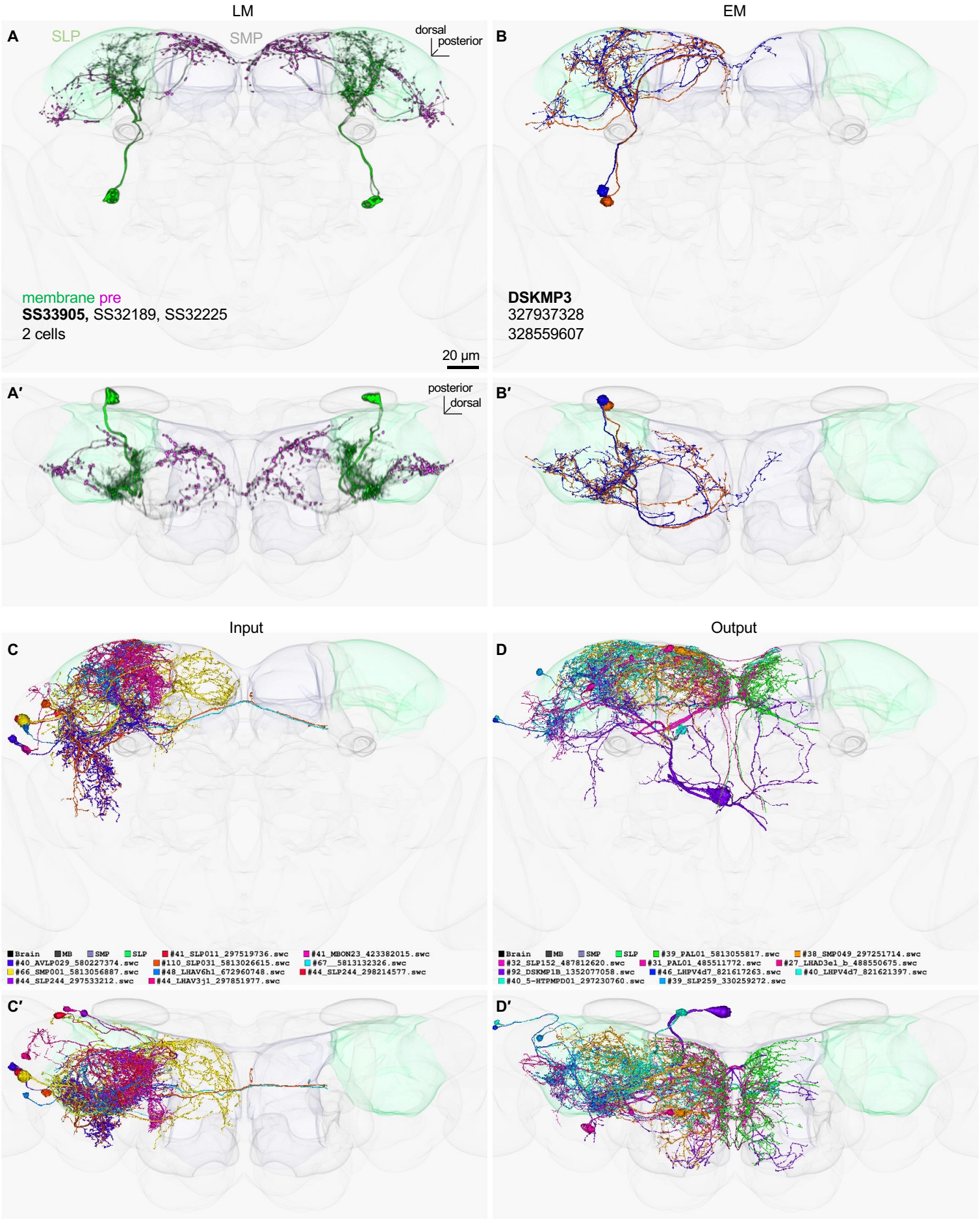


**Figure 2 – figure supplement 19**

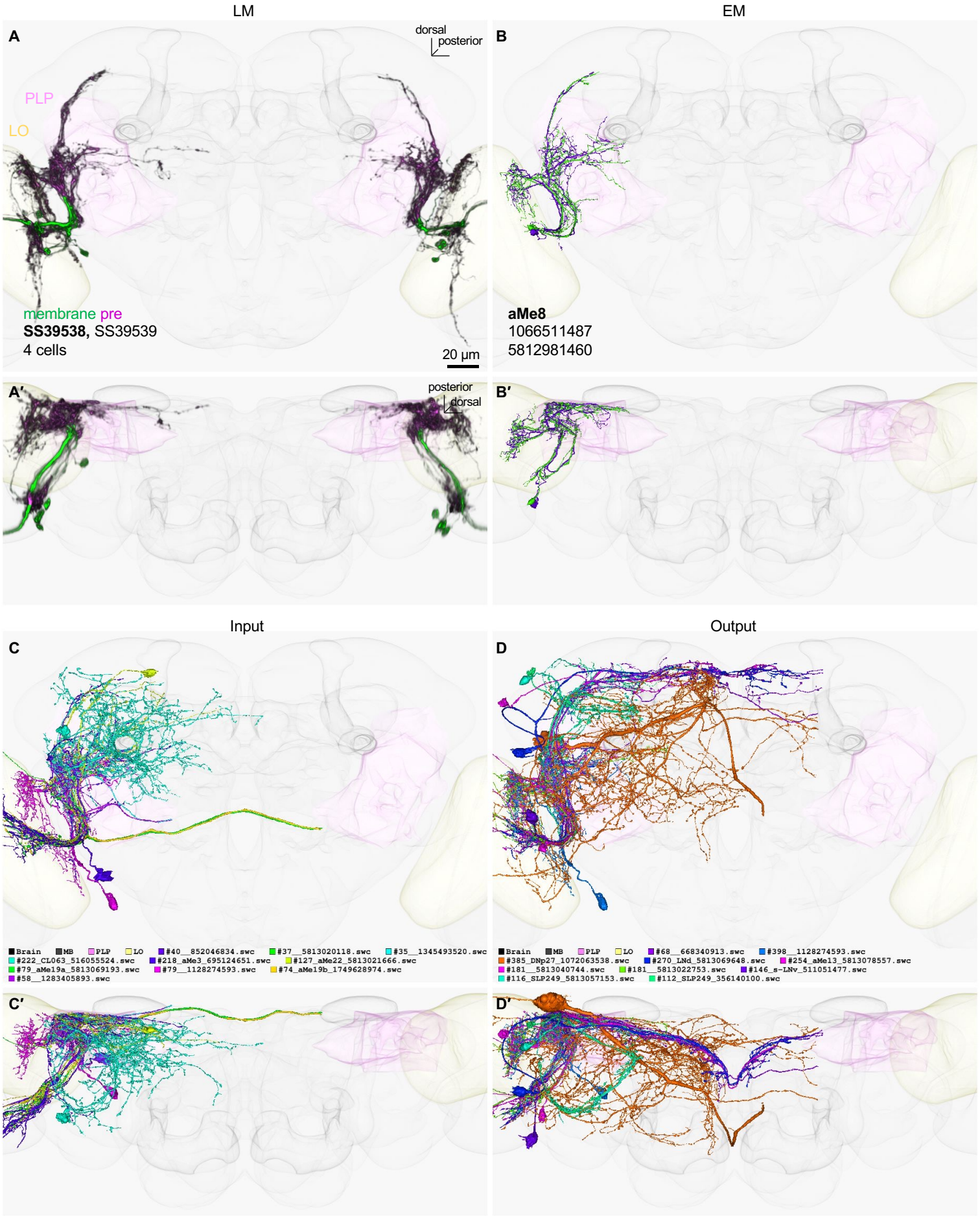


**Figure 2 – figure supplement 20**

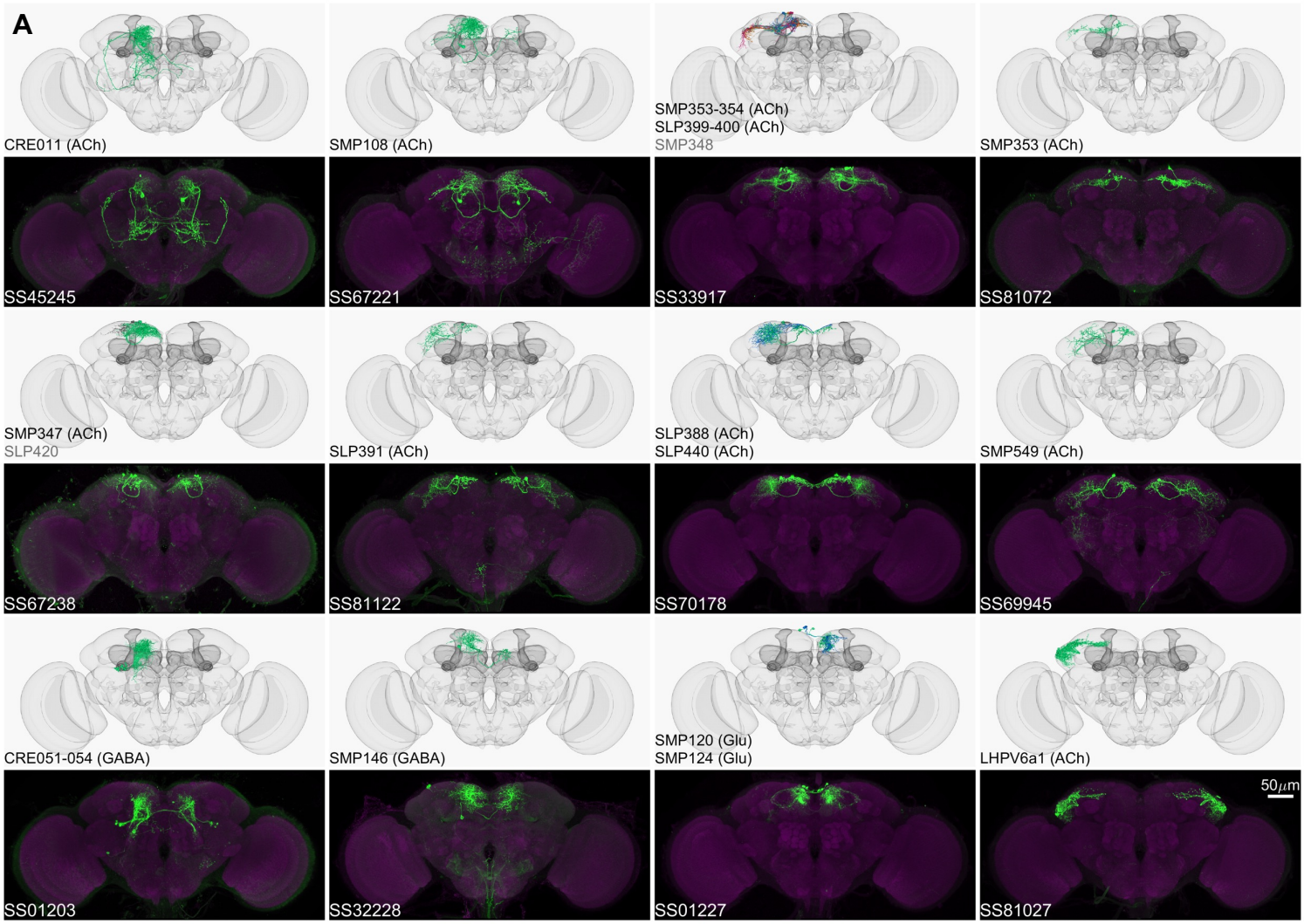


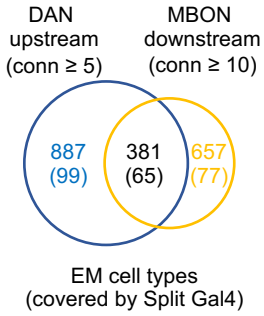


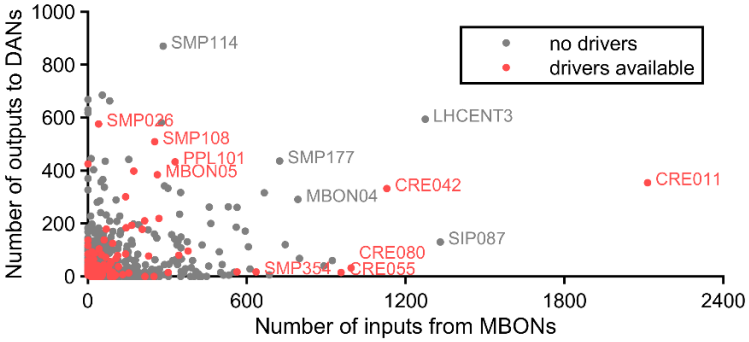


**Figure 3 Drivers for MBON downstream and DAN upstream neurons.**

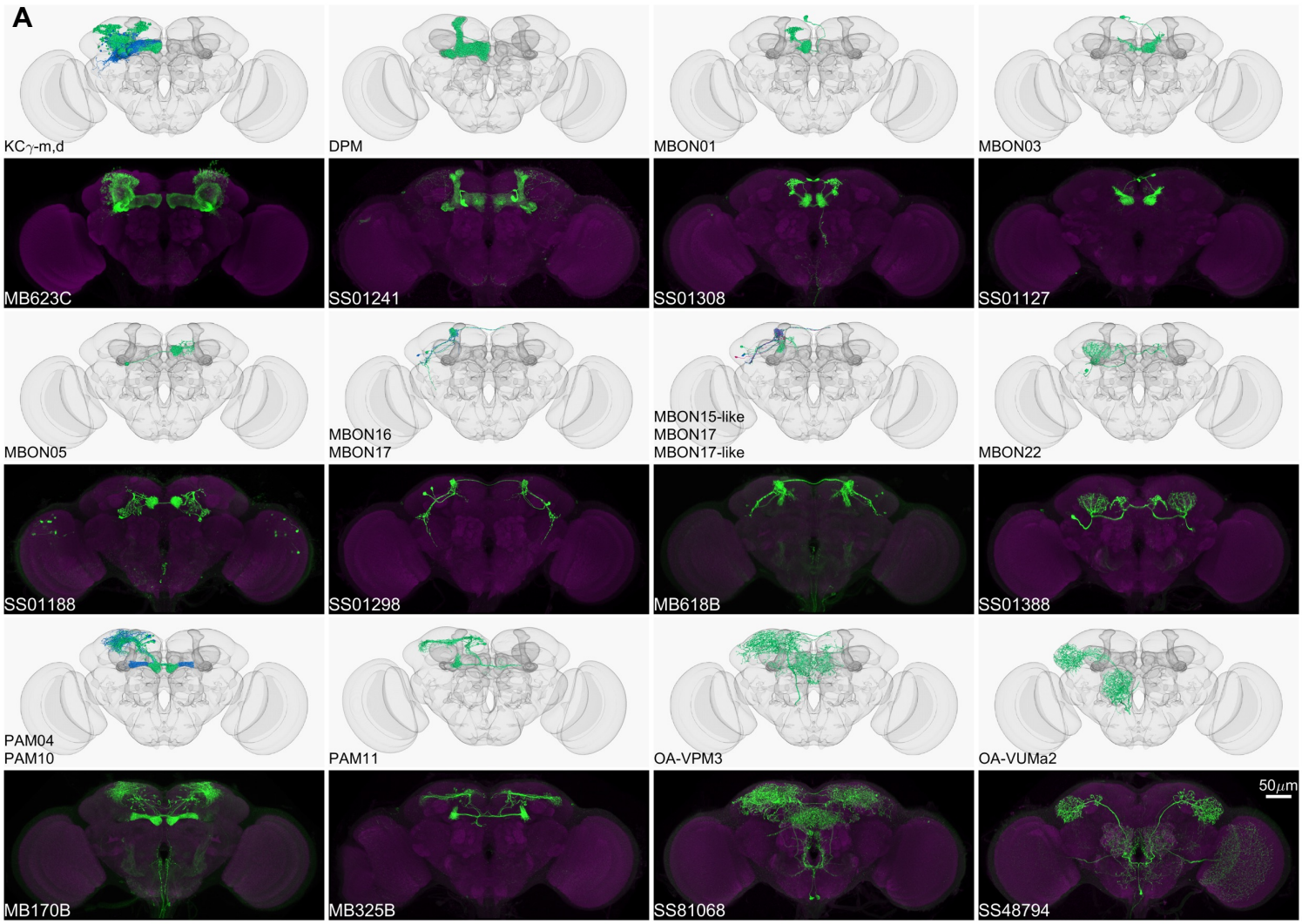


**B**

| MB cell types | Covered cell types | Total cell types | Missed cell types |
|---|---|---|---|
| Intrinsic neurons (excluding KCs) | 1 | 2 | APL |
| MBONs | 33 | 37 | MBON24-25, 27, 34 |
| DANs | 18 | 23 | PPL102, 201-202, PAM09,15 |
| Other modulatory | 6 | 6 | |
| Total | 58 | 68 | |

**Figure 3-supplemental figure 1 New or improved drivers for MB cell types**

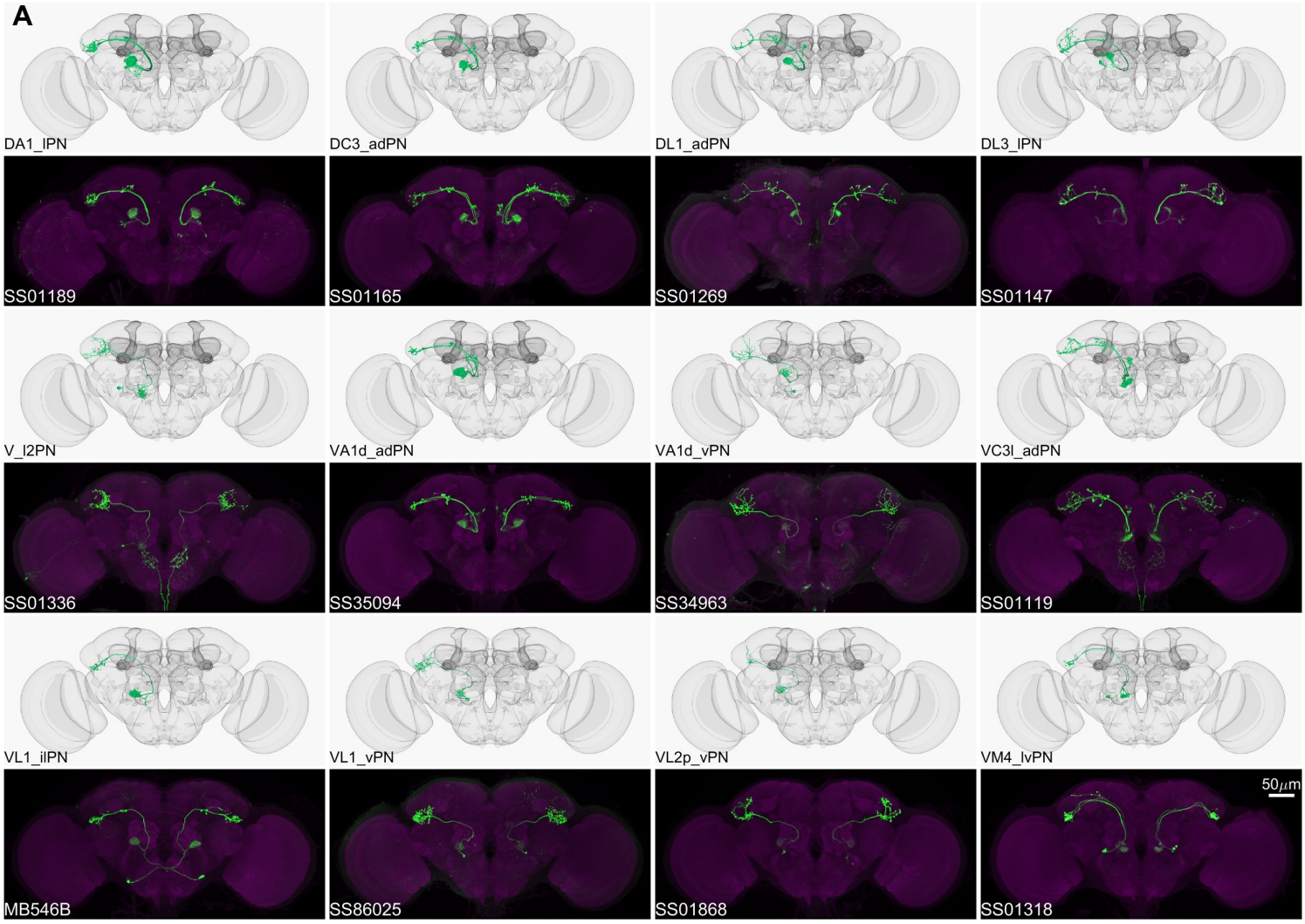


**B**

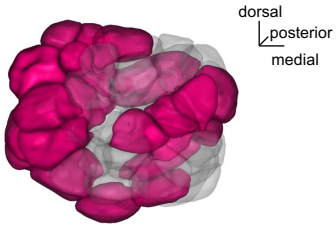


**C**

| PN types | Covered cell types | Total cell types |
|---|---|---|
| Olfactory uni-glomerular PNs | 26 | ~80 |
| Multi-glomerular PNs and non-olfactory PNs | > 22 | ~110 |
| Total | > 48 | ~190 |

**Figure 4 Driver lines for uni-glomerular projection neurons**

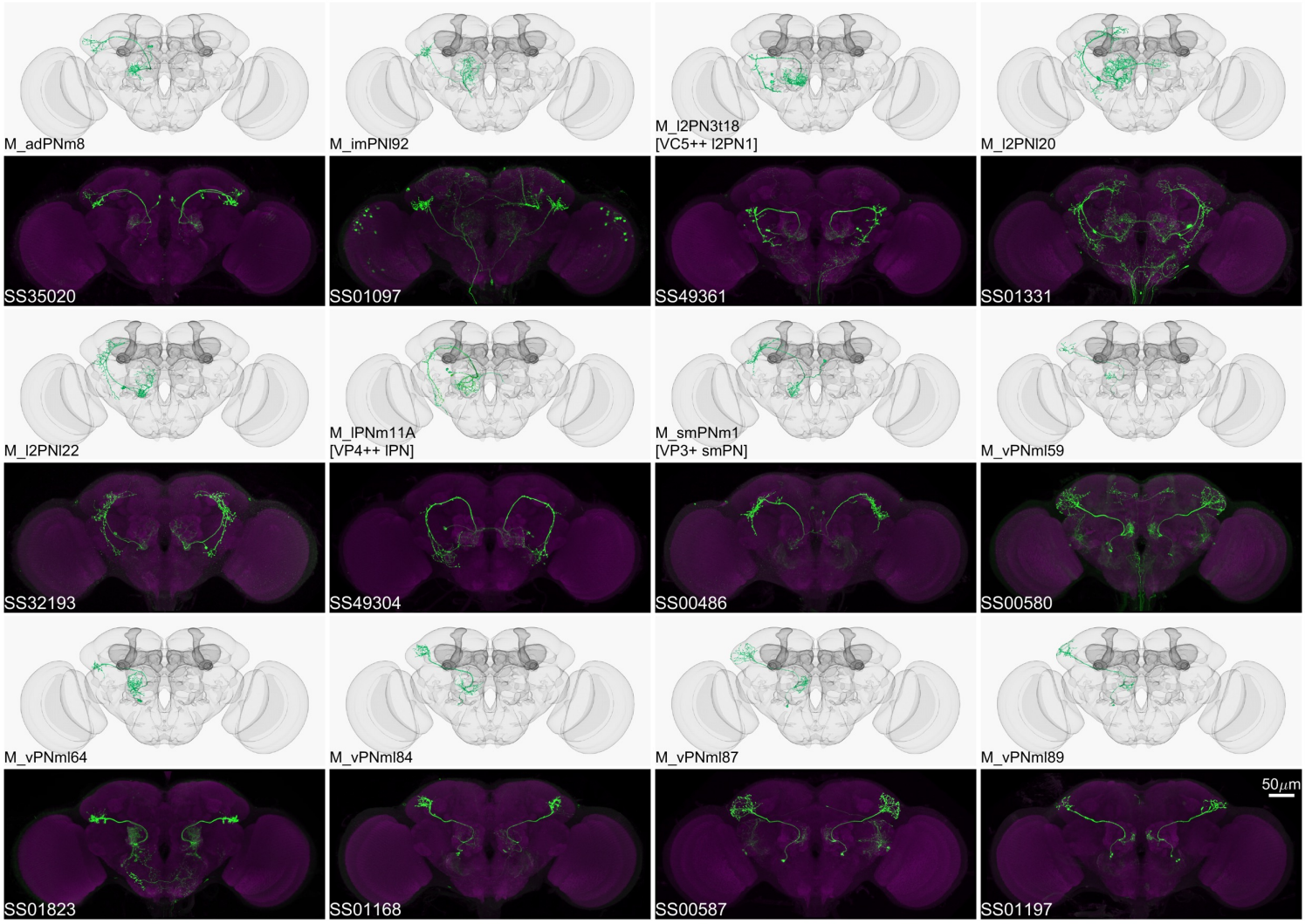


**Figure 5 Driver lines for multi-glomerular projection neurons**

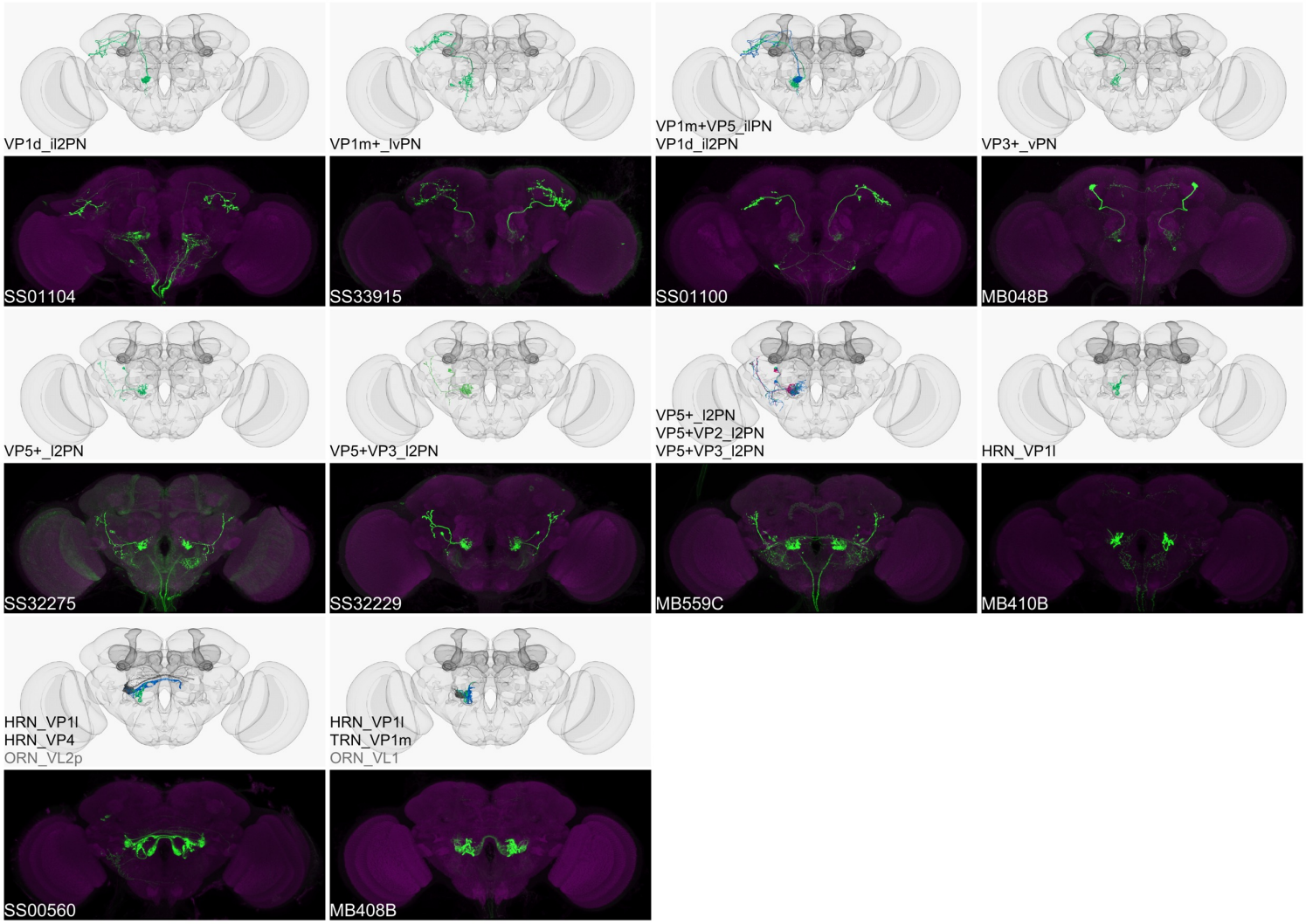


**Figure 6 Driver lines for non-olfactory projection neurons and sensory neurons**

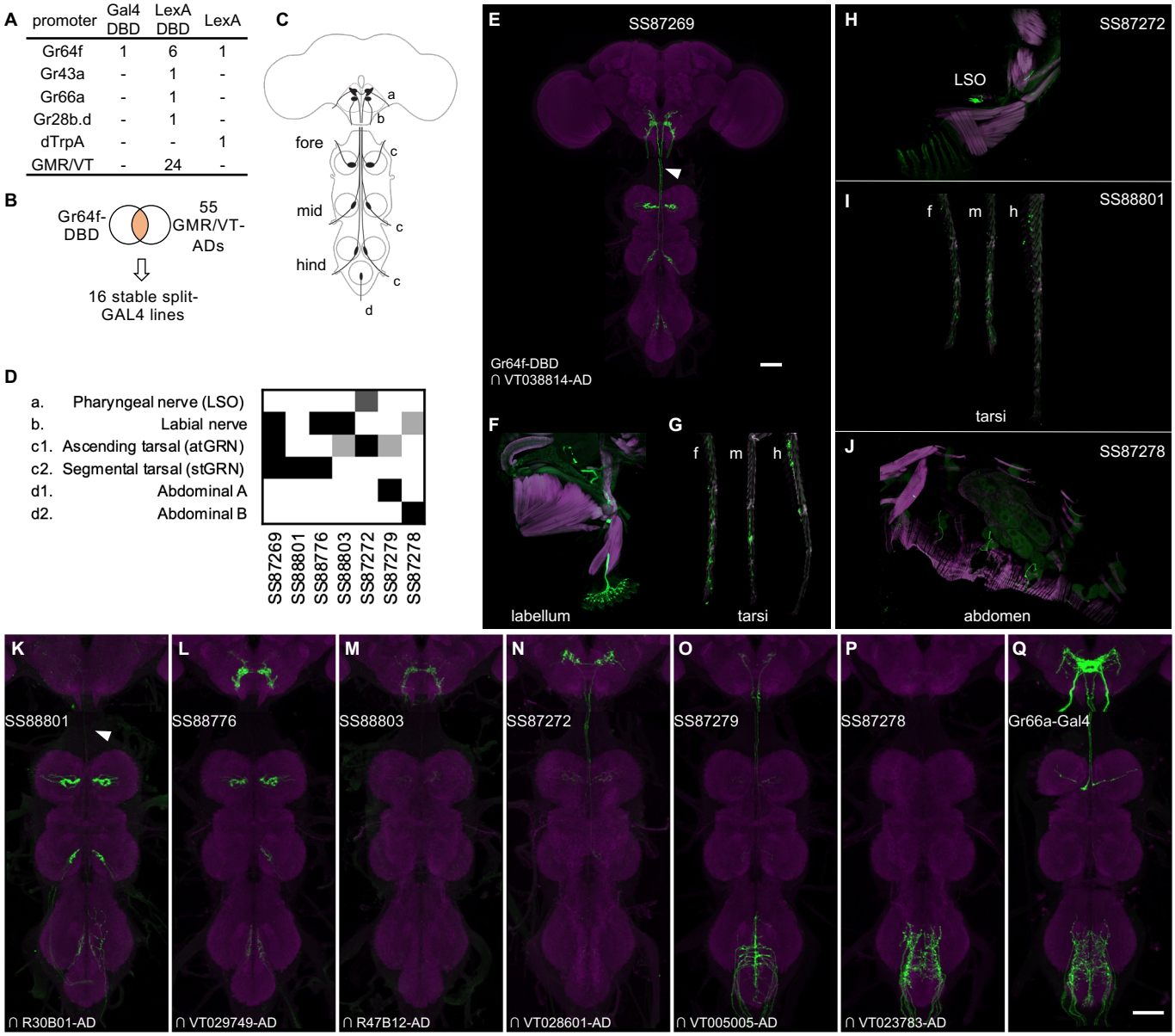


**Figure 7 Driver lines for gustatory sensory neurons**

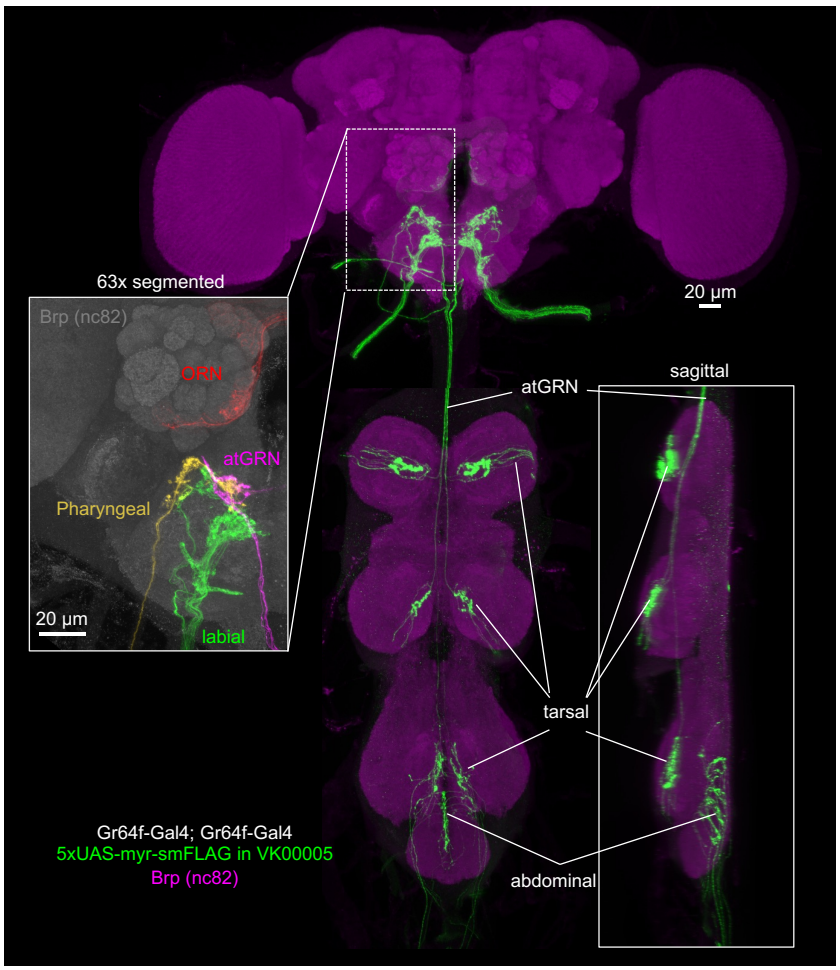


**Figure 7-figure supplement 1 Expression pattern of Gr64f-Gal4**

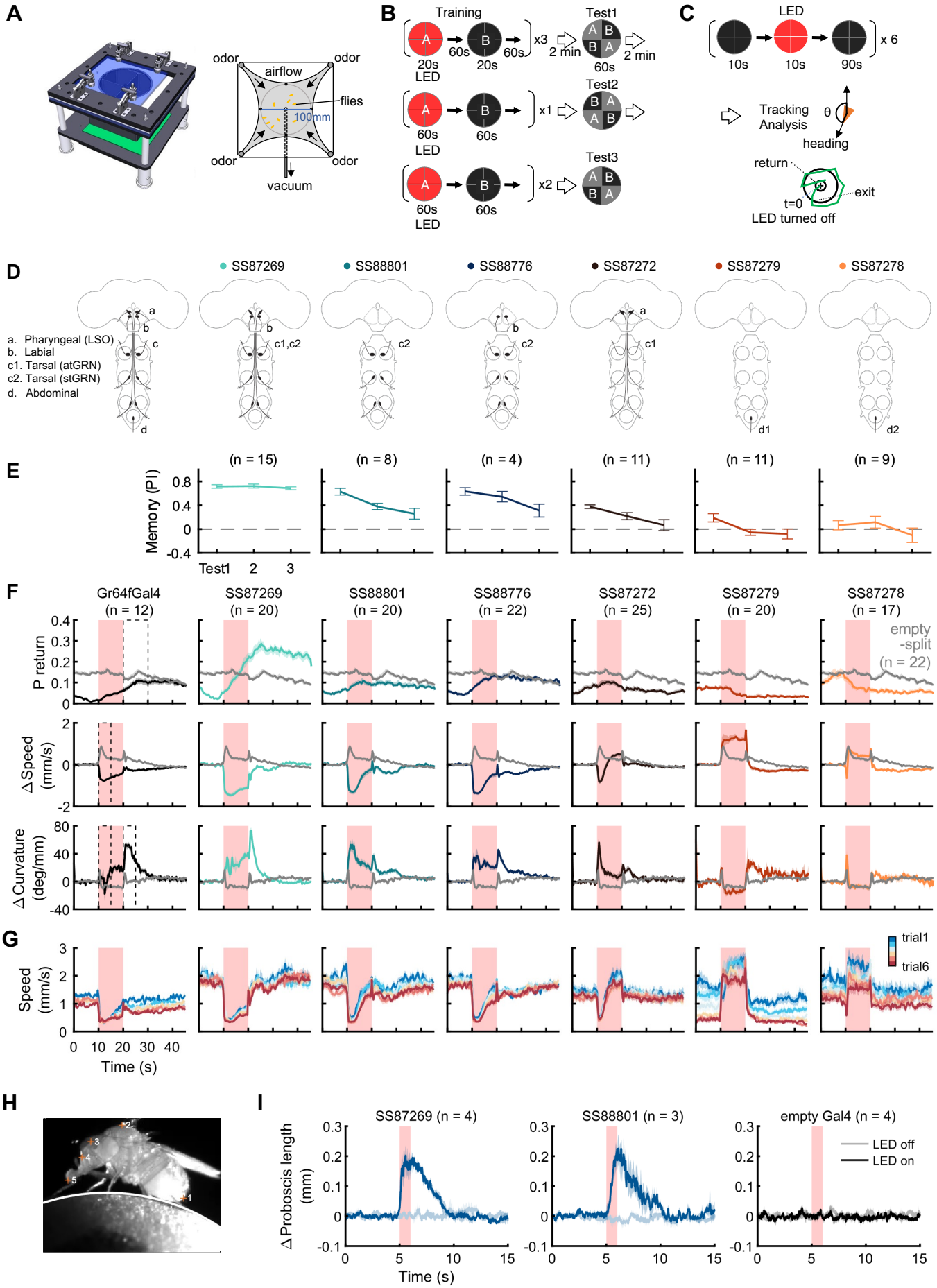


**Figure 8 Behaviors with Gr64f-split-GAL4 lines**

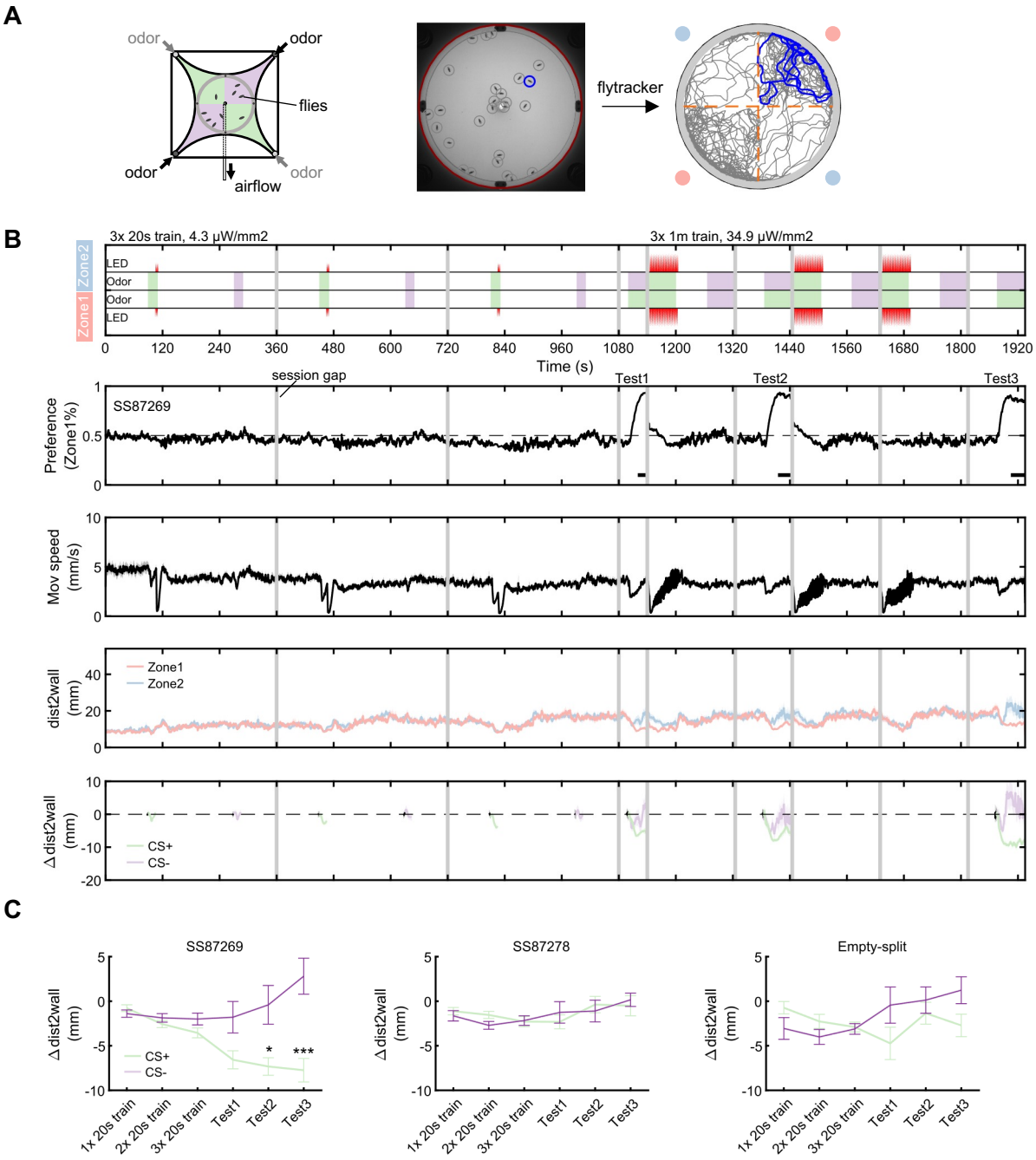


**Figure 8-figure supplement 1 Olfactory arena learning experiment, fly tracking and data analysis**

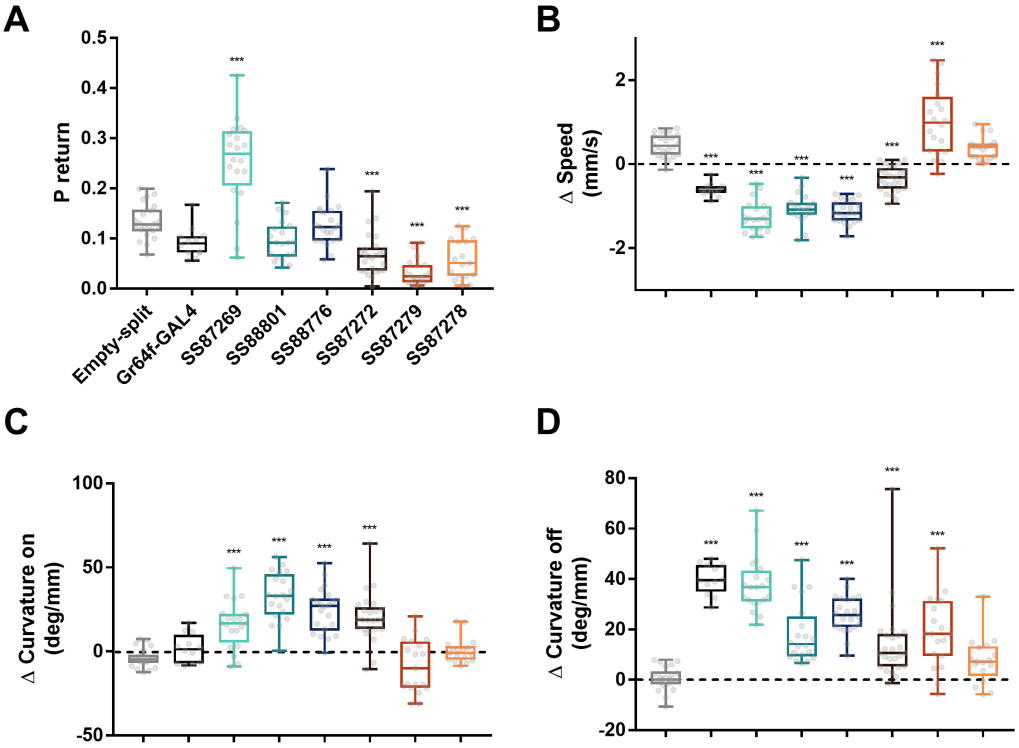


**Figure 8-figure supplement 2 Summary data of Gr64f-split-Gal4 activation phenotypes**

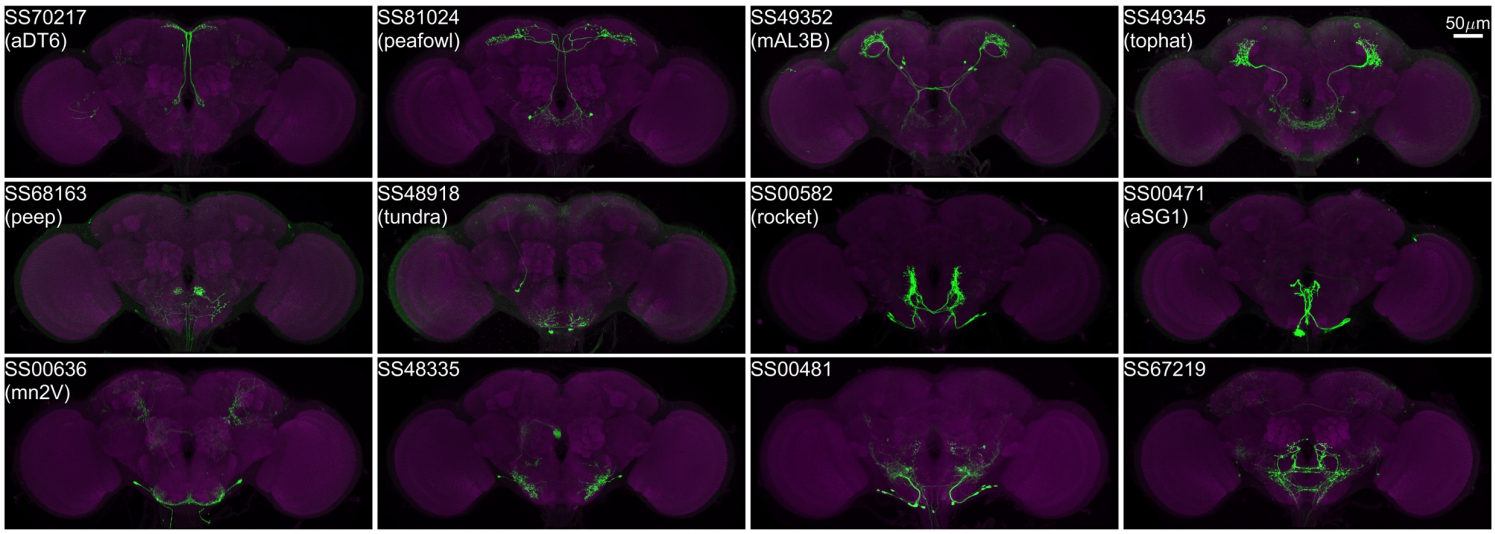


**Figure 8-figure supplement 3 Examples of covered SEZ neurons**

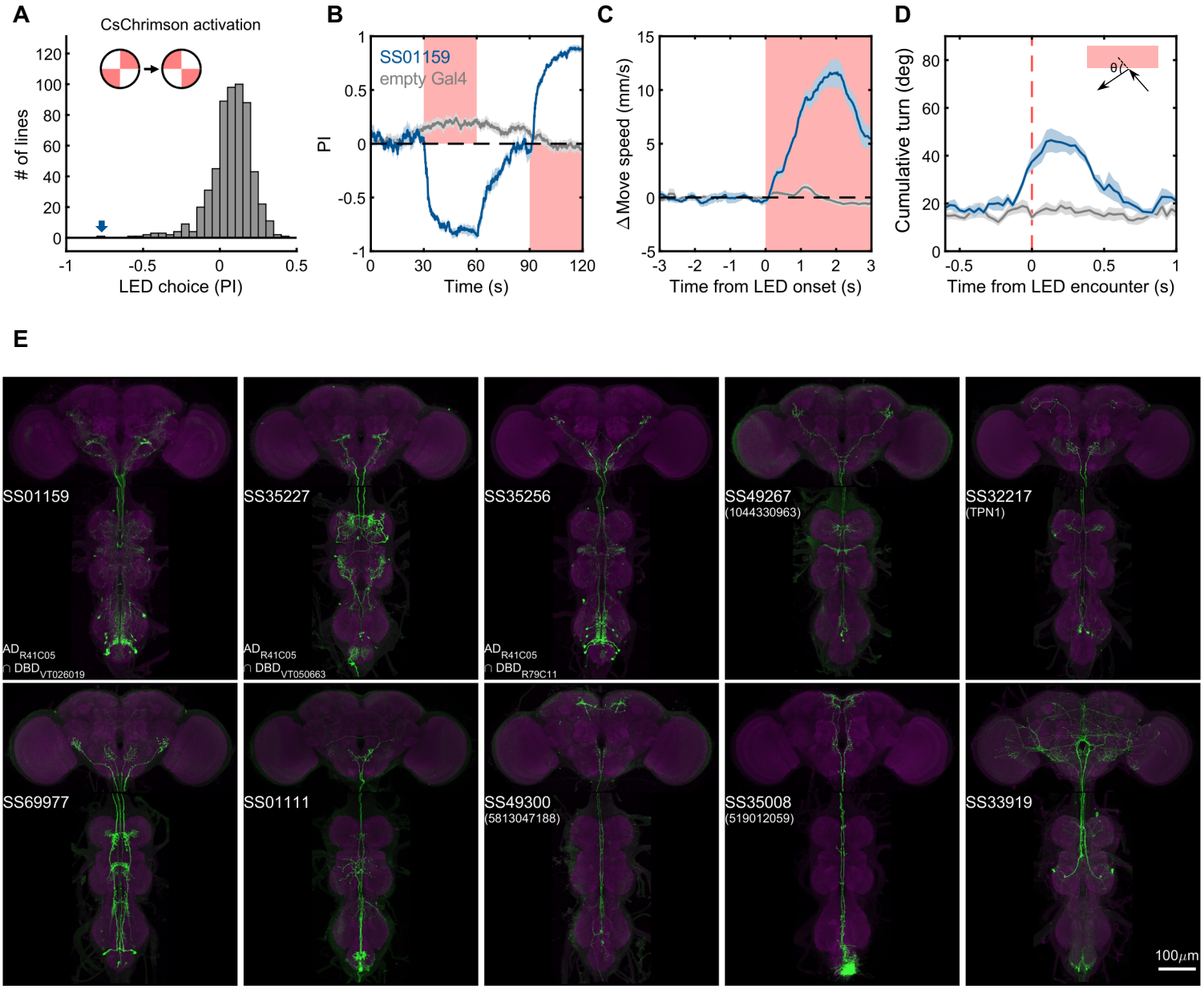


**Figure 9 Examples of covered ascending neurons**

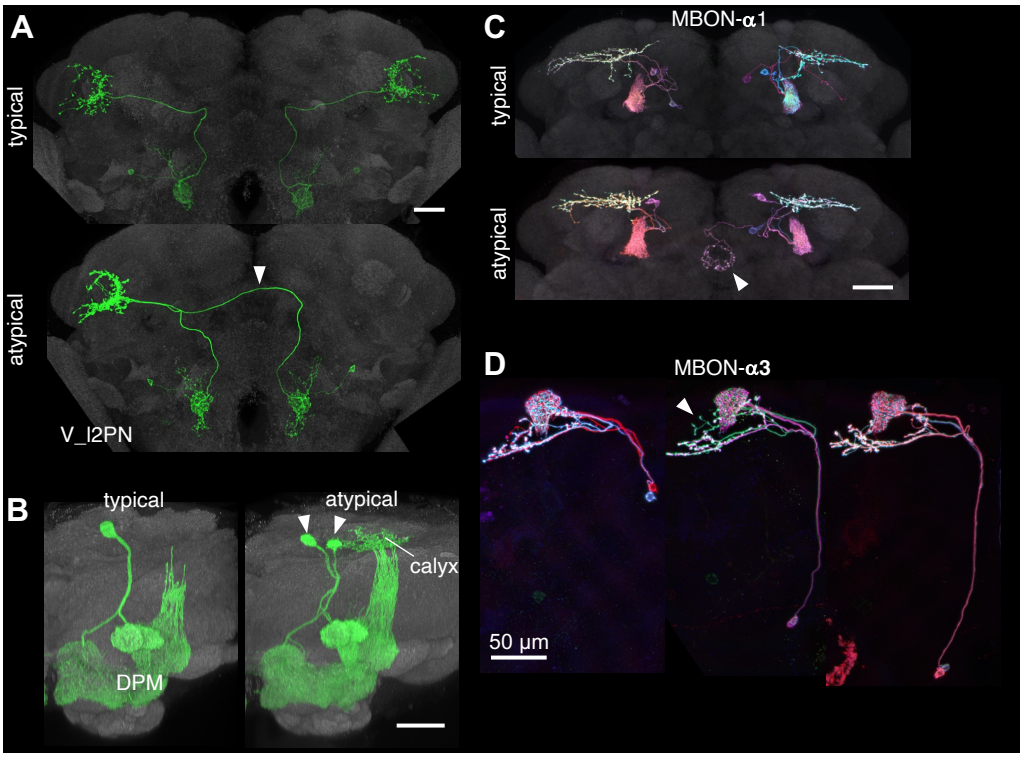


**E**

| Cell Type | MB compartments | N hemisphere examined | Typical number of cells | Different number of cells (%) | Mislocalization (%) Dendrite | Mislocalization (%) Axon | mode of errors |
|---|---|---|---|---|---|---|---|
| MBON01 | Y5, β'2a | 16 | 1 | 0.0 | 0.0 | 12.5 | mislocalization of axons |
| MBON02 | β2, β'2a | 96 | 1 | 1.0 | 1.0 | 1.0 | mislocalization of axons |
| MBON03 | β'2mp | 56 | 1 | 0.0 | 0.0 | 0.0 | |
| MBON05 | Y4 | 50 | 1 | 0.0 | 0.0 | 0.0 | |
| MBON06 | β1 | 38 | 1 | 0.0 | 0.0 | 0.0 | |
| MBON07 | α1 | 105 | 2 | 0.0 | 22.9 | 1.9 | dendrites outside the MB<br>axon in the ellipsoid body<br>third soma without neurites |
| MBON08/09 | Y3, β'1 | 338 | 2 | 0* | * | 0.6 | see Figure 11 |
| MBON11 | Y1, pedc | 136 | 1 | 0.7 | 0.7 | 1.5 | dendrites in Y2<br>axon in the calyx<br>lack of axon in α3 |
| MBON12 | Y2, α'1 | 106 | 2 | 0.0 | 0.0 | 0.0 | |
| MBON13 | α'2 | 82 | 1 | 0.0 | 1.2 | 0.0 | dendrites outside the MB |
| MBON14 | α3 | 44 | 1 | 0.0 | 0.0 | 2.3 | additional axon branch |
| MBON18 | α2sc | 36 | 1 | 0.0 | 0.0 | 0.0 | |
| MBON19 | α2p3p | 34 | 2 | 0.0 | 0.0 | 0.0 | |
| MBON22 | calyx | 56 | 1 | 1.8 | 17.9 | 0.0 | dendriets outside the calyx |
| MB-DPM | all | 48 | 1 | 8.3 | 4.2 | 4.2 | Second DPM<br>axons/dendrites in the calyx |

**Figure 10 Stereotypy and erroneous projections**

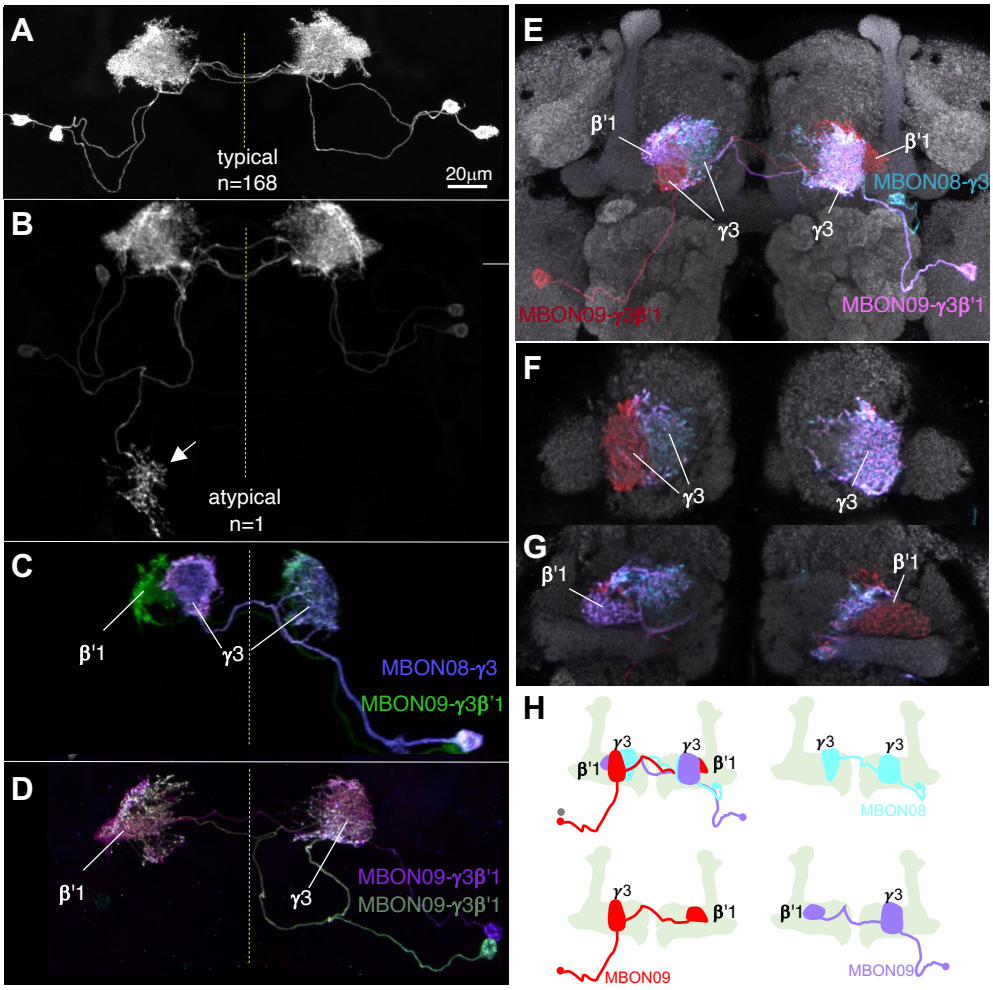


**I**

| | Female | Male | Total |
|---|---|---|---|
| MBON08 | 7 | 14 | 21 |
| MBON09 | 102 | 86 | 188 |
| % MBON08 | 6.4 | 14.0 | 10.0 |
| P only MBON09 | 0.77 | 0.55 | 0.65 |
| P at least One MBON08 | 0.23 | 0.45 | 0.35 |

**J**

| Left 2 cells | Right 2 cells | Left γ3 | Left β'1 | Right γ3 | Right β'1 | |
|---|---|---|---|---|---|---|
| 08/08 | 08/08 | + | | + | | P=2% (No occurrence in 169 flies) |
| 08/08 | 08/09 | + | + | + | | |
| 08/08 | 09/09 | + | + | + | | |
| 08/09 | 08/08 | + | | + | + | |
| 09/09 | 08/08 | + | | + | + | |
| 08/09 | 08/09 | + | + | + | + | P=3% (No occurrence in MCFO) |
| 08/09 | 09/09 | + | + | + | + | P=29% |
| 09/09 | 08/09 | + | + | + | + | |
| 09/09 | 09/09 | + | + | + | + | P=~65% of flies |
| MBON type | | MB compartments | | | | |

**Figure 11 Individuality and asymmetry of MBON08 and MBON09**

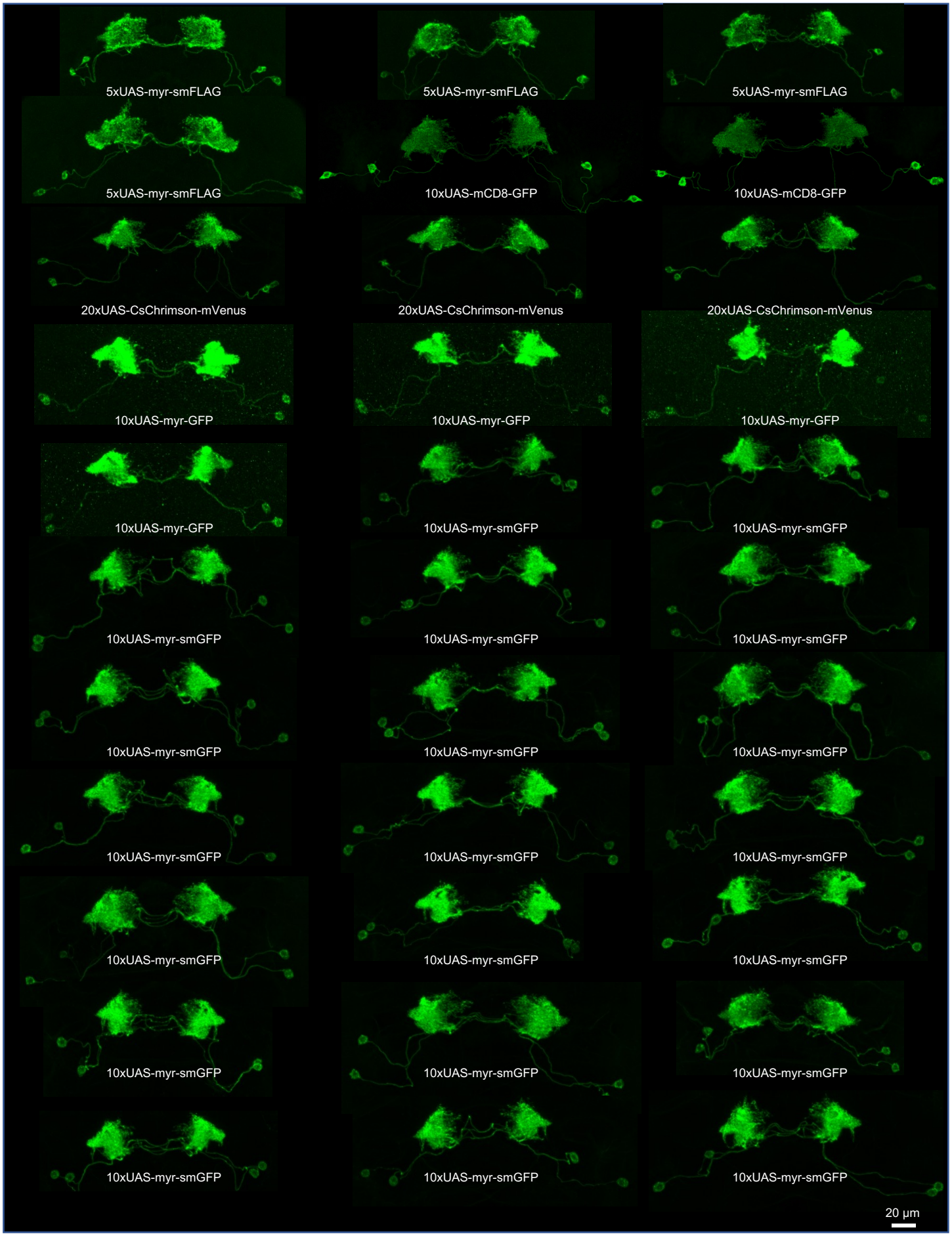


**Figure 11 – figure supplement 1 MB083C invariantly label two MBONs**

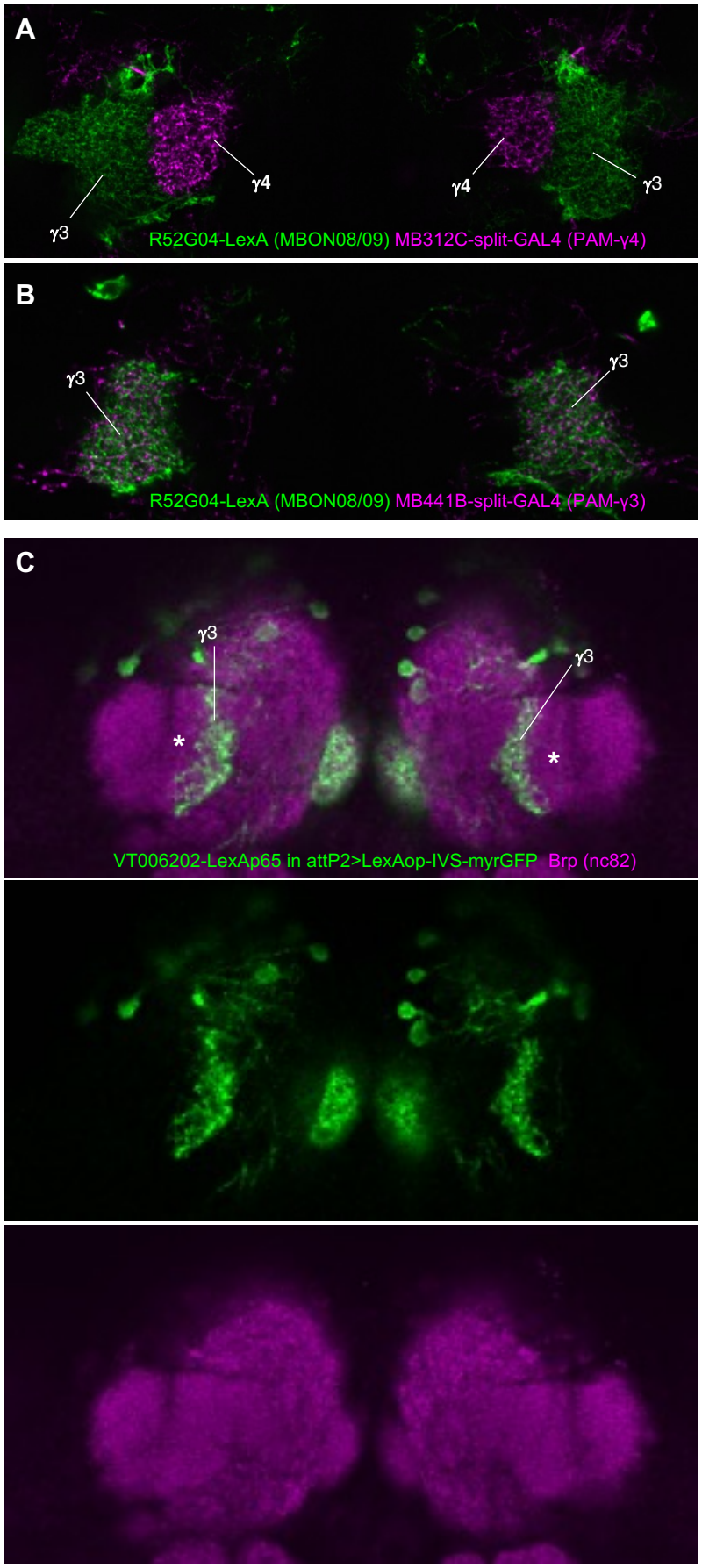


**Figure 11 – figure supplement 2 Subdivisions of medial and lateral γ3 compartments**

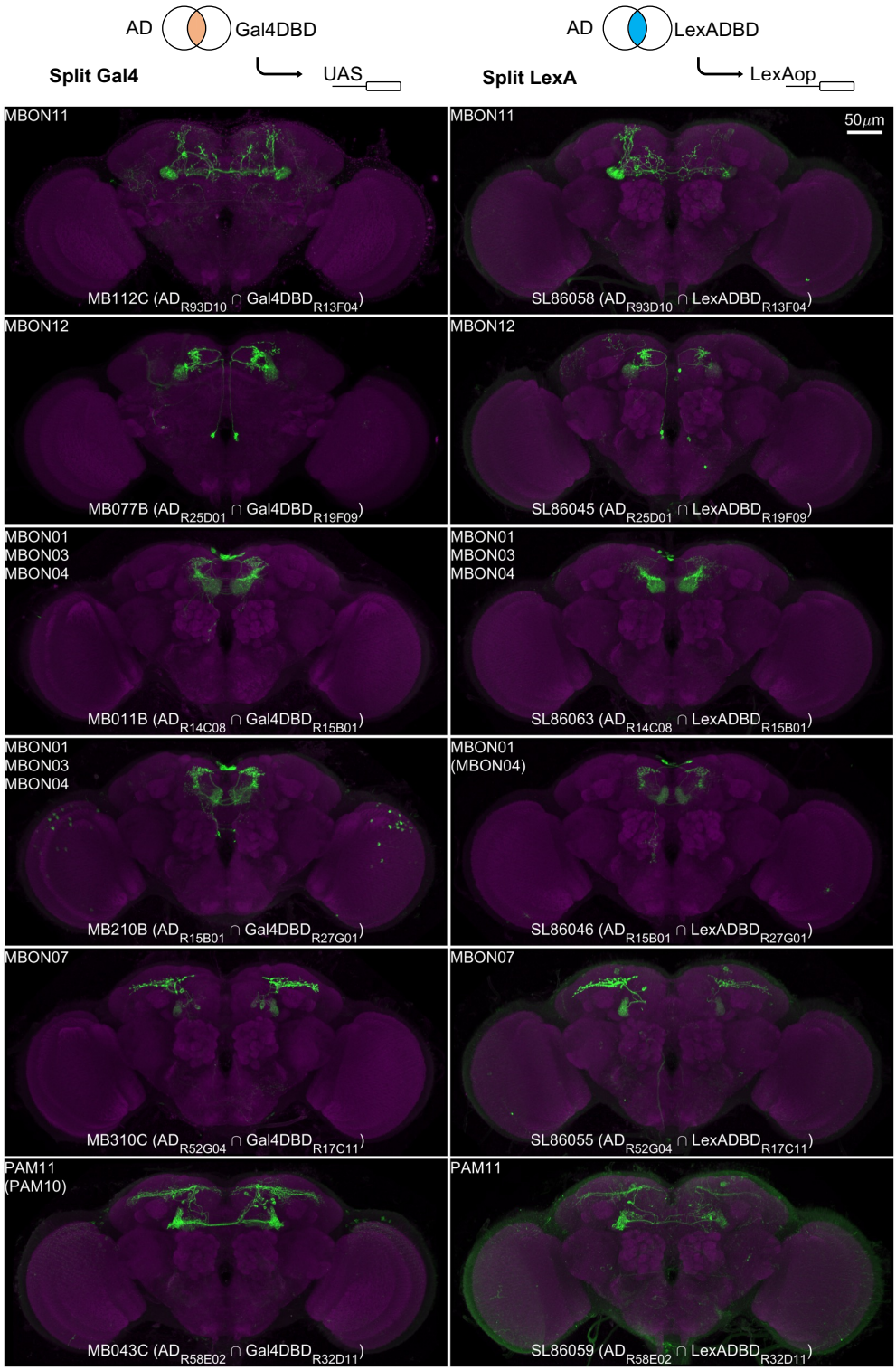


**Figure 12 Examples of split-LexA conversion**